# UC Riverside

## UC Riverside Electronic Theses and Dissertations

### Title

Using Cell Derived Extracellular Matrix to Advance the Physiological Relevance of Three Dimensional Tissue Models

### Permalink

https://escholarship.org/uc/item/5rj9g4kq

### Author

Salmeron, Lisa Vanessa

### Publication Date

2024

### Copyright Information

This work is made available under the terms of a Creative Commons Attribution-NonCommercial License, available at https://creativecommons.org/licenses/by-nc/4.0/

Peer reviewed|Thesis/dissertation

eScholarship.org Powered by the California Digital Library
University of California

UNIVERSITY OF CALIFORNIA
RIVERSIDE

# Using Cell Derived Extracellular Matrix to Advance the Physiological Relevance of Three-Dimensional Tissue Models

A Dissertation submitted in partial satisfaction of the
requirements for the degree of

Doctor of Philosophy

in

Bioengineering

by

Lisa Vanessa Salmeron

September 2024

Dissertation Committee:

Dr. Joshua Morgan, Chairperson
Dr. Huinan Liu
Dr. Hyle Park

Copyright by
Lisa Vanessa Salmeron
2024

The Dissertation of Lisa Vanessa Salmeron is approved:

_____

_____

_____

Committee Chairperson

University of California, Riverside

**Acknowledgments**

I thank the following individuals who have made this work possible:

The outstanding mentorship, advice, direction and insight of Dr. Joshua Morgan. The dedication and diligence of my undergraduate and graduate research assistants: Esther Chin, Jimmy Ho, and Rayyan Ayoub. The scientific discourse provided by fellow lab mates: Dr. Martina Sanchez, Isabella Bagdasarian, Dr. Shane Kennedy, William Darch, Dr. Abby Barlow, Jordan Rolsma, and Sara Nafar. The supervision and guidance provided to me throughout my undergraduate research in Dr. Kara E. McCloskey's research lab with mentor Dr. Edwin Shen and within the Mentored Summer Research Internship Program (MSRP) under Dr. Huinan Liu and mentor Dr. Wayne Leu. And my committee members for encouraging and challenging me.

To those who encouraged and supported me in my ambitions to achieve this goal: my amazing parents Laura and Luis Salmeron, my family and loved ones.

*Funding Sources:* RX1 Bioprinter Grant Program for Early Career Principal Investigators from Aspect Biosystems. The Dissertation Completion Fellowship Award (DCFA) from UCR Graduate Division.

ABSTRACT OF THE DISSERTATION

Using Cell Derived Extracellular Matrix to Advance the Physiological Relevance of Three-Dimensional Tissue Models

Lisa Vanessa Salmeron

Doctor of Philosophy, Graduate Program in Bioengineering
University of California, Riverside, September 2024
Dr. Joshua Morgan, Chairperson

Traditionally used natural biomaterials include purified biological polymers (e.g., collagen, fibrin). However, purified polymers do not retain the molecular diversity of native tissue, inhibiting their use in specialized tissues. As an alternative approach, there is increasing research in tissue derived matrix (TDM) biomaterials. TDM, while having increased similarity to native tissue, require harsh chemical processing and a considerable amount of site-specific donor tissues, difficult to achieve for rarer tissue like cornea. Here, we validate *in vitro* generation of a suitable biomaterial using tissue-specific cell types; this work is the foundation to scalable tissue-specific biomaterial production. Furthermore, in contrast to TDM collected from cadaver tissue; in vitro CDM methods allows for tighter batch consistency and incorporation of therapeutically useful transgenes. In this work, we generate CDM from mouse fibroblasts, human lung fibroblasts, and human corneal keratocytes. We quantify the composition and organization of the CDM, demonstrate use as a functional biomaterial, and further demonstrate transgenic CDM with green fluorescent protein (GFP) as a proxy for future therapeutically useful proteins. This work includes: 1) a cell-derived matrix (CDM) that includes tissue-specific ECM components; and 2) a 3D bio-printed system that replicates the tissue-scale 3D organization of the cornea. Corneal blindness is increasingly prevalent; with ~5 million bilateral cases and ~23 million unilateral cases

worldwide. Donor tissues remains the cure to blindness, however, due to shortage of donor corneas, ~12.7 million people are on waiting lists and 190,000 yearly transplants are performed. Tissue engineered corneas represent an alternative supply, however, the unique composition and structure of the cornea has hindered development. In collaboration with an industry partner, we developed a 3D corneal construct bio-printed with corneal CDH. Print patterns are designed with orthogonal layers interleaved by spiral cell-laden layers, mimicking the lamella and corkscrew pattern of native cornea. Corneal constructs were matured and tested for viability and morphology. Further, using rabbit cells in the bioprints, we tested *ex vivo* engraftment on rabbit eyes kept in culture, again testing viability and morphology. This research validates a novel approach for the creation of engineered tissues by harvesting extracellular matrix (ECM) from specialized cell types such as cornea.

# Table of Contents

List of Figures ..... x

List of Tables ..... xvi

List of Abbreviations ..... xvii

Introduction ..... 1

1.1 Tissue Composition ..... 1

1.2 Current State of Engineered Tissue Production ..... 6

1.2.1 Theory, Principles and Applications ..... 10

1.3 Thesis overview ..... 12

The Bio-Fabrication of a Customizable Cell Derived Matrix and its Translational Production as a Hydrogel ..... 15

2.1 Abstract ..... 15

2.2 Introduction ..... 16

2.3 Materials and Methods ..... 19

2.3.1 Cell Isolation and Culture ..... 19

2.3.2 CDM Production ..... 20

2.3.3 Decellularization ..... 22

2.3.4 Immunofluorescent Staining ..... 22

2.3.5 Quantification of Matrix Structure ..... 23

2.3.6 Matrix Solubilization ..... 23

2.3.7 Protein, GAG, and Collagen Quantification ..... 24

2.3.8 Alcian Blue Staining ..... 25

2.3.9 Turbidity Kinetics ..... 25

2.3.10 Gelation Controls ..... 26

2.3.11 Cell Transfection and Transduction ..... 26

2.3.12 Tensile Testing ..... 27

2.4 Results ..... 28
2.4.1 Generation of multilayer cell-derived matrices using variable cell types ..... 28
2.4.2 Collagen Type 1 Fibrils and Cellular Filamentous Actin Are Strongly Aligned in CDM 30
2.4.3 Minimal Variation of Collagen Fibril Morphology Across Diverse CDM Tissue Types 30
2.4.4 CDMs demonstrate tensile strength, genetic enhancements and stackable layering construction ..... 32
2.4.5 GAGs are retained after decellularization, and Protein are retained after Solubilization ..... 34
2.4.6 CDMs can be scaled to provide customized Cell Derived Hydrogels (CDH) ... 35
2.5 Discussion ..... 38
2.6 Supplemental Materials ..... 42
A Physiologically Relevant 3D Bio-Printed Cornea Using a Novel Cell Derived Hydrogel ..... 44
3.1 Abstract ..... 44
3.2 Introduction ..... 45
3.3 Materials and Methods ..... 47
3.3.1 Corneal Keratocyte (CK) Isolation ..... 47
3.3.2 RT-qPCR ..... 49
3.3.3 Bioink Formulation ..... 51
3.3.4 3D Bio-Printing Parameters ..... 51
3.3.5 Wound Healing Activation Method ..... 52
3.3.6 Post Print Processing ..... 52
3.3.7 Ocular Globe Dissection and *Ex vivo* Transplantation ..... 53
3.3.8 Viability Assays ..... 54
3.3.9 Immunofluorescent Staining ..... 54
3.3.10 Cellular Circular Formation Analysis ..... 54

3.4 Results ..... 55
3.4.1 Testing of CDH-enriched Bioink for 3D Bio-Printed Corneal Equivalent ..... 55
3.4.2 Physiologically Relevant Construction of 3D Printed BCE ..... 56
3.4.3 Increased Cellular Assembly of hCK-CDH enriched BCEs ..... 59
3.4.4 Consistent Viability of Printed Cells with Incorporated Post-Print Processing . 60
3.4.5 *Increased Viability of Transplanted BCE* ..... 61
3.5 Discussion ..... 63
3.6 Supplementary materials ..... 67
Closing Statements ..... 69
4.1 Impact ..... 73
4.2 Challenges, Limitations, and Future Improvements ..... 69
4.2.1 Scaling up Tissue Production ..... 69
4.2.2 Sustainably Tackling Metabolic Demands ..... 70
4.2.3 Combatting Insufficient Mechanical Properties ..... 70
4.2.4 Tissue Composition and Decellularization ..... 71
4.2.5 The Impact of Pepsin Digestions on Gelation Properties ..... 71
Appendix ..... 74
MATLAB Analysis and Quantification ..... 74
Layered Cellular Distribution in CDM ..... 74
Established Lab Protocols ..... 80
Alcian Blue Staining ..... 80
CDM Harvesting ..... 82
Bibliography ..... 84

# List of Figures

1.1 Structural Integrity of Tissue Ground Substances and Fibers A) Tissue cells synthesize and secrete collagen and proteoglycans which interact to form a highly organized macromolecular matrix. B) Hydrophilic GAGs maintain relative hydration. C) Collagen fiber assembly with resident proteins maintaining spatial regulation. D) This matrix is resistant to deformation. E) Proteoglycans coating fibers form an organized lattice with regular spacing that uses steric hinderances as a repellant to deformation ..... 3

1.2 An outline of the TDH process from isolation, homogenization, to gelation that we used. This gelation process was used as a control sample and became the framework for understanding the gelation process of isolated ECM ..... 12

2.1 CDM and CDH Production plus Analysis Workflow. A) 2D CDM production workflow, where a glass culture surface was APTES functionalized for enhanced cell and tissue adhesion throughout the extended culture period. After a 5-week culture with a chemically defined culture media cells will have deposited a CDM. B) CDM tissue tracing: Confluent CDM cultures are confocal imaged as regions of interest (ROI) in triplicate and traced using curvelet transforms. Collagen type 1 fibrils are stained and traced in green and filamentous actin is stained and traced in red. Traced tissue artifacts are line segments with various nodes that can then be quantified and studied. C) CDH Production: CDM is first decellularized then lyophilized as a dry-mass before solubilization in pepsin and final gelation ..... 21

2.2 Self-Assembled CDM Architecture. A) Confocal images of CDM cross-sectional area and XZ orthogonal view. Scalebar 25 μm in white; z-values also in μm. B) Cartoon depiction of CDM culture method used for 5-week *in vitro* culture. Volumetric rendering of cell nuclei separated by cell layers – illustrating the precise location of cells imbedded within dense tissue. C). An expositional quiver plot

revealing fibril and filamentous actin orientations throughout tissue bulk. Separated by layers that are labeled with color bars ..... 29

2.3 Traced Fibril Bundle Distributions: A) Histograms of the number of bundled collagen fibrils and their respective length, width and straightens. NIH 3T3 distributions in orange, IMR90 in blue and hCK in purple. B) Bar graphs of CDM lamella thicknesses, and average fibril lengths, fibril widths and cell density in culture ..... 31

2.4 Tensile Tested Properties of CDM. A) Shows the sample mounting of our rolled up CDM samples with both ends sandwiched between sandpaper before mounting on sample clamps. B) Representative stress strain curves of our parental control NIH 3T3 CDM (n = 6) and NIH 3T3 CDM transduced to express Fibulin-GFP (n = 5). C) Compared mechanical properties including the Yield and Ultimate Tensile Strength, Youngs Modulus, Elastic Limit, and Failure Strain with error bars ..... 33

2.5 Protein Composition after Decellularization. A) NIH3T3, IMR90 and hCK express sulfonated GAGs retention with alcian blue staining; scalebar 100 μm. B) Comparative bar graph of collagen, protein and chondroitin GAGs measured w/v% composition in solubilization solution ..... 35

2.6 TDH and CDH Cell Viability. A) Confocal imaging of cell morphology of lung IMR90, NIH 3T3, and hCKs on their respective lung TDH, lung CDH, NIH 3T3 derived CDH and hCK CDH that produced the matrix hydrogel with TG crosslinking and without TG. Scalebar 100 μm. B) Cytocompatibility results with and without TG crosslinking for each tissue type. ..... 37

2.7 TDH verses CDH Gelation Kinetics for Rat tail collagen control (n=13), lung TDH (n=15), Lung CDH (n=6), NIH 3T3 (n=3), hCK CDH (n=4). Measured via spectrophotometry at 405nm. A) the lag phase or initiation time to gelation B) time to reach 50% of maximum absorbance. C) Time to reach 95% maximum absorbance. D) The turbidimetric speed, S, or the slope of the linear portion of the curve. E) Image of gelled hCK-CDH sample birds eye view and cross-sectional view. F) Example curve and with gelation metrics labeling of rat tail collagen control, G) Lung-TDH, H) NIH-3T3 CDH, I) Lung-CDH, and J) hCK-CDH. ..... 37

2.S.1 Harvested CDM Drymass. Measured CDM dry weight in mgs per 100 cm2 after decellularization and lyophilization ($p > 0.0364$) ..... 42

2.S.2 Supplemental Figure 2.S.2: Stress Strain Curves of All Tensile Tested Samples. A) is the control NIH 3T3 CDM samples and B) is the Fibulin-GFP transduced NIH 3T3's CDM samples. ..... 43

3.1 Workflow from cellular isolation to BCE production. This schematic depicts the isolation process such that A) - C) the stroma is isolated and D) stromal explants are cut to 1mm cubes. In E) stromal cells migrate onto cell culture dish for expansion. F) is the CDM production process on APTES functionalized glass so that during the decellularization wash process in G) the matrix remains adherent to the glass and is easily harvested. H) is the lyophilization of isolated CDM while I) is the solubilization to a cell derived hydrogel (CDH) and J) is the bioink formulation in combination with sodium alginate (SA) and rat tail collagen type I (RCT). Finally, K) a diagram of the pneumatic pressure-based extrusion system used for 3D bioprinting ..... 48

3.2 Post Print Processing. A) the 3D bioprinting of our BCE. B) BCE directly after bioprinting. C) After 1 week in culture. D) A schematic of the apparatus used for plastic compression of BCEs for liquid expulsion. E and F) are post compression and show transparency of our BCEs ..... 53

3.3 3D Physiologically Relevant Print Design. A) The architectural makeup of the corneal stroma with respect to the preferential lamella layering and superimposed keratocyte network that corkscrews within the layered lamellae. B) A schematic diagram of the preferential corneal symmetry as reported by Meek and Bone (2004). C) The scrutinized fibril assembly in the cornea as reported by Meek and Bone (2004). D) The 3D printing pattern with 1. depicting the first layer as a longitudinal pattern printed rectilinearly within the corneal cylinder then 2. depicting the second layers concentric pattern for the corkscrew network and 3 depicting the laterally aligned fibers. This pattern had a repeating infill until the

desired thickness was reached and a diagram of the assemblage for 3D printing is shown ..... 57

3.4 Physiologically Relevant Corneal Construction. Confocal imaging of encapsulated corneal keratocytes with nuclei in cyan and filamentous actin in magenta. A) Cell alignment along the fibril edges scalebar 100 μm and B) close-up of cell spreading scalebar 50 μm. C) Imaging of highly interconnected cells within BCE scalebar 50 μm. D and E) additional cell imaging scalebar 100 μm. F) Diagram of print scheme and highlighted radial region for imaging. G) Stitched tile scans of radial slices in BCE, scalebar 100 μm, z position of the objective throughout the thickness of the BCE with filamentous actin in cyan and actin in magenta ..... 58

3.5 The Circularity of BCEs. A.) Preferential circular anisotropy of cells withing 3D printed BCEs. The kappa (κ) values are the circular dispersion values normalized to the mean with the green diamonds representing the average center-points of each sample and the blue triangles the leftmost and rightmost radial means. P-value = 0.0006. B.) Depicts collagen control confocal images of the leftmost and central point of a single sample and their respective kappa values. C.) Shows the collagen control radial distribution of cellular dispersion with each averaged peripheral and center point highlighted in blue and green respectively. D and E) Depicts confocal images and distributions of a single CDH sample respectively. Scalebar is 50 μm ..... 60

3.6 Cytocompatibility post bioprinting. A and B) Confocal imaging of 3D bio-printed BCEs with human cells collagen control based bioink in A) and CDH enriched bioink in B). C and D) Imaging of 3D bio-printed BCEs with rabbit cells collagen control based bioink in C) and CDH enriched bioink in D). Sample size n=3 for all samples except rabbit CDH n=4. Live cells in cyan and dead in magenta and scalebar 100 μm ..... 61

3.7 Transplantable Corneal Construct Response. A) 3D printed cornea directly after transplantation and before culture. B) 3D printed cornea 3.5 weeks in culture and 2 weeks after transplantation in ex-vivo culture. C) Re-transplant control in ex-vivo

culture where cornea was dissected cultured for 1 week and then retransplanted onto cornea for 2 weeks. D) Live dead viability of transplanted bioprint. E) Live dead viability of retransplanted control. Live in cyan dead in magenta scalebar 100 μm. F) Viability analysis sample size n=2 62

3.S.1 Figure 3.S.1 Corneal Specific Protein Expression. A) A time course analysis of cornea specific fibril proteins where collagen type 1 alpha 1 (COL1a1) is the prominent fibril protein of the cornea and collagen type 3 alpha 1 (Col3a1) is a wound fibril protein. Each week was normalized against week 2 measured against RPLPO (Large Ribosomal Protein) Endogenous Control. B) Corneal specific GAG keratocan (KERA) weekly amplification compared to decoran (DCRN) a wound specific GAG also normalized to week 2 under the same conditions. C) An endpoint analysis of protein expression after a 5-week CDM culture observing fibril collagens, GAGs and growth factor protein production for corneal reconstruction measured against GADPH. D) The melt curves verification of target specific amplification and fluorescent detection in the previous graphs. 67

3.S.2 The Circularity of BCEs after 3 weeks in culture. A.) Preferential circular anisotropy of cells withing 3D printed BCEs. The kappa (κ) values are the circular dispersion values normalized to the mean with the red diamonds representing the average center-points of each sample and the orange triangles the leftmost and rightmost radial means. B.) Depicts collagen control confocal images of the leftmost and central point of a single sample and their respective kappa values. C.) Shows the collagen control radial distribution of cellular dispersion with each averaged peripheral and center point highlighted in blue and green respectively. D and E) Depicts confocal images and distributions of a single CDH sample respectively. Scalebar is 50 μm 68

5.1 Merged Layer Distribution Breakdown. A) Binary thresholding of nuclear staining to identify centroid and extent through sample thickness in Z-axis. B) Stained nucleus confocal imaging at individual Z-slice for comparison. C) In order of code figure this is the position of the original centroid through the imaged CDM; X, Y,

and Z axis units in pixels. D) Updated view of nucleus within Z-slice. Outside of plane/layer separated by color scheme. E) Color-scheme-separated nuclear centroids distributed throughout CDM. F) Finalized merged layer distribution after removing rejected layers at individual Z-slice. This information was used to create the finalized image in Figure 2.2B ..... 79

# List of Tables

1.1 Table of Major Proteins in the Extracellular Matrix ..... 5

1.2 FDA Approved Cellular and Gene Therapy Products. Namely, treatments that utilize tissue engineering to turn cell and gene therapies into bioactive treatments for regenerative medicine therapies. ..... 7

3.1 Table of qPCR Primers their forward and reverse sequences as well as relevant citations. ..... 50

# List of Abbreviations

ECM – Extracellular Matrix
CDM – Cell Derived Matrix
TDM – Tissue Derived Matrix
CDH – Cell Derived Hydrogel
TDH - Tissue Derived Hydrogel
IMR90 – Human Lung Fibroblast Cell Line
NIH 3T3 – Immortalized Mouse Embryonic Fibroblasts
CKs – Corneal Keratocytes
GAGs – Glycosaminoglycans
PGs – Proteoglycans
GF – Growth Factors
TG – Transglutaminase
BCE – Bioengineered Corneal Equivalent
GFP – Green Fluorescent Protein
$T_{lag}$ – Lag Time
$T_{1/2}$ – Time Half-life
$T_{95}$ – Time to 95%
S – Turbidity Speed
ROI – Region of Interest
FGF – Fibroblast Growth Factor
VEGF – Vascular Endothelial Growth Factor
TGF-β – Transforming Growth Factor Beta
PDGFβ – Platelet Derived Growth Factor Beta
IL – Interlukin
HEK293TN – Derivative Cell Line Isolated from the Kidney of a Human Embryo
PsPAX2 – 2$^{nd}$ Generation Lentiviral Packaging Plasmid
pMD2.G – VSV-G Envelope Expressing Plasmid
DMEM – Dulbecco's Modified Eagle Medium
FBS – Fetal Bovine Serum
PS – Penicillin Streptomycin
APTES – (3-Aminopropyl) Triethoxysilane
LN – Liquid Nitrogen
EDTA – Ethylenediaminetetraacetic Acid
DPI – Dots Per Inch
DMMB – 1,9-Dimethylmethylene Blue

RT-qPCR – Reverse Transcriptase quantitative Polymerase Chain Reaction
GAPDH – Glyceraldehyde-3-Phosphate Dehydrogenase
PDGFRα – Platelet Derived Growth Factor Receptor Alpha
RPLPO – Large Ribosomal Protein
PC – Plastic Compression
XRD – X-ray Diffraction

# Chapter 1

# Introduction

## 1.1 Tissue Composition

Tissue is a complex assembly consisting of cells and structural components that organize to perform specific functions. There are four basic types of animal tissue: 1) epithelial tissue, 2) connective tissue, 3) muscle tissue, and 4) nervous tissue each with various subtypes and functional roles. Of these, the connective tissue is the most abundant;[1,2] providing mechanical structure, organization and transports nutrients/waste transports for the organism.[1] Connective tissue is predominantly populated with cells that originate from the embryonic mesenchyme embedded in an extracellular matrix (ECM) that is made up of fibrous proteins and ground substances.[3]

Protein fibers make up 20-25% of the protein content in humans.[4,5] Of these, collagen fibers are non-elastic and assemble in bundles of various thicknesses and flexibility that are the primary tensile elements of the tissue.[6,7] Collagens themselves have multiple different forms for supramolecular assembly. Major collagen classifications include: fibril forming collagens, fibril associated collagens, network forming collagens, transmembrane collagens, anchoring fibrils, and beaded filament forming collagen, there are even some collagens; additional unique collagen organizations exist.[8] In the spaces between fibers, a gel like

material termed ground substance provides structural and biological roles.[6] Ground substance is predominantly composed of glycosaminoglycans (GAGs) that link to proteoglycans (PGs) in a way that permits extracellular fluid to diffuse through.[9–11] More specifically, GAG-decorated proteoglycans are assembled by cells onto collagen bundles to maintain a consistent spacing between fibers – providing resistive properties to compressive forces (Figure 1.1).[6,12,13] This highly charged fibril assembly acts as a docking site for elastins, growth factors (GFs) and other ligands or mechanical signals that play a major role in signal transduction between cells and organs.[14–16]

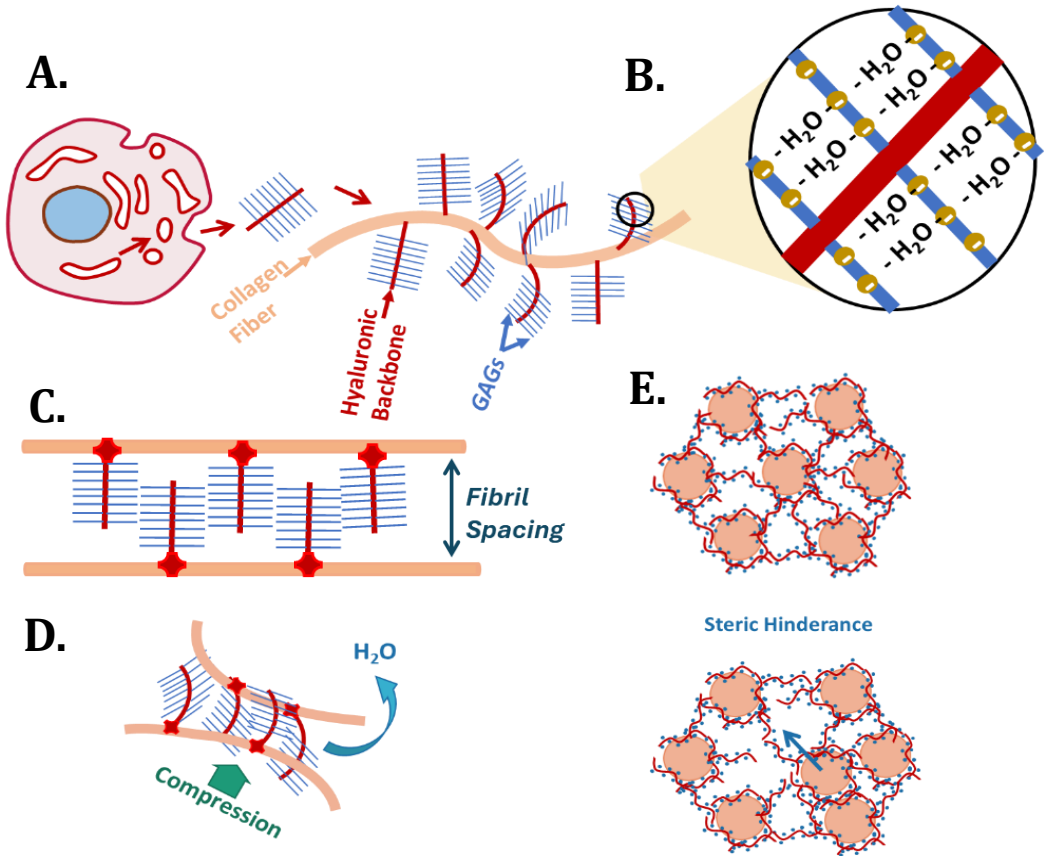



Figure 1.1: Structural Integrity of Tissue Ground Substances and Fibers A) Tissue cells synthesize and secrete collagen and proteoglycans which interact to form a highly organized macromolecular matrix. B) Hydrophilic GAGs maintain relative hydration. C) Collagen fiber assembly with resident proteins maintaining spatial regulation. D) This matrix is resistant to deformation. E) Proteoglycans coating fibers form an organized lattice with regular spacing that uses steric hinderances as a repellant to deformation.

Ultimately, collagens, GAGs, PGs, elastin, laminins, fibronectin, and other proteins/glycoproteins are the ultrastructural building blocks of a well-organized ECM (Table 1.1).[14,17–19] The composition and organization of these matrix components varies among tissues and with health and disease. Through the specific composition and organization, the ECM regulates cell processes like adhesion, differentiation, homeostasis, apoptosis, and wound healing in a tissue specific manner.[17,20] Alterations in the ECM due to damage, disease, or aging can lead to cellular dysregulation. Regenerative medicine aims to restore, replace and repair unhealthy tissue;[21] developing more representative ECM is therefore a key goal and ongoing research aims to recapitulate the complexity of native tissue in engineered models.[22]

## Table 1.1 Major Proteins in the Extracellular Matrix

| ECM Proteins | Major Types and Forms | Role |
|---|---|---|
| Collagens | 25 distinct chains forming structures:<br>Fibrillar<br>Non-fibrillar | Provides structural support. |
| GAGs | Hyaluronan,<br>Chondroitin sulfate,<br>Dermatan sulfate,<br>Heparan sulfate,<br>Keratan sulfate | Highly charged proteins used to sequester water for lubrication and shock absorption. |
| PGs | **Types**: Heparin sulfate PG<br>Chondroitin sulfate PG<br>Keratan sulfate PG<br>**Small**: Decorin, Biglycan<br>Testican, Bikunin<br>Fibromodulin, Lumican<br>**Large**: Aggrecan, Neurocan,<br>Versican, Brevican. | Regulator in the fibril spacing, and the assembly and maintenance of ECM. |
| Elastin | Topoelastins made of non-polar amino acids like glycine, valine, alanine, and proline that once assembled form elastic fibers including:<br>Elastin,<br>Elaunin<br>Oxytalan. | Resiliency to recoil and elastic properties |
| Laminin | Subunits: α1-5, β1-3,γ1-3<br>With 15 isoforms in trimeric combinations | Major basement membrane protein. Web-like structures that contribution tensile strength. Mediate cell attachment, differentiation, shape and movement. |
| Fibronectin | Insoluble (found in ECM)<br>Soluble (found in blood) | Large insoluble fibrils that comprise the ECM. Assist in various protein binding. |
| Glycoproteins<br>Docking proteins | Fibrillin<br>Ligands<br>Integrins<br>Growth factors<br>Chemokines | Help assemble elastin fibers<br>Mediate cell signaling with ECM |

## 1.2 Current State of Engineered Tissue Production

In the approximately three decades since the field of tissue engineering emerged the Food and Drug Administration (FDA) has approved 37 therapies for commercial production (Table 1.2).[23] They vary greatly in therapeutic targets and biological agents used, yet generally stimulate healing and regeneration where conventional treatments are insufficient.[24] The full restoration of tissue after injury or disease however, has not been generally addressed.[21,24] Current research uses a combination of biomaterials and scaffoldings in combination with cells and bioactive molecules.[25] The materials chosen must provide structural support and control the body's innate healing and inflammatory responses in much the same manner as ECM.

## Table 1.2 FDA Approved Cellular and Gene Therapy Products

| Name | Company | Therapeutic Target/Use | Major Biological Agent(s) Used |
|---|---|---|---|
| ABECMA (idecabtagene vicleucel) | Celgene Corporation, a Bristol-Myers Squibb Company | Multiple Myeloma | Genetically modified autologous T cells |
| ADSTILADRIN (nadofaragene firadenovec-vcng) | Ferring Pharmaceuticals A/S | Non-muscle invasive bladder cancer | Adenoviral vector |
| ALLOCORD (HPC, Cord Blood) | SSM Cardinal Glennon Children's Medical Center | Hematopoietic stem cell transplantation | Hematopoietic progenitor cells |
| AMTAGVI (lifileucel) | Iovance Biotherapeutics, Inc. | Metastatic melanoma | Autologous tumor infiltrating lymphocytes |
| BEQVEZ (fidanacogene elaparvovec-dzkt) | Pfizer, Inc. | Hemophilia B | AAV vector encoding FIX-Padua |
| BREYANZI (lisocabtagene maraleucel) | Juno Therapeutics, Inc., a Bristol-Myers Squibb Company | Large B-cell lymphoma | Genetically modified autologous T cells |
| CARVYKTI (ciltacabtagene autoleucel) | Janssen Biotech, Inc. | Multiple Myeloma | Genetically modified autologous T cells |
| CASGEVY (exagamglogene autotemcel) | Vertex Pharmaceuticals Incorporated | Sickle Cell Disease | CRISPR-modified autologous CD34+ hematopoietic stem cells |
| CLEVECORD (HPC Cord Blood) | Cleveland Cord Blood Center | Hematopoietic stem cell transplantation | Hematopoietic progenitor cells |
| Ducord, HPC Cord Blood | Duke University School of Medicine | Hematopoietic stem cell transplantation | Hematopoietic progenitor cells |
| ELEVIDYS (delandistrogene moxeparvovec-rokl) | Sarapeta Therapeutics, Inc. | Duchenne Muscular Dystrophy | AAV vector encoding micro-dystrophin |
| GINTUIT (Allogeneic Cultured Keratinocytes and Fibroblasts in Bovine Collagen) | Organogenesis Incorporated | Oral soft tissue regeneration | Allogeneic cultured keratinocytes and fibroblasts in bovine collagen |
| HEMACORD (HPC, cord blood) | New York Blood Center | Hematopoietic stem cell transplantation | Hematopoietic progenitor cells |
| HEMGENIX (etranacogene dezaparvovec-drlb) | CSL Behring LLC | Hemophilia B | AAV vector encoding FIX-Padua |
| HPC, Cord Blood | Clinimmune Labs, University of | Hematopoietic stem cell transplantation | Hematopoietic progenitor cells |

| | | | |
|---|---|---|---|
| | Colorado Cord Blood Bank | | |
| HPC, Cord Blood - MD Anderson Cord Blood Bank | MD Anderson Cord Blood Bank | Hematopoietic stem cell transplantation | Hematopoietic progenitor cells |
| HPC, Cord Blood - LifeSouth | LifeSouth Community Blood Centers, Inc. | Hematopoietic stem cell transplantation | Hematopoietic progenitor cells |
| HPC, Cord Blood - Bloodworks | Bloodworks | Hematopoietic stem cell transplantation | Hematopoietic progenitor cells |
| IMLYGIC (talimogene laherparepvec) | BioVex, Inc., a subsidiary of Amgen Inc. | Melanoma | Genetically modified oncolytic viral therapy (herpes simplex virus) |
| KYMRIAH (tisagenlecleucel) | Novartis Pharmaceuticals Corporation | B-cell acute lymphoblastic leukemia | Genetically modified autologous T cells |
| LANTIDRA (donislecel) | CellTrans Inc. | Type 1 Diabetes | Purified allogeneic islets of Langerhans |
| LAVIV (Azficel-T) | Fibrocell Technologies | Nasolabial fold wrinkles | Autologous fibroblasts |
| LENMELDY (atidarsagene autotemcel) | Orchard Therapeutics (Europe) Limited | Metachromatic leukodystrophy | Genetically modified autologous CD34+ cells |
| LUXTURNA (voretigene neparvovec-rzyl) | Spark Therapeutics, Inc. | Retinal dystrophy due to RPE65 mutation | AAV vector encoding RPE65 |
| LYFGENIA (lovotibeglogene autotemcel) | bluebird bio, Inc. | Sickle Cell Disease | Genetically modified autologous CD34+ cells |
| MACI (Autologous Cultured Chondrocytes on a Porcine Collagen Membrane) | Vericel Corp. | Cartilage defects | Autologous cultured chondrocytes on porcine collagen membrane |
| OMISIRGE (omidubicel-onlv) | Gamida Cell Ltd. | Hematopoietic stem cell transplantation | Cultured allogeneic hematopoietic stem and progenitor cells |
| PROVENGE (sipuleucel-T) | Dendreon Corp. | Prostate cancer | Autologous dendritic cells exposed to a prostate cancer antigen |
| RETHYMIC (allogeneic processed thymus tissue – agdc) | Enzyvant Therapeutics GmbH | Congenital athymia | Allogeneic processed thymus tissue |
| ROCTAVIAN (valoctocogene roxaparvovec-rvox) | BioMarin Pharmaceutical Inc | Hemophilia A | AAV vector encoding FVIII |

| | | | |
|---|---|---|---|
| SKYSONA (elivaldogene autotemcel) | bluebird bio, Inc. | Cerebral adrenoleukodystrophy | Genetically modified autologous CD34+ cells |
| STRATAGRAFT (allogeneic cultured keratinocytes and dermal fibroblasts in murine collagen-dsat) | Stratatech Corporation | Deep partial-thickness burns | Allogeneic cultured keratinocytes and dermal fibroblasts in murine collagen |
| TECARTUS (brexucabtagene autoleucel) | Kite Pharma, Inc. | Mantle cell lymphoma | Genetically modified autologous T cells |
| VYJUVEK (beremagene geperpavec) | Krystal Biotech, Inc. | Dystrophic Epidermolysis Bullosa | HSV-1 based gene therapy |
| YESCARTA (axicabtagene ciloleucel) | Kite Pharma, Incorporated | Large B-cell lymphoma | Genetically modified autologous T cells |
| ZYNTEGLO (betibeglogene autotemcel) | bluebird bio, Inc. | Transfusion-dependent β-thalassemia | Genetically modified autologous CD34+ cells |
| ZOLGENSMA (onasemnogene abeparvovec-xioi) | Novartis Gene Therapies, Inc. | Spinal Muscular Atrophy | AAV vector encoding SMN1 |

Table 1.2 FDA approved treatments that utilize tissue engineering to turn cell and gene therapies into bioactive treatments for regenerative medicine therapies. Table adapted from FDA reports. [23]

Both synthetic and natural materials are frequently used as biomaterials for medical and research applications. Synthetic polymers,[26] ceramics,[27] metals,[28] glass[29] and even living cells or tissues have been molded into devices, coatings, fibers, sponges, films, meshes, and hydrogels for biomedical use. However, synthetic ingredients and matrices derived from isolated biological materials (i.e. collagen, fibrin, hyaluronan) do completely recapitulate the intricacies of cell-ECM signaling[30] observed in native tissue. Natural biomaterials have become a promising alternative with initial clinical tests accessible for acellularized tissues.[21,24,31,32] Tissue derived matrix (TDM) from decellularized allogenic or xenogeneic tissues seemingly maintain native material composition and microstructure.[33,34] These tissue sources however are hindered by inadequate tissue supply and inconsistencies that arise from donor age, gender, and health. In response to these limitations, TDM production has been mirrored by increased interest in in vitro cell derived matrix (CDM). In contrast to TDM, CDM offers more control over material production environment, is more customizable and can even be augmented or suppressed through genetic modifications to cater to certain therapeutic targets.[35]

### 1.2.1 Theory, Principles and Applications

Fibroblasts capably secrete their own ECM that may then be extracted and repurposed as structural and functional bio activators in regenerative medicine. The basis for CDM production is the confluent culture of fibroblasts induced to secrete and organize their own ECM.[35,36] Common approaches for CDM production use a variety of culture methods including 2D adherent cultures that deposit a self-assembled lamella on the surface. For more control of the 3D organization and thickness biodegradable and synthetic scaffolds can be

used as a carrier for embedded CDM depositing fibroblasts. Finally, multicellular aggregates[37,38] of fibroblast and differentiating stem cells are also commonly employed to obtain CDM.

The initial matrix deposition occurs after 5-9 days of confluent culture with ascorbic acid.[39,40] CDM is then typically extracted after a 2–5-week culture using various decellularization methods designed to preserve as much of the matrix composition and architecture as feasible.[39,41–45] Human clinical applications of this biomaterial are derived from a variety of tissues, including heart valves, blood vessels, skin, nerves, skeletal muscle, tendons, ligaments, small intestinal submucosa, urinary bladder and liver in the form of dried and hydrated sheets.[46]

The production of CDM to CDH is a highly anticipated biomaterial[36,47] with limited success.[48,49] While harvesting *in vitro* CDM is a new concept, it draws many parallels to the established practice of TDM harvesting. The widespread utilization of TDM to tissue derived hydrogels (TDH)[47,50,51] provides the fundamental principles for our success in the production of CDH. Our recreation of this process with rabbit lungs involves: 1) decellularization, 2) lyophilization, 3) liquid nitrogen (LN) homogenization 4) pepsin digestion and 5) gelation (Figure 1.2).

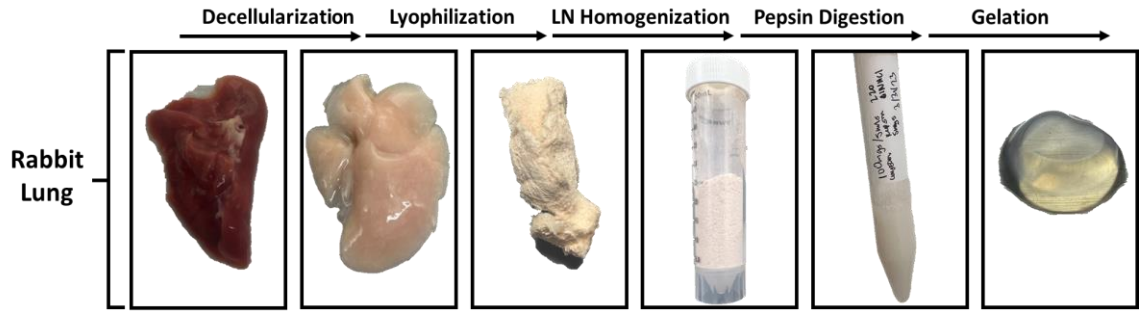



Figure 1.2: An outline of the TDH process from isolation, homogenization, to gelation that we used. This gelation process was used as a control sample and became the framework for understanding the gelation process of isolated ECM.

## 1.3 Thesis overview

This thesis demonstrates the feasibility and customization of tissue produced *in vitro*. Our findings broadly impact the ***integrity, specificity, availability and compatibility*** of naturally derived matrices, hydrogels and bio-inks. Providing the framework for a viable approach to 3D bioprinting physiologically relevant tissue with customizable bioinks that can be produced in culture and cater to tissue specific needs.

***(i) Specificity and Integrity of CDMs***: First, CDM deposition is induced by triggering the ECM production process of activated human corneal keratocytes (hCKs), NIH 3T3s and IMR90s over a 5-week culture period. Tissue organization is then measured histologically, and through PCR and image analysis. We then demonstrate the customization of such a tissue by genetically modifying cells to incorporate additional matrix proteins. The structural integrity of our genetically engineered CDM is confirmed with tensile testing.

***(ii) Connective Tissue Availability***: The CDMs deposited *in vitro* secrete a relevant composition of ECM proteins. Commercial biological coatings make these components available separately. A specialized blend derived straight from the tissue source provides an

innately applicable tissue combination that is convenient and reproducible. The CDM production process is established to increase ECM deposition and customization. The CDM yield obtained from this prolonged culture system provides sufficient ECM components for translation to hydrogels.

***(iii) Successful Conversion of Harvested CDMs into CDHs***. We fabricate and characterize cell derived matrices and hydrogels composed of resident ECM components with various assays. The CDH process is established to: preserve the biochemical make up of CDM during decellularization, dehydrate the isolated CDM, increase solubilization, and confirm gelation.

***(iv) Cytocompatible Hydrogels***: Our results confirm the functionality and compatibility of hydrogels of various tissue types by seeding resident cells that maintain viability above 80%.

***(v) Competent CDH Bioprinting and Construction of a Bioengineered Corneal Equivalent:*** Finally, our de novo hCK-CDH is used as an enriching bio-ink component for the novel 3D bioprinting of a bioengineered corneal equivalent. Our alternative approach to BCEs model assessment focuses on cell organization provided by our novel substrate; where cell arrangement properties and tissue development replicate native human corneas.

The development of cell derived hydrogels has immense applicability in regenerative medicine, drug deliveries, sealants, food additives, tissue engineering, transplantable tissue, bio-inks, wound dressing, and bioregulators. This tool opens up the field of hydrogel fabrication to become more specialized and customizable. This is a promising manuscript

and by making these findings accessible researchers will have a method for manufacturing tissue tailored hydrogels, matrices, and physiologically relevant tissues with 3D bio printing.

# Chapter 2

# The Bio-Fabrication of a Customizable Cell Derived Matrix and its Translational Production as a Hydrogel

## 2.1 Abstract

Prior work has established the potential of decellularized extracellular matrix derived from animal donor tissue (tissue derived matrix; TDM) as a viable biomaterial for research and therapy. More recently, the development of cell derived matrix (CDM) has garnered interest as an alternative to allogenic and xenogeneic TDM. Here we establish a 5-week culture system that produces CDMs of average thicknesses 30 ± 21.8 μm. Then, imaging cellular filaments and fibrillar collagen type I we were able to trace these artifacts and confirm their alignment as well as better understand the tissues fibrillar distribution when produced *in vitro*. We further compare the biochemical makeup of primary human corneal keratocytes, human lung fibroblasts (IMR90) and immortalized mouse NIH 3T3s CDMs produced *in vitro* to xenogeneic rabbit lung TDM. Using various assays and spectrophotometer techniques we establish the matrix composition of collagen (TDM: 5.75 ± 0.68 w/v% and CDM: 5.12 ± 4.5 w/v%), bulk proteins (TDM: 43 ± 11.5 w/v% and CDM:

46.6 ± 21.5 w/v%), and chondroitin glycosaminoglycans (TDM: 2.7 ± 0.48 w/v% and CDM: 1.1 ± 0.55 w/v%) to be comparable for TDM and CDM. Using these culture methods, we were also able to demonstrate the practical potential of engineering a genetically enhanced CDM. Tensile testing confirmed the ultimate tensile strength of our CDMs (65.7 ± 47.3kPa NIH 3T3 controls n = 6; 45.6 ± 24.5kPA Transduced Samples n = 5) as a workable tissue. Finally, we demonstrated dissolution and reconstitution of CDM into cell derived hydrogel (CDH) as a de novo biomaterial with limited characterization. We establish a robust method for gelation without crosslinkers that works for CDH from IMR90, NIH3T3, and primary human corneal keratocytes at a gelation time that is relevant for research needs (30min) and demonstrates cytocompatibility. In conclusion, this study shows the practical potential of CDM and CDH as a customizable biomaterial in research and therapeutic development.

## 2.2 Introduction

Naturally deposited extracellular matrix (ECM) provides a network of tissue specific components essential for maintaining homeostasis as well as regulating development, differentiation, and wound responses within the body.[17] To achieve this, the ECM must be a highly organized network that provides cells with appropriate chemical and mechanical cues, as well as tissue structure. Within ECM this organization is preserved through the interactions of glycosaminoglycans (GAGs, e.g. heparan sulphate, chondroitin sulfate, keratan sulfate, hyaluronan) and fibrillar proteins (e.g. collagens, fibronectin, laminins).[20] The organization and density of these components helps to regulate tissue functionality. For instance, a highly negatively charged assembly of proteoglycans sequesters water, much like a sponge, creating

a clear tissue highly resistive to compressive force and beneficial for fluid and nutrient transport (ex. the corneal stroma) while a more mineralized ground substance creates a rigid body solid enough to structurally support the body (ex. bone). More specifically, the mechanical properties and fiber organizations are strongly dependent on the modification of collagen fibrils by GAGs; collagen fibril organization and spacing is determined by the type and density of these GAGs.[52] Furthermore, the charged surface of polysaccharide constituents in GAGs provide docking sites for chemokines and growth factors important for cellular function (e.g. FGF, VEGF, TGF-β, IL).[15] Overall, this ECM organization facilitates tissue specific functionality that can be difficult to replicate or model *in vitro*. Nonetheless, as the field of tissue engineering advances there is increasing need for cost-effective generation of tissue-mimetic ECM biomaterials.[34]

Currently, typical *in vitro* culture biomaterials are amniotic membrane, synthetic hydrogels, or purified proteins such as rat-tail collagen; they do not possess the full complexity of native tissue.[51] For instance, natural hydrogels available commercially include isolated biological components (e.g. collagens, elastins, hyaluronic acids, laminins, fibronectins). While isolated components are derived from biologicals they are classically purified and do not retain other biochemical constituents specific to the native tissue (e.g. proteoglycans, procollagens, growth factors, and other extracellular matrix proteins). As a result, most cell culture substrates only contain one of these components instead of a blend native to their respective tissue types.[50] A notable exception being Engelbreth-Holm-Swarm tumor extract (e.g. Matrigel™), a tumor derived cocktail of basement membrane proteins that is poorly defined and lot dependent.[51,53]

The practice of reconstituting hydrogels from site-specific ECM is an expanding field meant to retain a more complete assortment of resident proteins native to tissue. Since 2017, more than 70 papers have shown successes in creating tissue-specific hydrogels from native source tissues.[51] Donor sources include xenografts and allograft of high demand tissues such as skin, cardiac, bone vascular and corneal grafts. ECM harvested from source tissue can then be used as the basis for 3D organotypic culture models or as stimulants for wound healing and tissue regrowth.[41]

These methods, while promising, require a considerable amount of site-specific donor tissue. Current research typically uses xenogeneic tissue extracts that undergo harsh decellularization and solubilization.[42] Post extraction these methods remain largely dependent on high doses of immunosuppressants that subject patients to a higher risk of infection.[54,55] Allografts do not induce as many cellular immune responses; however, tissues are not widely available and must undergo additional processing and testing, donor screenings and compliances to meet surgical requirements. Furthermore, despite evolving techniques, many decellularization methods strip the tissue of much of its distinct site-specific proteins such as growth factors and GAGs.[33,42] In contrast to tissue-derived ECM (TDM) autologous tissue cultured *in vitro* otherwise known as cell derived ECM (CDM) can be obtained to minimize potential pathogen transfer, inflammation and immune responses thus addressing this the above limitations.[56–58]

By allowing different types of fibroblasts to synthesize cell-type specific extracellular matrix proteins the basic approach for engineering autograft tissue that can be cultured and harvested in vitro becomes achievable. This involves the *in vitro* production and extraction of tissue specific ECM components such as collagens, GAGs, and growth factors as bulk

CDM. Furthermore, in contrast to TCM; *in vitro* CDM methods allows for modulation of external stimuli, genetic modification of cell source, and controlled culture system such as 2D vs 3D.[35,46]

In this work, we generate CDM with cultures of mouse fibroblasts, human lung fibroblasts (IMR90s), and human corneal keratocytes (hCK). We quantify the structure and organization of deposited matrix. We further demonstrate use as a biomaterial through both lamination of intact lamella, and gelation of dissolved CDM. Biomaterial usage is validated with cell viability and morphology assessments. This CDM production and isolation method has the potential to generate cost effective tissue specific matrix and hydrogels *in vitro*.

## 2.3 Materials and Methods

### 2.3.1 Cell Isolation and Culture

Primary corneal keratocytes (CKs) were isolated from human donor corneoscleral rims (Saving Sight, St. Louis, MO). Briefly, corneas were isolated at the limbal region and placed in 5 mM EDTA and 1.2 U/mL protease overnight at 4 °C. The epithelial and endothelial cell layers were removed and the remaining stromal tissue was cut into approximately 1 mm × 1 mm cubes. Explant tissues were cultured for one week in a media blend containing a base of 70% MCDB 131 (CM034-050; genDEPOT, Baker, TX) and 30% DMEM/F12 with 7% fetal bovine serum (FBS), 1% penicillin-streptomycin (PS), 0.5 µg/mL Amphotericin B, 35 µg/mL bovine pituitary extract, 5 µg/mL insulin, 5 ng/µL epithelial growth factor, and 0.5 µg/mL hydrocortisone. Cells which migrated out of the tissue were

passaged and cultured in the same media. Primary lung fibroblasts (IMR90s; ATCC, Manassas, VA) and mouse fibroblasts (NIH3T3; ATCC) and HEK293TN cells were cultured in DMEM/F12 (Product No. 10-092-CV; Corning, Manassas, VA) supplemented with 10% FBS, 1% PS, and 0.5 μg/mL Amphotericin B.

### 2.3.2 CDM Production

A 3.5-5 week culture of hCK, IMR90, and NIH3T3s was employed to produce a comparable bulk tissue (Figure 2.1A). For all cultures 100-300 μg/mL ascorbic acid, and 0.5 μg/mL TBF-β2 (Peprotech, Cranbury, NJ) were added fresh every 2 to 3 days to increase ECM production. Ascorbic acid concentrations were increased by 100 μg/ml weekly. Either 186 $cm^2$ or 58 $cm^2$ glass culture surfaces were functionalized with (3-aminopropyl) triethoxysilane as previously described to allow for the CDM to adhere to the glass throughout culture and decellularization.[59]

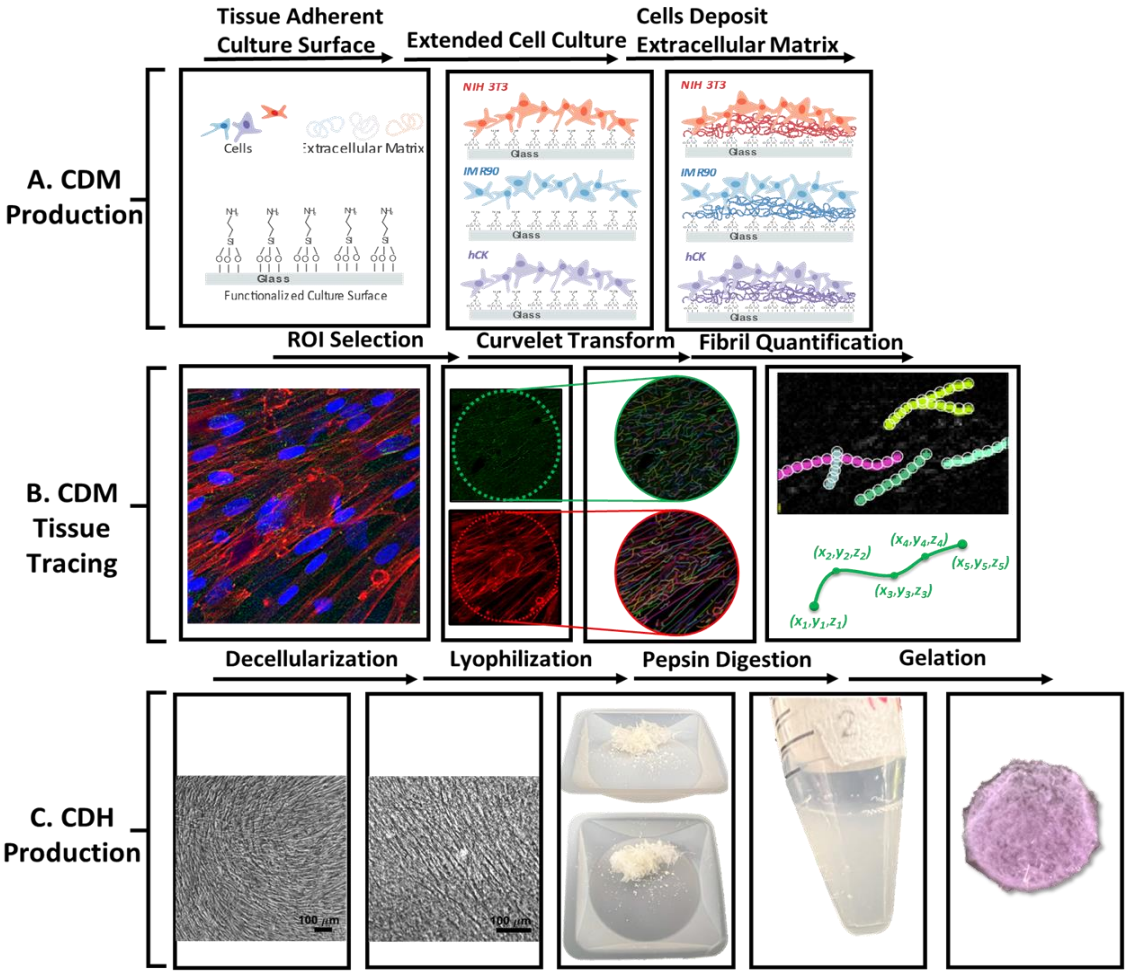



Figure 2.1 CDM and CDH Production plus Analysis Workflow. A) 2D CDM production workflow, where a glass culture surface was APTES functionalized for enhanced cell and tissue adhesion throughout the extended culture period. After a 5-week culture with a chemically defined culture media cells will have deposited a CDM. B) CDM tissue tracing: Confluent CDM cultures are confocal imaged as regions of interest (ROI) in triplicate and traced using curvelet transforms. Collagen type 1 fibrils are stained and traced in green and filamentous actin is stained and traced in red. Traced tissue artifacts are line segments with various nodes that can then be quantified and studied. C) CDH Production: CDM is first decellularized then lyophilized as a dry-mass before solubilization in pepsin and final gelation.

### 2.3.3 Decellularization

To harvest extracellular matrix, the cultures were washed 3× with 0.5% Triton X-100 (Sigma Aldrich, St. Louis, MO), 20 mM ammonium hydroxide (ThermoFisher Scientific), and 2.21 mM Ethylenediaminetetraacetic acid (EDTA; Santa Cruz Biotechnology, Santa Cruz, CA) in distilled water (~15 min each). Acid-base washes were performed for additional cellular lysis as well as removal of remnant salts from culture media.[42] This is done by alternating the Triton-$NH_4OH$ blend with 0.1% acetic acid for 3× ~7.5 min washes. Tissue isolates that were not fixed and stained for image analysis were further incubated in 0.1% glacial acetic acid for 7 d.

### 2.3.4 Immunofluorescent Staining

CDM samples of IMR90, hCK, and NIH3T3 were cultured for 5 weeks on APTES functionalized coverslips and then fixed with 4% paraformaldehyde/0.05% Triton X-100 in PBS. Fixed CDMs were then stained overnight in 4 °C with rabbit anti-Collagen 1α1 (1:500; A16891; ABclonal, Woburn, MA). After a 3× PBS wash DyLight 488 conjugated goat anti-rabbit IgG (1:500; 35552, ThermoFisher Scientific, Waltham, MA), DRAQ7(1:500; D15106, Invitrogen, Waltham, MA) and DyLight 550 conjugated phalloidin (1:500; A22283, ThermoFisher Scientific) were added overnight. Samples were then mounted on a glass slide with Gelvatol and imaged with Leica TCS SPE-II laser scanning confocal microscope with an oil immersion 40X (Leica, Buffalo Grove, IL). All experiments were conducted in triplicate.

### 2.3.5 Quantification of Matrix Structure

Confocal images of CDM samples (IMR90, hCK and NIH3T3) were analyzed. Analysis was performed on both individual image tiles as well as stitched regions of approximated 618 × 618 $\mu m^2$. Stitching was performed using previously published phase correlation methods.[60] Fiber thickness, length, and straightness analysis was performed using Curve Lab 2.1.2 and custom scripts using ridgelet and curvelet multiscale transforms.[61,62] Line segment tracings were characterized to have a minimum length and maximum width of 10 and 5 pixels as depicted in Figure 2.1B. The orientation of each individual traced segment was measured in degrees; this directional data was statistically quantified using circular statistics.[63] Analysis of cellular and fibril layering using custom MATLAB scrips can be seen in the appendix.

### 2.3.6 Matrix Solubilization

Previously harvested CDM or TDM was lyophilized at 0.120 mBar and -86 °C (FreeZone Plus 6; Labconco Co., Kansas City, MO) (CDH gelation process depicted in Figure 2.1C). The lyophilized CDM was resuspended without homogenization. Lyophilized TDM was homogenized under liquid nitrogen in a pre-cooled (-80°C) mortar and pestle. Crosslinked CDM and TDM samples were enzymatically digested in 1 mg/mL of pepsin for every 10 mg of dry mass in 0.1% glacial acetic acid and 0.025N HCl at a pH ~2. Samples that did not require crosslinking were adjusted to 1 mg/mL of pepsin for every 6.55 mgs of dry mass. The solution was continuously stirred at room temperature for 48-96 h until fully solubilized. The newly solubilized CDM solution was neutralized to pH 7.4 using 0.1 N

NaOH and subsequently diluted to the desired concentration using 10× PBS and distilled water. Finally, solutions are allowed to hydrolyze and gel by incubating at 37°C for 2-5 h. Crosslinked samples were gelled using a 10% w/v transglutaminase (SKU 1201; Modernist Pantry, Eliot, ME) solution is added at a 1:1 ratio of gelation volume and incubated overnight.

### 2.3.7 Protein, GAG, and Collagen Quantification

For overall protein, previously digested samples were quantified using a DC Protein Assay (Bio-Rad, Hercules, CA) per manufacturer protocol. The standard curve (bovine serum albumin) was prepared in the digestion solution. Glycosaminoglycan content was analyzed using a dimethyl methylene blue (DMMB) assay. 16 mg of 1,9-Dimethyl-Methylene Blue zinc chloride double salt (341088, Sigma-Aldrich, Darmstadt, Germany), 3.04 g glycine, 1.6 g NaCl was dissolved with 95 mL of 0.1 M acetic acid in a total volume of 1 L as previously described.[64] Absorbance measurements were taken at wavelengths of 525 nm using a SpectraMax M2 UV-Vis Spectrophotometer (Molecular Devices, San Jose, CA). A standard curve was created using chondroitin sulfate in a digestion solution of 1 mg/mL pepsin in 0.1% glacial acetic acid and 0.025N HCl. Using previously digested samples, collagen content was quantified per Collagen Assay Kit manufacturer protocol (MAK322; Sigma-Aldrich, MO) measured at $\lambda_{ex}$ = 375/$\lambda_{em}$ = 465 nm using a spectrophotometer. The assay was repeated three times with independent samples in triplicate.

### 2.3.8 Alcian Blue Staining

CDM cultured on APTES functionalized glass coverslips were decellularized prior to Alcian blue staining. Preparations of 5 mg/mL rat tail collagen gel was used as a control. Gelled rat tail collagen controls were flattened at a concentration of 5 mg/ml using a previously published plastic compression method.[65] Excess liquid was expelled by compressing gelled collagen within a porous layer. The presence of acidic polysaccharides was measured using Alcian blue staining. Briefly, samples were washed with 0.1% glacial acetic acid (3 min) prior to 30 min incubation in a 1% Alcian blue (33864-99-2; Thermo Scientific Chemicals,) solution of 0.1N HCl (pH = 1). Samples were then rinsed with deionized water. Stained samples were subsequently mounted on a glass slide with Gelvatol. IMR90, NIH3T3, and hCK samples were stained and imaged in triplicate.

### 2.3.9 Turbidity Kinetics

The gel solution was neutralized on ice at 4 °C and immediately placed into a 48 well plate (200 μL/well). The plate was transferred to a SpectraMax M2 UV-Vis Spectrophotometer (Molecular Devices, San Jose, CA) preheated to 37 °C, and absorbance was measured at 405 nm every minute for 2 hours. Absorbance was normalized and used to calculate gelation metrics as previously discribed.[66–68] The lag phase, $t_{lag}$, calculated by extrapolating the onset of the linear portion of the curve. The time to reach 50% and 95% maximum absorbance; denoted as $t_{1/2}$ and $t_{95}$. The turbidimetric speed, S, of gelation was determined by calculating the growth portion slope of the curve normalized to max absorbance.

### 2.3.10 Gelation Controls

Rat tail collagen controls were established using a previously published method.[69] Briefly, isolated rat-tail collagen was chemically treated with acetone, 70% isopropanol and 0.1% glacial acetic acid. These rat-tail collagen type 1 isolates were later lyophilized, reconstituted, and gelled. Decellularized rabbit lung derived ECM (L-TDM) was isolated per previously published protocol.[67] This included the sequential treatments of 0.1% Triton X-100 treatment (24 h, 4 °C), 2% w/v sodium deoxycholate (24 h, 4°C), 1 M NaCl (1 h, RT), and a final DI $H_2O$ rinse. Once decellularized the L-TDM was lyophilized and processed as described above.

### 2.3.11 Cell Transfection and Transduction

Lentiviral transduction of NIH3T3s was performed in accordance with previously published work.[70,71] Lentiviral generation was completed by first transfecting HEK293TN (System Biosciences, Palo Alto, CA) cells with transfection agent *Trans*IT™-2020 (MIR5400; Mirus Bio, WI) in combination with packaging gifted from Didier Trono (psPAX2; Addgene plasmid #12260; http://n2t.net/addgene:12260 RRID:Addgene_12260, Addgene, MA), envelope also gifted from Didier Trono (pMD2.G; Addgene plasmid # 12259; http://n2t.net/addgene:12259 RRID:Addgene_12259), and transfer gift from Mariano Viapiano[71] (FL-fibulin-3-V5-lentiviral-GFP; Addgene plasmid #29703 http://n2t.net/addgene:29703 RRID:Addgene_29703) plasmid at a mass ratio of 1.00:0.30:1.05 (package:envelope:transfer). Cells were incubated for 72 h before viral media was harvested, centrifuged at 1000×*g* for 10 minutes, and filtered (0.22 μm, ThermoFisher

Scientific). The viral supernatant was transferred to a culture of NIH3T3, which were incubated in viral media for 24-48 h before CDM production.

### 2.3.12 Tensile Testing

Parental and fn-GFP NIH3T3 were cultured in 90mm APTES functionalized glass petri dishes similar to above. Live cultures were coated with 4% w/v gelatin solution to stabilize the ECM and carefully scraped off glass with a cell scraper while keeping the ECM intact. Then CDM was submerged in PBS for 10 min in an incubated shaker (SHKE4450; Thermo Scientific) at 40 °C and 120 RPM to remove gelatin. Replicates of parental and fn-GFP NIH3T3 cultures respectively were extracted and kept hydrated in PBS until mounting on 3D printed clamps with sandpaper (samples covered ≥50% of sandpaper) using ethyl cyanoacrylate glue (Krazy Glue, Atlanta, GA) to prevent slippage. Tensile testing was conducted with a vertical Tensile Tester (1103013-01A, Test Resources, Minnesota, USA) with P/Q Series Operator (firmware version 0.3Q) and Xy software (version 4.00.10). When mounting, actuator heads were slowly jogged apart to remove slack and the starting position ($L_0$) was designated. Tensile forces were measured with an actuator-mounted 0.5 N transducer (model ULC-0.5N, Interface, USA). A preload of 0.0 mN with a strain rate of 127.00 mm/min was employed until failure. Software outputs for time, load, and actuator displacement were exported for analysis. The exported sample displacement was used to calculate strain against the sample length; measured with calipers. Stress was calculated using the cross-sectional area of rolled up CDM lamellae; measured using calipers. Mechanical properties were extrapolated from the stress strain curves as follows: the toe region was selected at the initial slope increase, the elastic endpoint selected as the last of the

linear region, the plastic after yielding where the rate of straining is no longer linear and finally the ultimate tensile strength being the maximum stress that the CDM samples withstood.

## 2.4 Results

### 2.4.1 Generation of multilayer cell-derived matrices using variable cell types

Stromal fibroblasts from human lung (IMR90), cornea (hCK), and mouse immortalized embryonic fibroblasts (NIH3T3) were induced to deposit extracellular matrix over a 5-week period. The resultant CDM lamella produced from adherent 2D monolayers is qualitatively consistent with prior reports in this field.[14,16–18,38] At 5 weeks, cells and deposited matrices were fixed, stained and imaged under confocal microscopy (Figure 2.2A). This imaging format allows for a volumetric evaluation of the cellular population embedded in CDM. Custom MATLAB algorithms implement watershedding techniques to reveal multilayered arrangements based on segmented trends within the cell's distribution. Indeed, NIH3T3s average $4.\overline{66} \pm 0.58$ distinct layers while IMR90s and hCK specify strata at values of $4 \pm 1.73$ and $7 \pm 1$ respectively (each with a sample size of n=3) (Figure 2.2B). Interestingly, low passage primary hCK produced matrices with significantly more cell layers than that of IMR90 and NIH3T3 cultures (ANOVA followed by Tukey's HSD; $p = 0.0498$).

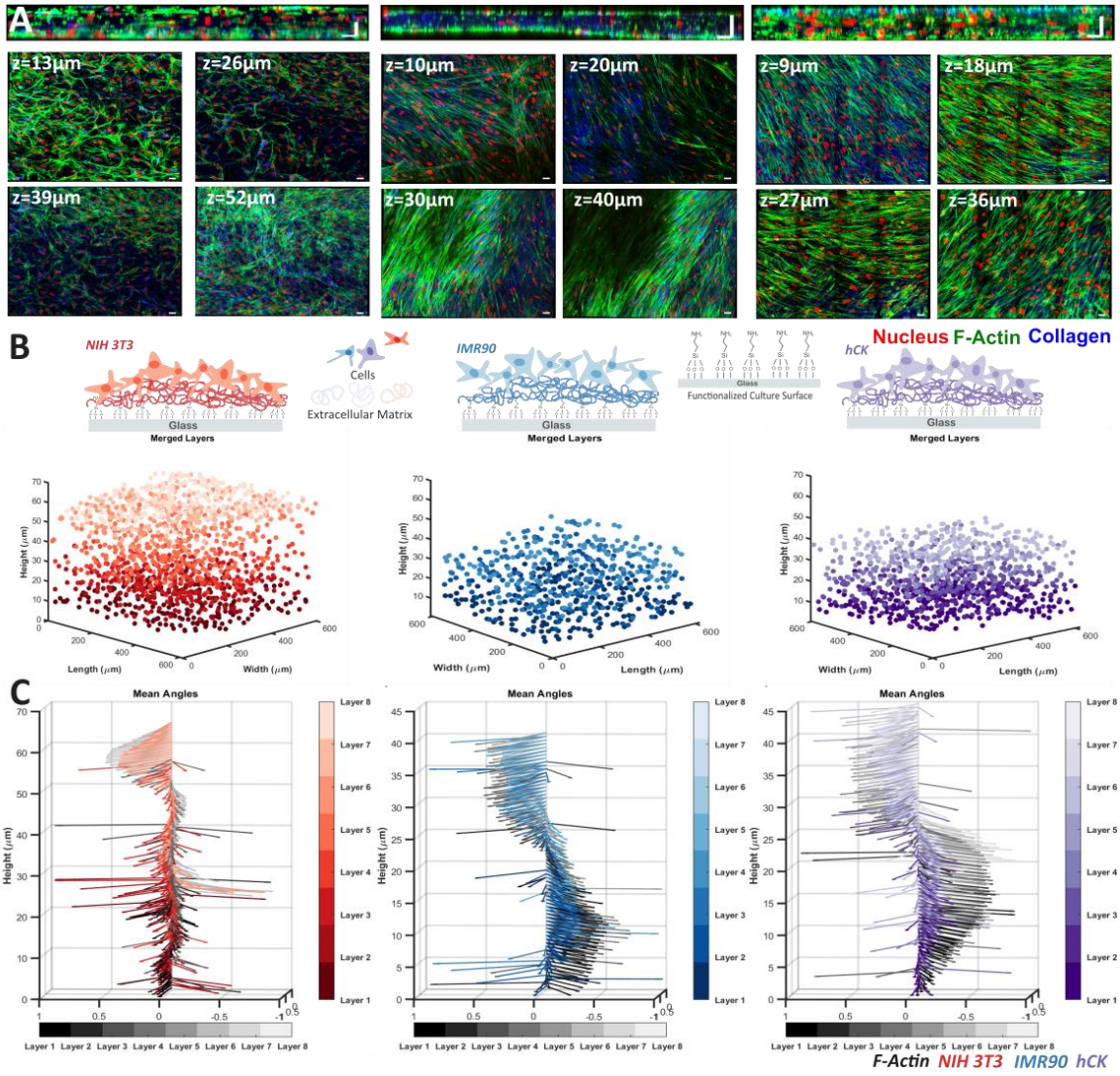



Figure 2.2: Self-Assembled CDM Architecture. A) Confocal images of CDM cross-sectional area and XZ orthogonal view. Scalebar 25 µm in white; z-values also in µm. B) Cartoon depiction of CDM culture method used for 5-week *in vitro* culture. Volumetric rendering of cell nuclei separated by cell layers – illustrating the precise location of cells imbedded within dense tissue. C). An expositional quiver plot revealing fibril and filamentous actin orientations throughout tissue bulk. Separated by layers that are labeled with color bars.

### 2.4.2 Collagen Type 1 Fibrils and Cellular Filamentous Actin Are Strongly Aligned in CDM

We applied curvelet-based image processing to both stained collagen type 1 fibril bundles and cellular filamentous actin.[73] Further analysis of these tissue artifacts reveals a snake like pattern is prevalent throughout the CDM lamella (Figure 2.2C). Wherein, F-actin appears to be acting as the leading strand at the inflection points of each woven pattern formed with deposited collagen type 1a1. Indeed, based on Pearson correlation coefficient a strong association is measured among the curvelet distributions of cell filaments and their deposited matrix. R values include 0.853±0.0754, 0.9065±0.0099 and 0.8999±0.0586 for NIH3T3, IMR90 and hCK respectively.

### 2.4.3 Minimal Variation of Collagen Fibril Morphology Across Diverse CDM Tissue Types

Tracking bundled collagen fibrils allows for analysis of trends in length, width, and straightness throughout these deposited tissue lamellae (Figure 2.3A). With all 3 CDM tissue types there are no statistically significant differences in these properties. However the distribution of IMR90 fibrils width has a wider interquartile range at $p = 0.028$; likewise, the cell density throughout tissue culture IMR90 remains the lowest of all three groups. Meanwhile, hCKs and NIH3T3 CDMs seem to have less variability in length and width. Finally, the CDM lamellas express literature relevant thicknesses of 33.61 μm ± 21.15 (NIH3T3 $n = 5$), 20.62 μm ± 12.18 (IMR90 $n = 7$) and 36.79 μm ± 25.93 (hCK $n = 6$) (Figure 2.3B). Regardless of cell type there was no significant variation ($p = 0.3$).

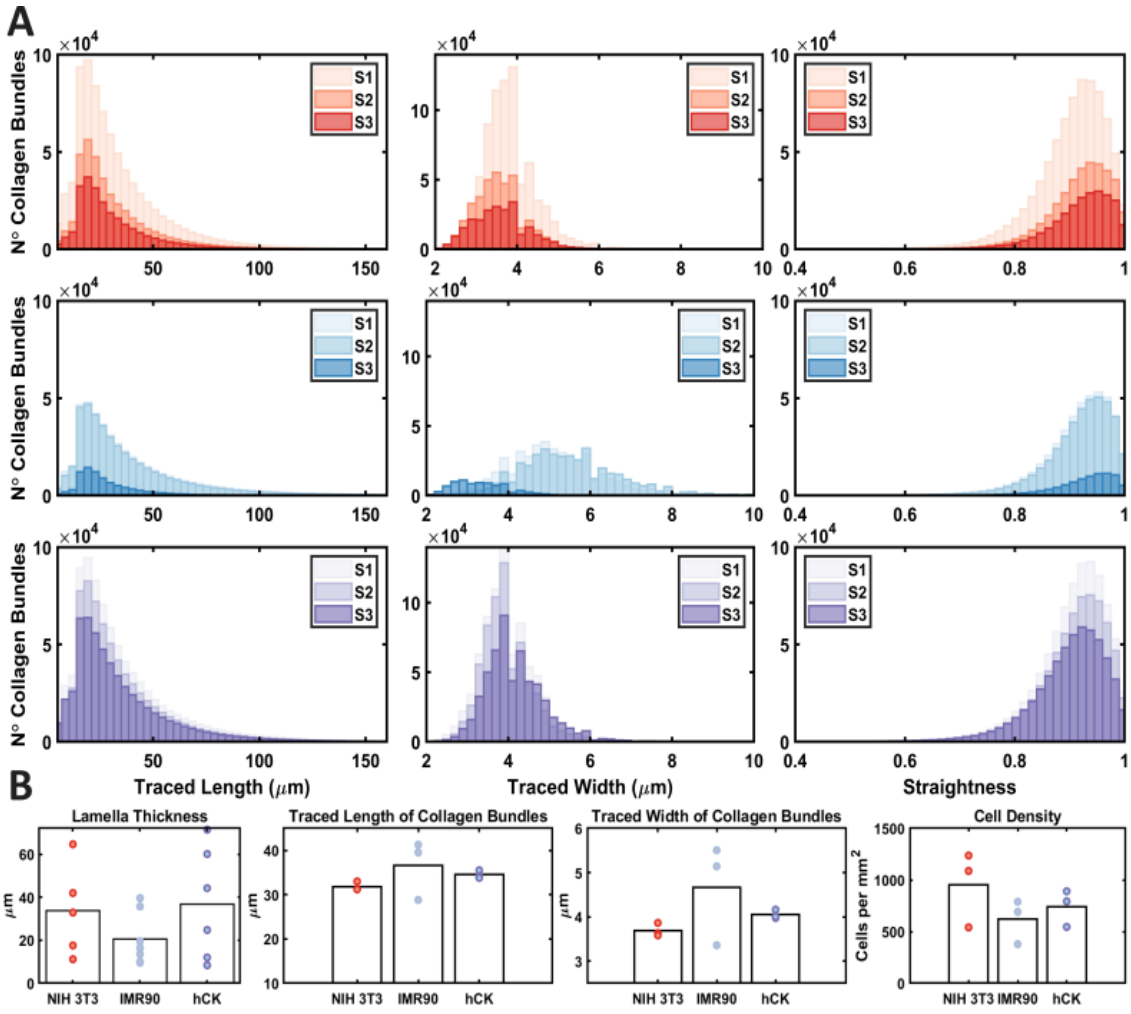



Figure 2.3: Traced Fibril Bundle Distributions: A) Histograms of the number of bundled collagen fibrils and their respective length, width and straightens. NIH 3T3 distributions in orange, IMR90 in blue and hCK in purple. B) Bar graphs of CDM lamella thicknesses, and average fibril lengths, fibril widths and cell density in culture.

### 2.4.4 CDMs demonstrate tensile strength, genetic enhancements and stackable layering construction

A key advantage of CDMs in contrast to TDMs as a biomaterial is the capability for customization. To this end, fibulin tagged with GFP viral loads were expressed in NIH3T3 CDM to produce stromal tissue rich in this basal GAG protein. Further, we tested the tensile properties of CDM from fibulin-GFP expressing and parental (unmodified) NIH3T3s (Figure 2.4). We observed no significant differences between the CDMs, suggesting this type of modification does not result in any gross defects. We demonstrate the CDM lamellae are amenable to these techniques.

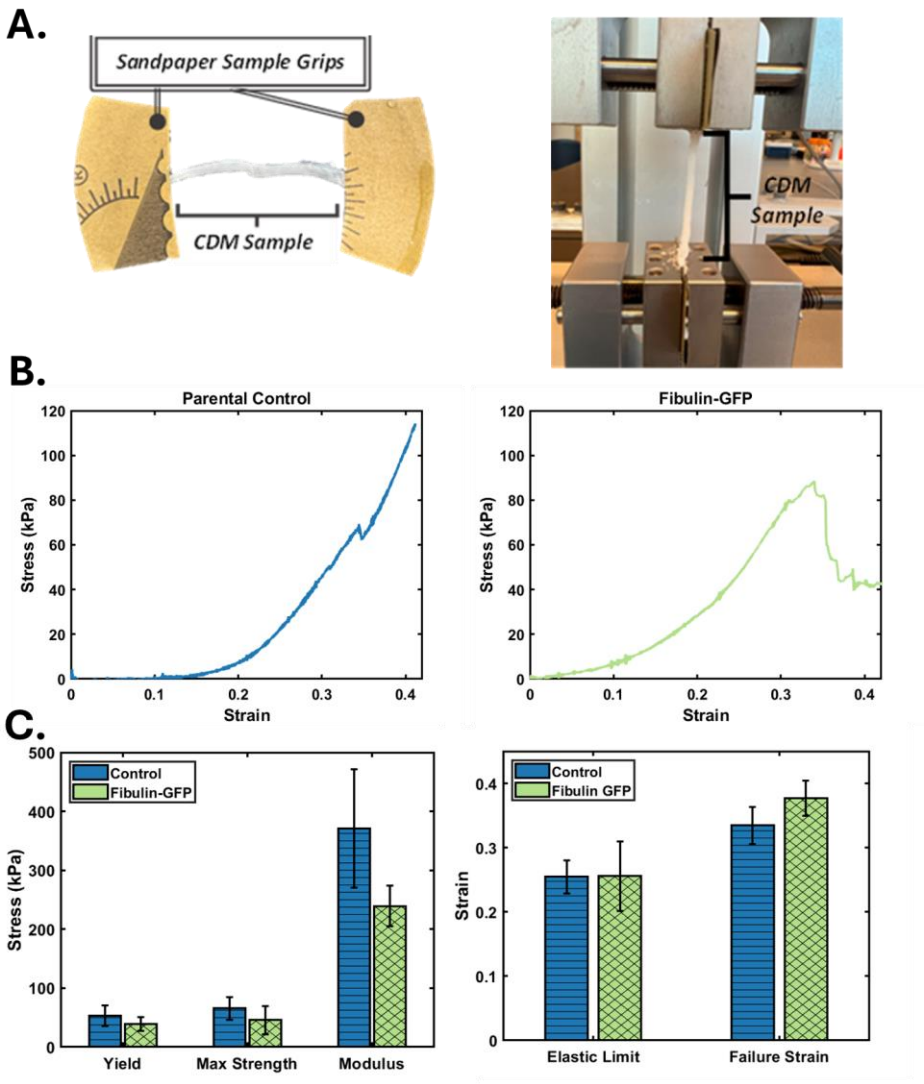



Figure 2.4: Tensile Tested Properties of CDM. A) Shows the sample mounting of our rolled up CDM samples with both ends sandwiched between sandpaper before mounting on sample clamps. B) Representative stress strain curves of our parental control NIH 3T3 CDM (n = 6) and NIH 3T3 CDM transduced to express Fibulin-GFP (n = 5). C) Compared mechanical properties including the Yield and Ultimate Tensile Strength, Youngs Modulus, Elastic Limit, and Failure Strain with error bars.

### 2.4.5 GAGs are retained after decellularization, and Protein are retained after Solubilization

Alcian Blue staining was performed to determine the extent of sulfation of mucins in CDM tissues (Figure 2.5A). Viable acidic polysaccharides content was determined in CDM after decellularization localizing to fibers of the tissue. Protein, collagen and DMMB assays were conducted as a quantitative measure of ground substance composition with decellularized rabbit lung tissue as an *in-situ* TDM equivalent. CDM dry mass was obtained via decellularization of 2D-CDM cultures then freeze dry lyophilization. These harvested CDMs had dry weights of 2.8mgs (NIH3T3 n = 5), 1.8mgs (IMR90 n = 3), and 1.8 mgs (hCK n = 8) per 100 $cm^2$ (Supplemental Figure 2.S.1). Harvested NIH3T3 and hCK dry mass very significantly at a p-value of 0.036. Finally, when solubilizing bulk dry weights at ranges of 25-35 mgs per ml protein retention compared to decellularized rabbit lung tissue does not vary statistically with a measured retention of 43% of harvested rabbit lung, 42%, 52% and 46% for 3T3, IMR90 and hCK respectively (Figure 2.5B). GAG retention was measured against Chondroitin with TDM samples having a statistically higher retention of solubilized chondroitin compared to CDM; results indicate that solubilized solutions contain 2.7% Chondroitin GAGs for TDM and 0.8%, 1.3% and 1.3% for NIH3T3, IMR90 and hCK CDM samples respectively. Finally, solubilized collagen in solution did not vary and was measurable at 5.8%, 5.9%, 5.8% and 3.7% for TDM, NIH3T3, IMR90 and hCK CDM respectively.

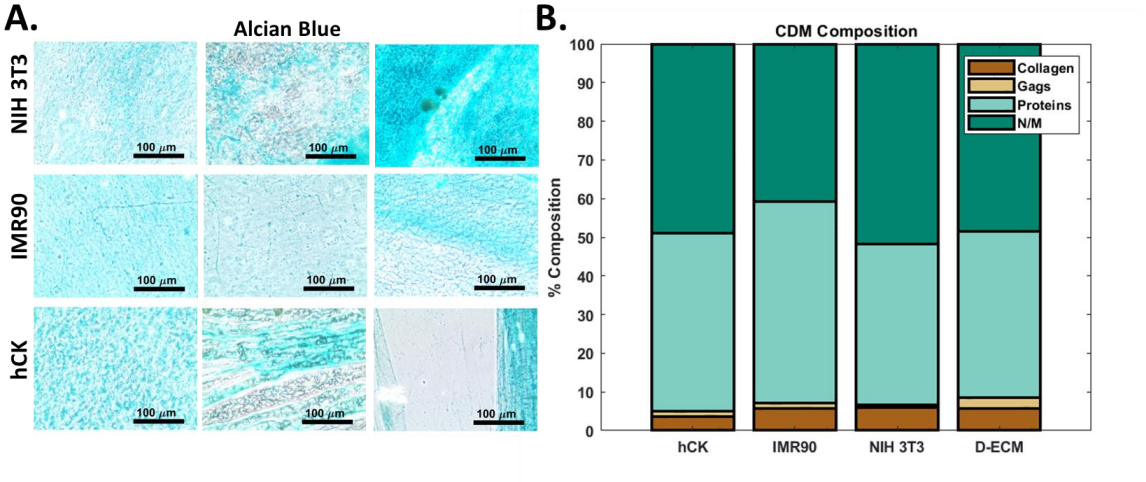



Figure 2.5: Protein Composition after Decellularization. A) NIH3T3, IMR90 and hCK express sulfonated GAGs retention with alcian blue staining; scalebar 100 μm. B) Comparative bar graph of collagen, protein and chondroitin GAGs measured w/v% composition in solubilization solution.

### 2.4.6 CDMs can be scaled to provide customized Cell Derived Hydrogels (CDH)

Using the previously published standards we were able to gel CDH at 1mg/ml of pepsin for every 10mgs of CDM. However, gelation was inconsistent (for both CDH and TDH) and in order to get 100% gelation we crosslinked with TG. We were able to obtain consistent gelation without additional crosslinkers by increasing CDM w/v% and pepsin concentrations. Cytocompatibility tests confirm that both methods have viability above 80% and gelation without the use of additional crosslinkers had consistently higher cellular retention ($p = 0.03$) (Figure 2.6). Gelation kinetics for these samples could then be measured via spectrophotometry. We find that hydrogels derived from corneal keratocytes take longer to gel effecting $T_{lag}$ ($p = 0.0005$), $T_{1/2}$ ($p = 0.0001$), and $T_{95\%}$ ($p = 0.0001$) while culture derived lung tissue hydrogels takes less time to gelation compared to both hCK and rat tail collagen ($p = 0.0001$) (Figure 2.7A-C). The turbidimetric speed, S-value, of cell derived lung

hydrogels is also higher than that of tissue derived lung hydrogels; in addition, rat tail collagen hydrogels are also significantly higher than lung TDHs ($p > 0.0001$) (Figure 2.7D). Representative gels and gelation curves with these labeled metrics can be seen in Figure 2.7E-J.

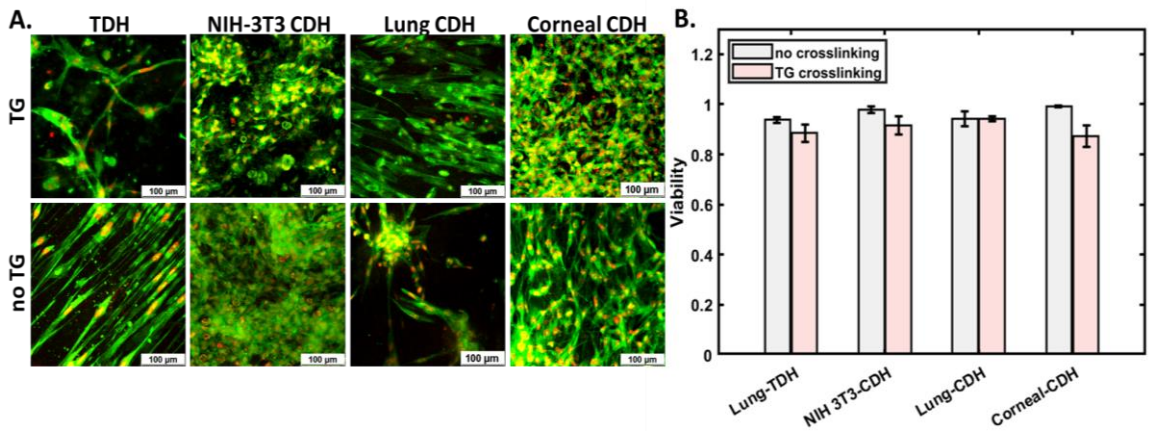



Figure 2.6: TDH and CDH Cell Viability. A) Confocal imaging of cell morphology of lung IMR90, NIH 3T3, and hCKs on their respective lung TDH, lung CDH, NIH 3T3 derived CDH and hCK CDH that produced the matrix hydrogel with TG crosslinking and without TG. Scalebar 100 µm. B) Cytocompatibility results with and without TG crosslinking for each tissue type.

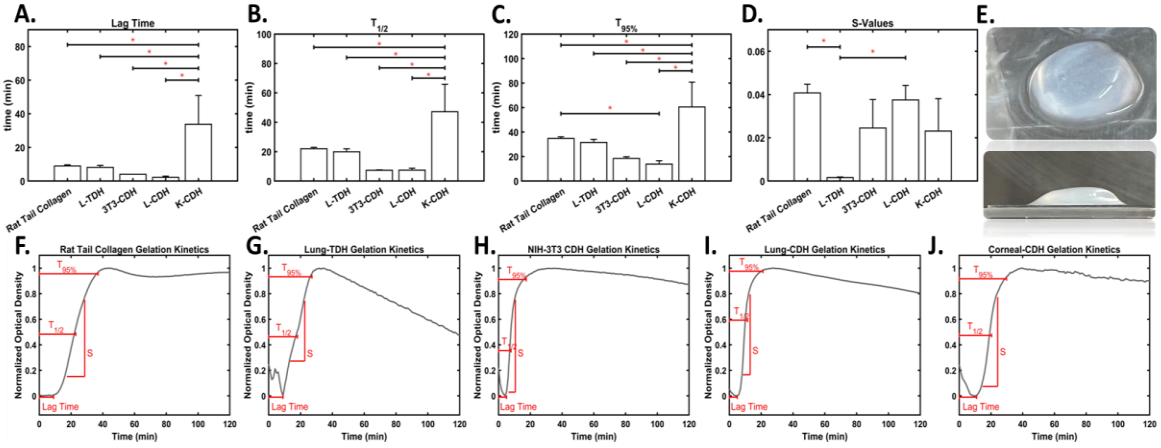



Figure 2.7: TDH verses CDH Gelation Kinetics for Rat tail collagen control (n=13), lung TDH (n=15), Lung CDH (n=6), NIH 3T3 (n=3), hCK CDH (n=4). Measured via spectrophotometry at 405nm. A) the lag phase or initiation time to gelation B) time to reach 50% of maximum absorbance. C) Time to reach 95% maximum absorbance. D) The turbidimetric speed, S, or the slope of the linear portion of the curve. E) Image of gelled hCK-CDH sample birds eye view and cross-sectional view. F) Example curve and with gelation metrics labeling of rat tail collagen control, G) Lung-TDH, H) NIH-3T3 CDH, I) Lung-CDH, and J) hCK-CDH.

## 2.5 Discussion

In this study we demonstrate a straightforward and reproducible protocol for the *in vitro* generation of workable cell specific CDM. We quantify CDM structure and macromolecular composition of three cell types, including generally available NIH3T3 and IMR90 cells. Further, we demonstrate robust gelation of CDM from multiple cell types and its biocompatibility as a culture material.

Since early demonstrations of CDM,[58,74] the technology has been considered as a potential biomaterial for grafting, scaffolding, and *in vitro* tissue models. While techniques and utilized cell types vary,[36] 2D CDM deposition is one of the most accessible and widely used methods for tissue engineering ECM.[75] For this reason, we focus on quantifying the structure and function of 2D CDM deposition from multiple stromal cells including human primary cells (corneal keratocytes) and more commonly available IMR90 and NIH3T3 cells. For CDM scaffolding, a key parameter of CDM is overall thickness; recently published protocols show 2-7 week cultures produce CDM with observed thicknesses ranging from 2-20 μm.[39,72] In our studies, we find the lower range of thickness across all three cell types is consistent with these protocols and can be substantially thicker with an upper range of ~80 μm. These findings are more consistent with early CDM studies on porous membranes, with ~125 μm thicknesses or ~395 μm utilizing chemically defined media.[74]

A common component of our work and prior studies is ascorbic acid, which is a well-established precursor for collagen synthesis and deposition.[76,77] Further studies have revealed ascorbic acid activates mitochondria thus affecting cell proliferation and metabolism with results demonstrating a more efficient preparation of cells over extended cultures.[77,78] The importance of ascorbic acid motivated the increased dosing throughout the 3-5 week culture

period. We further introduced TGF-β2 which is well understood to strongly drive ECM synthesis.[59,79,80] With the interest of further development of resilient tissue we noted that the CDM material yield is consistent with previously published increases with TGFβ.[81]

Given the overall thickness of our CDM, we wished to determine the localization of the cells, more specifically, if cells were distributed throughout or limited to the top or bottom of the CDM. Analysis of confocal images revealed a layered phenotype, with apparent cell sheets stacked vertically. While a time dependent growth study was not conducted, this is consistent with a layered vertical growth of ECM, with each layer providing a substrate for the one above. In our studies, we utilized curvelet-based analysis of collagen morphology. Research shows collagen fibers present a cord-like shape 1-20 μm wide of closely packed fibrils with interwoven lengths of 1-45 μm.[7,82–84] Importantly, our results are consistent with this and show a unimodal distribution of fiber thickness across all conditions. In tissue, collagen fibril bundle diameter distribution can be either unimodal or bimodal depending on tissue function, with unimodal distribution indicative of a more mature fibrillogensis.[85]

Collagenous tissues typically exhibit high tensile strength, and their fibril diameter distribution is proportional to resistance to plastic deformation; i.e. tissues with larger fibril diameters tend to withstand higher stresses.[85,86] Further, in loose connective tissue, intermolecular covalent crosslinks join these collagen fibrils both axially and laterally providing cushion and resilience. These interactions are dependent on the fibril specific alignment and spacing maintained by GAGs.[52,85] Indeed, studies show that at low stress levels fibrils exhibit a D-period crimp that allows fibers to move freely and prevent plastic deformation and fiber rupture.[46,85] Thereby, the orientation of collagen fibrils closest to the direction of applied stress are able to compensate for increased tensile strength; some fibers

even turn to the direction of stress.[46] This property leads to a larger and more variable toe region,[85] consistent with those seen in our tensile tested tissues (Supplemental Figure 2.S.2).

These studies demonstrated effective CDM generation from multiple cell types, including both primary cells and commonly available immortalized cells such as NIH3T3s. In overall composition, measured protein, GAGs, and collagen amount were comparable among the CDM regardless of source, although chondroitin GAGs were significantly reduced in CDM compared to decellularized rabbit lung tissue. Alcian Blue staining was able to validate a wide distribution of sulfonated GAGs throughout the tissue. Unaddressed in this study is the expression patterns of specific GAGs in the different cell-type CDMs; we would expect different cell populations to secrete distinct patterns of extracellular proteins including GAGs.

As the CDM field evolves from research to product production, removing influences in age, source, and resilience of cells allows for more control of CDMs composition. While primary or stem cell sources may provide improved physiological relevance, many applications may benefit from the increased consistency and flexibility of immortalized cells to generate specific CDM types. As a proof of concept we transduced NIH3T3s to deposit GFP expressing fibulin into the ECM, demonstrating the potential to create designer CDMs utilizing transgenic matrix proteins.

Harvesting, homogenizing, and lyophilizing these tissues allows for easy storage and delivery as a dry mass. Prior studies have used powdered ECM for its bioinductive properties.[87–90] The further solubilization and gelation of CDM into CDH allows for even broader use. There are limited prior reports of CDM gelation,[48,49] and no demonstrations with multiple cell types, as shown here. Further, gelation has been found to be inconsistent and

various techniques have been used to strengthen gels with the use of genipin, collagen 1 and fibrin.[48] These samples also contain additional proteins, GAGs, and salts which may hinder gelation. Here, we demonstrate gelation through both TG crosslinking and by self-assembly without TG crosslinking. Absent TG, we observe gelation at concentrations of ~25 mg/mL of CDM. This is consistent with the gelation of collagen, ideally performed at concentrations ≥1 mg/mL,[91] considering that collagens are approximately 5% of our CDMs. The average gelation time across all tissue types was approximately 30 min, which is similar to previous reports of 32 min,[48] and within a range acceptable for research use. While it's not clear exactly why gelation rates are slower for some CDH samples our findings indicate that the lag phase initiation is more limiting than the actual rate of gelation once begun, consistent with prior studies on pepsin treated samples.[92] More time to gelation has been shown to be consistent with increase in pepsin digestion times;[67] although we kept digestion time consistent, some samples may have inhibited pepsin activity. Studies postulate that an increase in GAG content could play a factor in steric hindrance, slowing gelation, but more work needs to be done to confirm this.[66,67]

In summary, we were able to demonstrate the creation of CDM lamella from multiple cell sources, including human primary cells. We further quantified the cellular and fibril organization to provide insight on the *in vitro* architecture of this widely used and easily scalable culture system. We were further able to quantify lamella mechanics (tensile strength and elastic modulus) and the biochemistry (overall protein, collagen, and GAG composition). Beyond the workability and versatility of this reproduceable tissue we've established that it is amendable to genetic modification through the use of transgenic cells. Finally, the translation of CDM to CDH for each of these cell types is the first of their kind; we establish

a method for decellularization, lyophilization and reconstitution that is consistent, reproducible and cytocompatible. We expect that these contributions to the bio-fabrication of CDM and CDH biomaterials will encourage a deeper understanding of the *in vitro* tissue self-assembly for the advancement of customizable tissue matrices and hydrogels.

## 2.6 Supplemental Materials

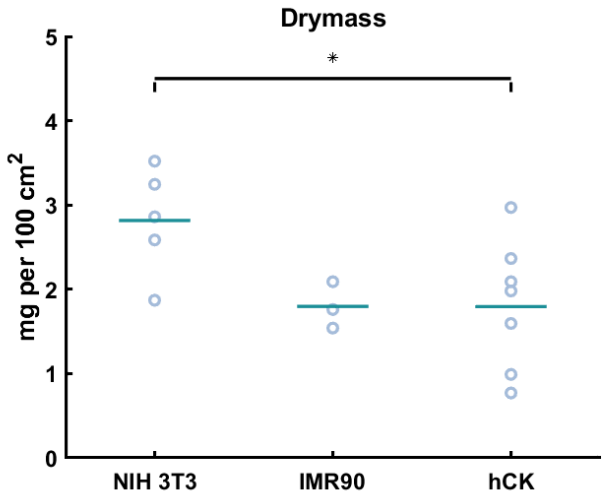
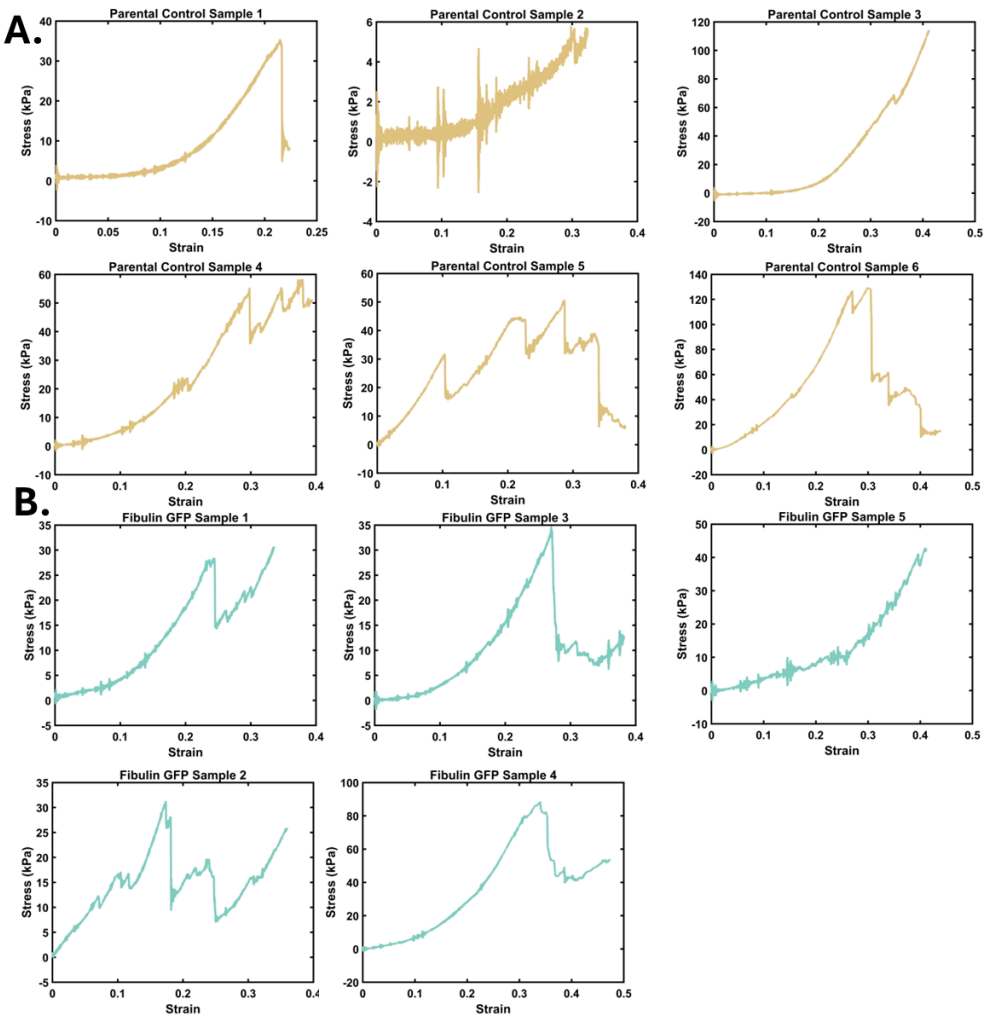



Figure 2.S.1: Harvested CDM Drymasses. Measured CDM dry weight in mgs per 100 cm2 after decellularization and lyophilization ($p > 0.0364$).




Supplemental Figure 2.S.2: Stress Strain Curves of All Tensile Tested Samples. A) is the control NIH 3T3 CDM samples and B) is the Fibulin-GFP transduced NIH 3T3's CDM samples.

# Chapter 3

# A Physiologically Relevant 3D Bio-Printed Cornea Using a Novel Cell Derived Hydrogel

## 3.1 Abstract

The aim of this work is to reproduce a corneal stroma analog using novel engineering methods to trigger tissue remodeling and mimic the development of the highly organized nature of the stromal matrix; it is not to provide clinically available transplantable tissue but to gain a better understanding of bioengineered tissue assembly. We utilized primary human corneal keratocytes (hCK) to produce cell-derived matrix (CDM) in vitro that possesses both collagenous and glycosaminoglycan components of the native tissue for use as the first studied cell derived hydrogel (CDH) bioink component in 3D bioprinting. Bioengineered corneal equivalents (BCE) were printed with a rat tail collagen and alginate based bioink (control) or with additional hCK-CDH; BCEs were assessed for post print viability and hCK morphology. In all cases, hCKs exhibited expected viabilities post bioprinting (62.4±4.7% rabbit-control 66.5±4.8% rabbit-CDH 70.5±3.4% human-control 72.6±4.5% human-CDH). BCEs printed with hCK-CDH enriched bioink exhibited increased spreading and

alignment with the local print orientation. Finally, as a precursor to future in vivo work, we assess cell viability of primary rabbit keratocytes in an ex vivo rabbit transplantation study. Overall, these findings demonstrate that bioinks enriched hCK-CDH improve cell phenotype in BCEs and encourage further study in the development of substitutes for corneal allografts.

## 3.2 Introduction

There is a pressing need for corneal transplant tissue, as corneal blindness is increasingly prevalent on a global scale. Globally, ~5 million people have bilateral corneal blindness, with another ~23 million with unilateral blindness.[93] Donor tissues remain the primary treatment, however, less than 190,000 transplants are performed worldwide due to shortage of transplantable corneas; waiting-list data show that ~12.7 million people are awaiting transplantations.[94] A bioengineered cornea would represent an alternative supply; however, the unique biochemical and structural makeup of the cornea has hindered development.

The unique structure of the corneal stroma enhances functionality. The cornea is a transparent tissue predominantly composed of a highly organized collagen lattice.[95] The regular spacing and alignment of collagen lattice is key to light transmittance, structural integrity, water retention and homeostasis. The human corneal stroma is composed of highly organized tissue with 200-250 distinct flattened lamella (layers) leading to an overall thickness of roughly 500 μm. Each lamella is aligned and rotated approximately 90° from neighboring lamella. Spacing is regulated through incorporation of specific glycosaminoglycans (GAGs) coating each collagen fibril. Corneal keratocytes maintain functionality and restore it after damage. The unique matrix of the cornea is maintained by a

network of quiescent corneal keratocytes (CKs) which form a "corkscrew" throughout the cornea.[96,97] In healthy tissue, the cells provide an organizational role for the collagen lattice through specialized fenestrations that space and orient the fibers.[97] In response to damage, corneal cells release TGFβ and PDGF, triggering differentiation of CKs to myofibroblasts,[98] which deposit fresh matrix into the wound. As the wound heals, IL1α/β levels increase, triggering apoptosis and clearance of the myofibroblasts.[99,100] The remaining cells revert to the quiescent phenotype, remodeling the matrix and restoring functionality.[101]

This research develops a novel approach to producing a bioengineered corneal equivalent (BCE) as a first step to providing a transplantable tissue supply. Many models have been tested for the use of exogenous materials (i.e. silk, chitin, collagen-chitosan hydrogels, fibrin-agarose hydrogels, and polyacrylic acid hydrogels), which can result in inflammation at the graft site.[102] As a result, natural cell-based models have emerged. Prior work by Zieske and colleagues has demonstrated a collagen and cell based 3D corneal construct built on the principle of self-assembly as a model to study physiological processes.[103,104] Despite interest in developing a transplantable BCE, as of yet there are no successful demonstrations in humans, although initial animal tests have been conducted.[102,103,105,106] Tissue derived hydrogels (TDH) (i.e. hydrogels derived from decellularized xenograft tissue) has shown promise due to their native biochemical composition, however, multiple corneas are needed for hydrogel formation[33,51,107] and animal studies of these models are limited.[108] . Our design takes a novel approach to tissue engineering corneal substitutes by using scalable ECM production to produce a novel CDH substrate for 3D tissue production.

Three major challenges when developing BCEs include ensuring (1) adequate matching of the *in vivo* layered collagen lattice; (2) the preferential cellular organization of a viable population of CKs; and (3) the unique mix of collagen and GAGs required for tissue functionality. To address these, we use bioprinting to recreate an aligned[109] and lamellar corneal structure, incorporate CK-derived matrices as a bioink to ensure the presence of relevant GAGs, and "hijack" the native corneal wound healing process for the development of embedded CKs. This work highlights our BCEs potential contributions as future substitutes for grafting purposes that could advance technological gaps in tissue supply.

## 3.3 Materials and Methods

### 3.3.1 Corneal Keratocyte (CK) Isolation

Primary corneal keratocytes (CKs) were isolated from human donor corneoscleral rims deemed unsuitable for transplant (Saving Sight, St. Louis, MO). Whole rabbit ocular globes (Animal Technologies, Tyler, TX) were also obtained and excised at the corneoscleral rim for CK isolation. Corneas were isolated at the limbal region using surgical scissors the tear film was removed samples then placed in a 5 mM EDTA and 1.2 u/L protease solution at 4 °C overnight. Then as depicted in Figure 1A-E the epithelial and endothelial layers were removed with the use of a cell scraper. The remaining stromal tissue was cut into ~1 mm cubes and incubated for one week in a culture media blend containing a base of 70% MCDB 131 (CM034-050; genDEPOT, Baker, TX) and 30% DMEM/F12 with 7% FBS, 35 µg/mL bovine pituitary extract, 5 µg/mL insulin, 5 ng/µL epithelial growth factor, and 0.5 µg/mL hydrocortisone; cells which migrated from the tissues were trypsinized and expanded. All

primary cultures were maintained in the above media blend and used between passages 2 and 11.

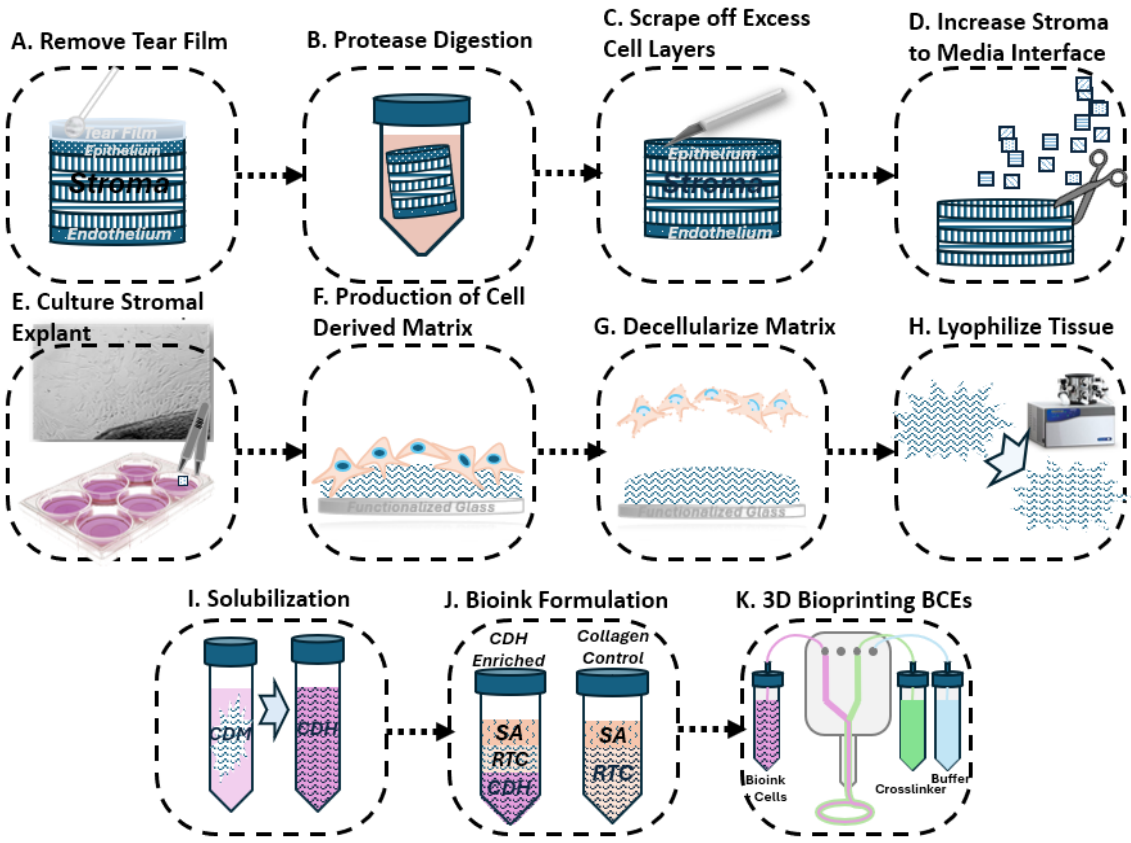



Figure 3.1 Workflow from cellular isolation to BCE production. This schematic depicts the isolation process such that A) - C) the stroma is isolated and D) stromal explants are cut to 1mm cubes. In E) stromal cells migrate onto cell culture dish for expansion. F) is the CDM production process on APTES functionalized glass so that during the decellularization wash process in G) the matrix remains adherent to the glass and is easily harvested. H) is the lyophilization of isolated CDM while I) is the solubilization to a cell derived hydrogel (CDH) and J) is the bioink formulation in combination with sodium alginate (SA) and rat tail collagen type I (RCT). Finally, K) a diagram of the pneumatic pressure-based extrusion system used for 3D bioprinting.

### 3.3.2 RT-qPCR

Following each week and at a 5-week endpoint CDM production cells were lysis and total RNA was extracted using the GeneJET RNA Purification Kit in accordance with the manufacturer's instructions (K0702, Thermo Fisher Scientific, Waltham, MA). The concentration and purity of the RNA were assessed using a SpectraMax M2 UV-Vis Spectrophotometer (Molecular Devices, San Jose, CA) by measuring the optical density values at 260 and 280 nm. For each sample, quantitative PCR (qPCR) was conducted in triplicate. As per the manufacturer's guidelines (Biomolecular Systems, Upper Coomera, Australia), 40 ng reactions were carried out in a total volume of 10 μL according to manufacturer instructions (SensiFAST SYBR® No-ROX One-Step Mix, Meridian Bioscience, Memphis, TN). GAPDH expression was used as an internal control, successful amplification of a primer pair was marked as positive expression. Melting curves were checked for single peaks. Changes in mRNA expression over the time course study was determined relative to RLPL0 expression at week 2 using the ΔΔCT method.

| Primers | Forward | Reverse | Reference |
|---|---|---|---|
| GAPDH | acagtcagccgcatcttctt | acgaccaaatccgttgactc | |
| RPLP0 | tggtcatccagcaggtgttcga | acagacactggcaacattgcgg | |
| PDGFRα | aactgatcccgagactcctg | ccgcacctctacaacaaaatg | [110] |
| VEGF | agtggtgaagttcatggatgtc | tgctctatctttctttggtctg | [111] |
| Decorin | tgctgttgacaatggctctc | gccttttggtgttgtgtcc | [112] |
| Lumican | tgagctggatctgtcctataa | atcttgcagaagctctttatg | [113] |
| Keratocan | caaacctcagactgagacac | atagacctgcctcacacttc | [114] |
| Collagen 1a1 | gagagcatgaccgatggatt | ccttcttgaggttgccagtc | [115] |
| Collagen 3a1 | ggtgctcggggtaatgacg | tccagggaatccggcagtt | [116] |

Table 3.1 Table of qPCR Primers their forward and reverse sequences as well as relevant citations.

### 3.3.3 Bioink Formulation

Previously published keratocyte cell derived hydrogels (CDHs) were used to enrich bioinks (Chapter 2). Briefly, hCKs were cultured for 5 weeks to produce cell derived matrix (CDM). CDM was decellularized, lyophilized, and solubilized at a concentration of ~1.77 mg/mL to enrich an AGC-10 Matrix Bioink (Aspect Biosystems) as depicted in Figure 1F-K. AGC-10 Matrix is a two-part bioink material containing 1.5% w/w alginate in Part A and 3.2 mg/mL collagen in Part B. Bioink controls contained AGC-10 matrix bioink with no additional CDH. Corneal prints were ~1.5 mL and ~3.2 million cells; cell density is based on human cornea.[117]

### 3.3.4 3D Bio-Printing Parameters

The corneal equivalent was printed as a cylinder with a 16 mm diameter and 4 mm height at an infill of 40%. A perimeter of 3 concentric lines with an estimated line width of 0.11 mm was printed at a speed of 20 mm/s and variable extrusion pressure of ~100-200 mBar. The calcium chloride crosslinker solution (Aspect Biosystems) extrusion pressure was ~80-110 mBar and a saline buffer solution's extrusion pressure was 60 mBar. Each layer was deposited with a layer height of ~0.3 mm and width ~0.15 mm. A repeated sequence of (1) a 0° rectilinear pattern with a speed of 9 mm/s followed by (2) a concentric spiral at print speed 8 mm/s and (3) another rectilinear pattern with a speed of 9 mm/s at 90° was achieved.

### 3.3.5 Wound Healing Activation Method

hCK BCEs were grown for an extended period of 5 weeks with varying serum, vitamin, growth factor and chemokine concentrations to mimic the wound healing and tissue repair response. For this protocol hCKs were cultured in the previously described media blend. Supplemental components were diluted to reduce serum and growth factor use and were adjusted weekly for the first three weeks. These include 1, 0.5 and 0.1 μg/ml TGF-β2 (Weeks 1, 2, 3, respectively), 10%, 5%, 2% FBS (Weeks 1, 2, 3, respectively), and 100, 200, 300 μg/mL of ascorbic acid (Weeks 1, 2, 3, respectively). 100 pg/mL IL-1α was added for the fourth week of culture. Media was changed every 2 to 3 days for 5 weeks to reach a serum and transforming growth factor free culture by week 4.

### 3.3.6 Post Print Processing

After at least 1 week of culture samples were then subjected to unconfined compression by applying a 100 g load for 8 min per previously published protocol.[65,118] Briefly, BCEs were plastically compressed (PC) between layers of nylon plastic (307 mesh size) and stainless steel (60 mesh size) meshes as depicted in Figure 2. Liquid expelled from the BCE during compression was wicked into the filter paper base. This reduced BCE thickness and increased density. The resulting corneal constructs were transferred to a 6 well plate and maintained in culture until transplantation and viability testing.

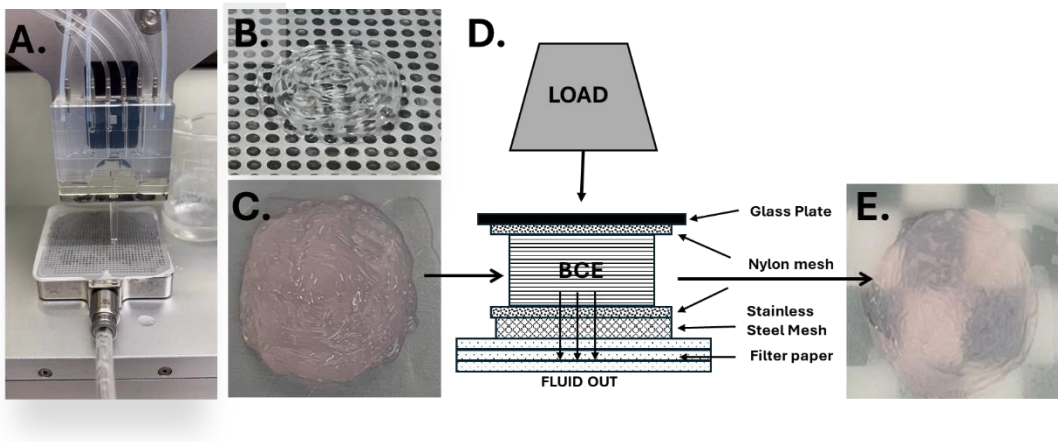



Figure 3.2 Post Print Processing. A) the 3D bioprinting system of our BCE. B) BCE directly after bioprinting. C) After 1 week in culture. D) A schematic of the apparatus used for plastic compression of BCEs for liquid expulsion. E) Post compression transparency of our BCEs.

### 3.3.7 Ocular Globe Dissection and *Ex vivo* Transplantation

Whole rabbit ocular globes (Animal Technologies, Tyler, TX) were used as a proxy tissue for transplantation. Sterile surgical clamp forceps were used to grip back excess tissue and expose cornea with adequate pressure. 2-4 surface incisions on the anterior region of the eye between tissue and visible iris were made. The anterior stroma was gently separated from the posterior stroma using blunt dissection. Microdissection scissors were used to extend incisions, allowing the anterior cornea to be removed. Anterior corneas were maintained in culture and used as transplantation controls. The corneoscleral rim was then isolated from the posterior globe using surgical scissors and maintained in culture until transplantations were conducted (3-5 days); the remaining ocular tissue was discarded. Partial corneal transplantations were conducted by applying surgical grade glue dropwise along the edges of the isolated corneoscleral rims with the anterior central cornea removed; BCEs or anterior

cornea controls were immediately adhered. Glue was allowed to dry for 5 minutes before transplants were cultured for an additional 7 days.

### 3.3.8 Viability Assays

Live dead viability staining was conducted one week after printing, prior to transplantation (2.5 weeks post print) and 14 days after transplantation. To determine cell viability after bioprinting BCEs were reacted with 2 mM calcein AM and 4 mM ethidium homodimer for 30 min per manufacturer protocol (30002; Biotium, Fremont, CA) and imaged under confocal (Leica, Buffalo Grove, IL) at 10× magnification.

### 3.3.9 Immunofluorescent Staining

After 5 weeks in culture BCEs were fixed with 4% paraformaldehyde/0.05% Triton X-100 in PBS. Fixed BCEs were then stained overnight in 4 °C with fluorescent-dye conjugated draq7(1:500; D15106, Invitrogen, Waltham, MA) and phalloidin (1:500; A22283, Thermo Fisher Scientific, Waltham, MA). Samples imaged with Leica TCS SPE-II laser scanning confocal microscope.

### 3.3.10 Cellular Circular Formation Analysis

BCEs were imaged at a cross-sectional diameter of the cylinder using a tile scanning method. Using custom MATLAB (R2022b; Version: 9.13.0 MathWorks Inc, Natick, Massachusetts) scrips and circular statistics toolbox[63] each individual tile scan was arranged in a maximum intensity projection and circularity was calculated as an approximation to the maximum likelihood estimate (MLE) of the concentration parameter kappa (κ) of the von Mises distribution ($1/\kappa$ is equivalent to the variance, $\sigma^2$, of a normal distribution).

## 3.4 Results

### 3.4.1 Testing of CDH-enriched Bioink for 3D Bio-Printed Corneal Equivalent

In this work, we take a novel approach to creating BCE utilizing bio-ink enriched with hCK-CDH. We have previously shown that decellularized CDM produced *in vitro* contains similar protein compositions to decellularized xenograft matrices isolated from *in vivo* tissue (Chapter 2). We then further established a protocol for solubilization and gelation of CDM into CDH that exhibits cytological compatibility and gelation times consistent with hydrogels previously used in microfluidic devices. However, to gain a better understanding of relevant matrix gene expression throughout the 5-week culture a time course and endpoint analysis of RT-qPCR was conducted (Supplemental Figure 3.S.1). These findings confirm the expression of GAGs necessary for corneal function (keratocan and lumican) including transparency and deturgescence.[119–121] With attenuated expression of decorin which can disrupt collagen fibril structure and organization.[122] Wound remodeling constituents such as collagen 3, VEGF and PDGFβ were also expressed during the CDM production process.[100,110,111,123] After this five-week endpoint culture, the harvested cornea specific CDM was lyophilized; the resulting dry mass was then successfully solubilized to generate the CDH pre-gel solution that was used to enrich a standard bioink blend of rat tail collagen type I and sodium alginate.

### 3.4.2 Physiologically Relevant Construction of 3D Printed BCE

Our print design is based on X-ray data of Meek and Boote (2004) (Figure 3.3 B&C) in which a circularly symmetrical increase in tissue organization occurs with radial distancing outside the central optical zone of the cornea (7-8mm), and aligned tissue contours were focused across the peripheral cornea in a curved path (Figure 3.3 C).[124] The print perimeter in Figure 3.3 D is imitative of the limbal region that forms a discrete anulus at the central cornea;[125] this additionally provides support for the print. The print consists of alternating layers of parallel fibers and concentric fibers (Figure 3.3 D). Each parallel layer was separated by a concentric layer mimetic of the corkscrew networking of stromal cells[96,97] (Figure 3.3 A and D2). As the printhead built upward each parallel layer was rotated 90° from the prior (Figure 3.3 D3&4). A radial slice was used to visualize the symmetry between the central anulus and periphery of our BCEs; we observed the desired design in our prints (Figure 3.4).

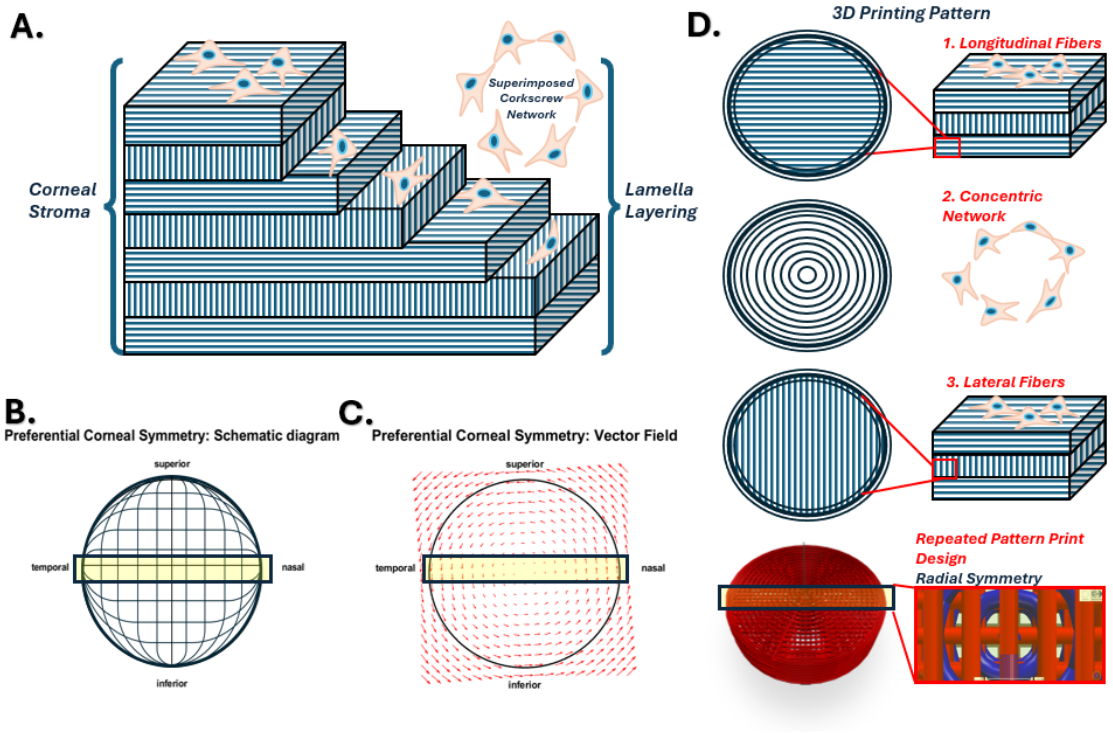



Figure 3.3 3D Physiologically Relevant Print Design. A) The architectural makeup of the corneal stroma with respect to the preferential lamella layering and superimposed keratocyte network that corkscrews within the layered lamellae. B) A schematic diagram of the preferential corneal symmetry as reported by Meek and Bone (2004). C) The scrutinized fibril assembly in the cornea as reported by Meek and Bone (2004). D) The 3D printing pattern with 1. depicting the first layer as a longitudinal pattern printed rectilinearly within the corneal cylinder then 2. depicting the second layers concentric pattern for the corkscrew network and 3 depicting the laterally aligned fibers. This pattern had a repeating infill until the desired thickness was reached and a diagram of the assemblage for 3D printing is shown.

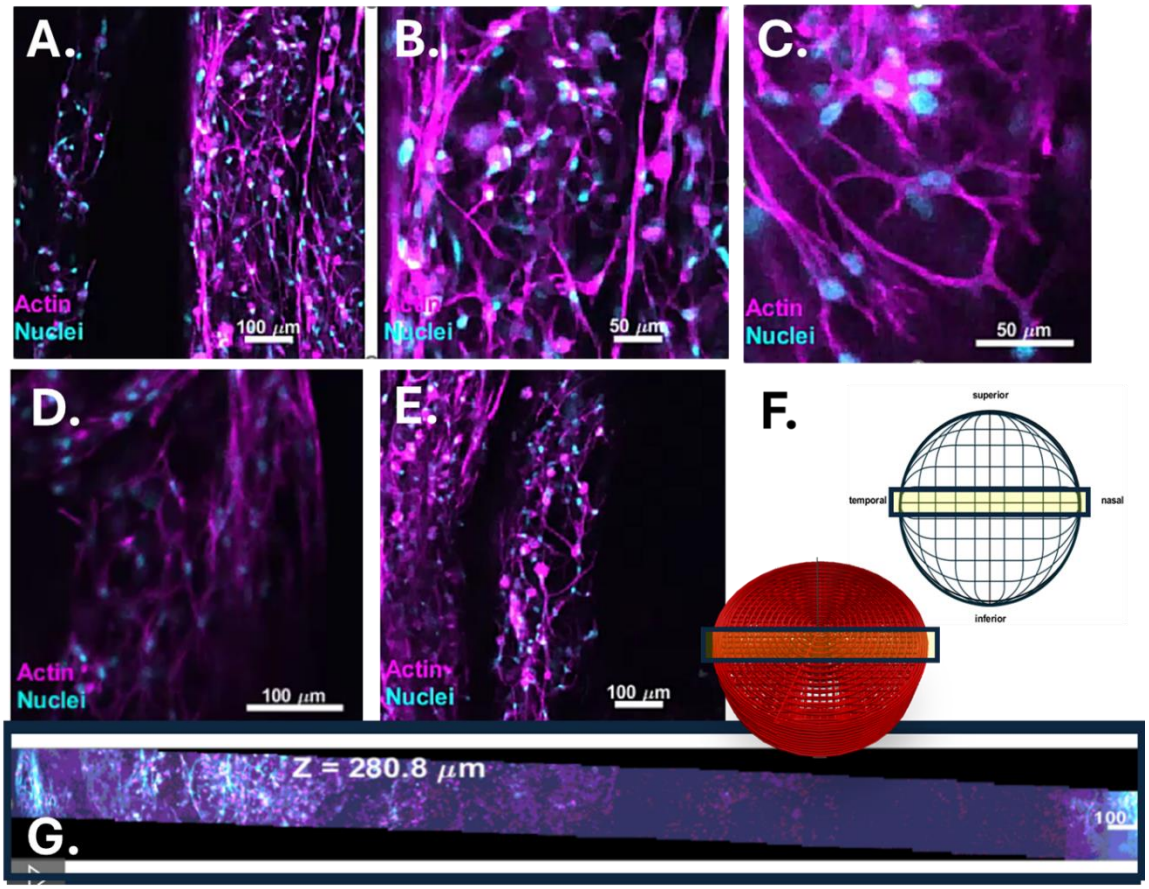



Figure 3.4 Physiologically Relevant Corneal Construction. Confocal imaging of encapsulated corneal keratocytes with nuclei in cyan and filamentous actin in magenta. A) Cell alignment along the fibril edges scalebar 100 μm and B) close-up of cell spreading scalebar 50 μm. C) Imaging of highly interconnected cells within BCE scalebar 50 μm. D and E) additional cell imaging scalebar 100 μm. F) Diagram of print scheme and highlighted radial region for imaging. G) Stitched tile scans of radial slices in BCE, scalebar 100 μm, z position of the objective throughout the thickness of the BCE with filamentous actin in cyan and actin in magenta.

### 3.4.3 Increased Cellular Assembly of hCK-CDH enriched BCEs

We also wished to assess the impact of our print design on cellular morphology. As a primary metric, we assessed the orientation of the phalloidin stain fit to a von Mises distribution. In the BCE models with hCK-CDH, we compared the distribution concentration, $\kappa$, indicated increased alignment, between the periphery and central regions (Figure 3.5). There was a statistically significant ($p = 0.0008$) increase in central $\kappa$ compared to the periphery in our hCK-CDH enriched BCEs (Figure 3.5). This contrasted our collagen controls BCEs in which the cellular organization did not vary between the periphery and central region. Morphologically both sample types express increased linearity about the periphery and have increased cell spreading after 5 weeks maturation compared to 3 weeks. Confocal imaging of samples only matured to 3 weeks had a less ubiquitous symmetry in circular assembly (Supplemental Figure 2A) and limited cell spreading (Supplemental Figure 2B and C). By inspection, hCK-CDH enriched BCEs had more visible spreading than collagen controls at 3 weeks.

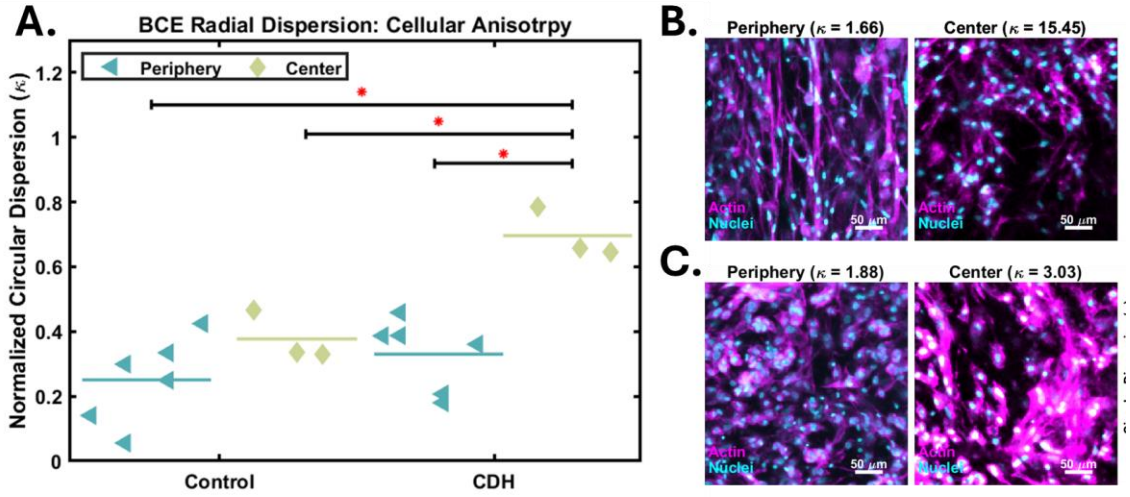



Figure 3.5 The Circularity of BCEs. A.) Preferential circular anisotropy of cells withing 3D printed BCEs. The kappa (κ) values are the circular dispersion values normalized to the mean with the green diamonds representing the average center-points of each sample and the blue triangles the leftmost and rightmost radial means. P-value = 0.0006. B.) Depicts collagen control confocal images of the leftmost and central point of a single sample and their respective kappa values. C.) Depicts confocal images and distributions of a single CDH sample respectively. Scalebar is 50 μm.

### 3.4.4 Consistent Viability of Printed Cells with Incorporated Post-Print Processing

Bioprinting associated shear stress and hydrostatic pressure are unavoidable stresses that can impact cell viability.[126] To test cell viability through the print process, cells were assayed using Live/Dead staining at 1 week post-bioprinting, for both human CKs and rabbit CKs (Figure 3.6 A). As bioink may influence viability, we compared the cell recovery of rat tail collagen control bioinks and hCK-CDH enriched bioinks. We saw no significant differences of viability between the control or hCK-CDH enriched bioinks, with overall viability between approximately 60% and 80% (Figure 3.6 B).

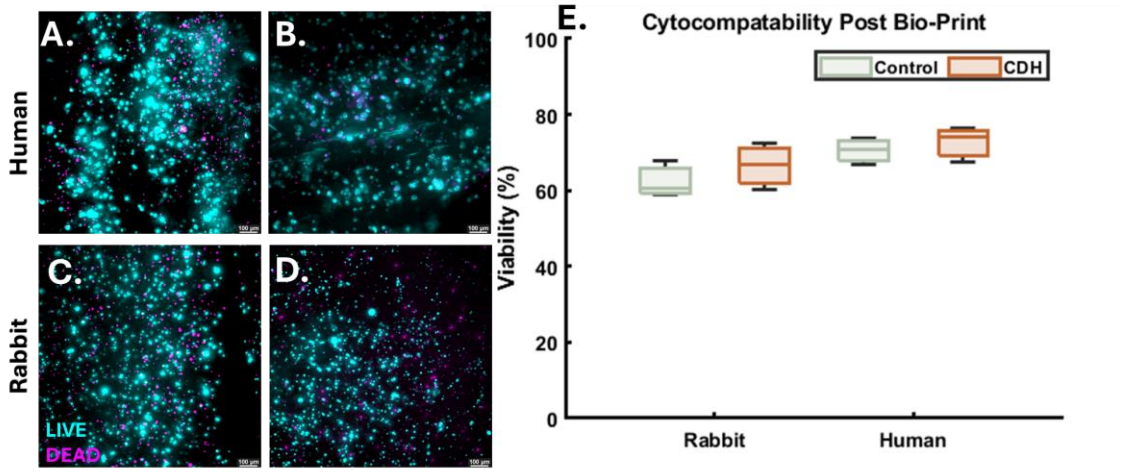



Figure 3.6 Cytocompatibility post bioprinting. A and B) Confocal imaging of 3D bio-printed BCEs with human cells collagen control based bioink in A) and CDH enriched bioink in B). C and D) Imaging of 3D bio-printed BCEs with rabbit cells collagen control based bioink in C) and CDH enriched bioink in D). Sample size n=3 for all samples except rabbit CDH n=4. Live cells in cyan and dead in magenta and scalebar 100 μm.

### 3.4.5 *Increased Viability of Transplanted BCE*

To verify the transplant-ability, cellular response, and therapeutic potential of our CDH-enriched BCEs we performed a partial thickness anterior laminar keratoplasty on rabbit ocular globes *ex vivo*. Directly after transplantation (Figure 3.7 A) explants were cultured and allowed to integrate for 14 days (Figure 3.7 B). Prior to transplantation (day 0) the viability of CDH-enriched BCE samples was confirmed to be consistent with previous results. Post-transplantation samples were cultured *ex vivo* for 14 days before assessing viability. These samples displayed an upward trend in viability after ex-vivo culture similar to those of re-transplantation controls (Figure 3.7 C).

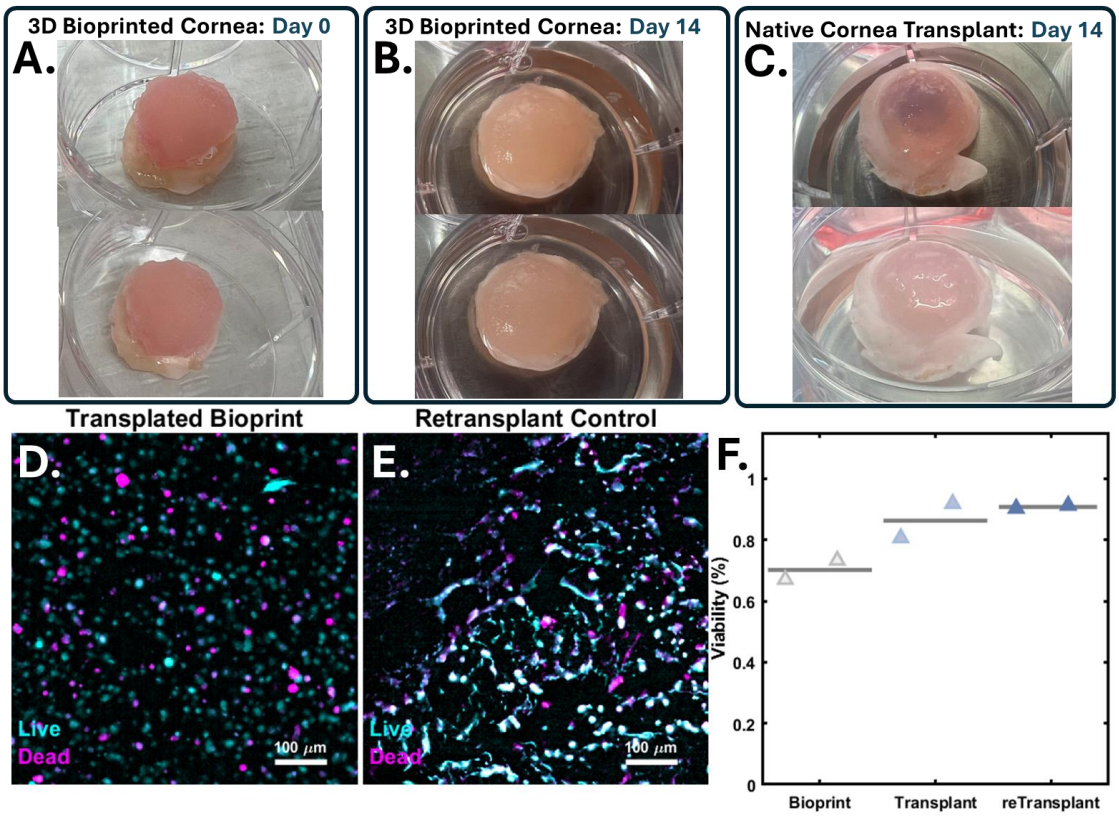



Figure 3.7 Transplantable Corneal Construct Response. A) 3D printed cornea directly after transplantation and before culture. B) 3D printed cornea 3.5 weeks in culture and 2 weeks after transplantation in ex-vivo culture. C) Re-transplant control in ex-vivo culture where cornea was dissected, then cultured for 1 week and finally retransplanted onto cornea for an additional 2 weeks culture. D) Live dead viability of transplanted bioprint. E) Live dead viability of retransplanted control. Live in cyan dead in magenta scalebar 100 μm. F) Viability analysis sample size n=2.

## 3.5 Discussion

To our knowledge, this is the first study to use cells to produce and derive extracellular matrix into a hydrogel-based bioink for 3D printing. Decellularized ECM has many advantages as a biomaterial because it mimics the composition and complexity of the native tissue microenvironment.[34] However, for cornea, the application of tissue derived ECM is limited by the constrained supply of donor corneal tissue; making it difficult to harvest sufficient ECM required for tissue applications.[107] An alternative source for ECM is *in vitro* CDM from cultured corneal keratocytes. Recent advancements in CDM production and characterization have confirmed the bioavailability of these tissue models,[35] including our recent demonstration of corneal CDM (Chapter 2).

In this study we investigate the self-assembly between cells and our novel tissue equivalent post bioprinting. In particular, we show a recapitulation of the preferential corneal and cellular architecture, consistent biocompatibility post bioprinting and a transplantation proof of concept. At a macroscopic level the corneal tissue assembly and interwoven pattern is important in maintaining shape.[124,127] Further, the keratocyte cell distribution through the stroma provides a functional intercommunicating network active during wound healing.[96,128,129] These fundamental corneal properties have potentially important tissue handling and response implications when considering the tissues inherent anisotropy and post-surgical amalgamation to the eye.[130,131] As a result, we took special care in designing the print pattern of the cornea to better match the known organization. Interleaved concentric layers were devised to mimic the “corkscrew” cellular network of the cornea.

During the extrusion-based printing processes cells are subjected to various mechanical, physical, and biological stresses that cause considerable cell damage and death.[126] Factors that have been found to effect cell viability when using pneumatic extrusion printing of cells in collagen-based matrix include: cell density, pressure, nozzle/gauge size, and bioink viscosity with their impact becoming most prevalent after at least 3 days post printing.[132] These factors in combination with printing speeds have additional effects on line width and uniformity during extrusion. Post-print, the viability of our constructs is consistent with other extrusion based robotic dispensing printheads that also employ pneumatic print systems under similar conditions.[132–134]

We place further consideration on the cellular responses to our biomimetic corneal construct. Namely, *in situ* keratocytes are not randomly distributed but "corkscrew" through the stromal thickness; further each cell is highly interconnected via cell-cell junctions that regulate corneal function.[97,135–138] However, in tissue, the cellular interface to this organizational structure is difficult to visualize with respect to the spatial organization of keratocyte networks.[139] Some studies have begun to use confocal imaging to better understand cell spreading along the Z axis.[140] With our proposed novel tissue design, we successfully recreate the orthogonally layered framework and the preferential radial anisotropy from the perimeter to center. In the cells, we show the corneal symmetry is preserved when comparing the periphery and center of our BCEs. Increasingly so when interfacing with the tissue specific matrix of our CDH enriched-bioink.

In the cornea, it is well understood that GAGs are critical for tissue function; this is especially true of the regularly spaced fibril proteins and sulfonated-GAGs that are necessary for transparency. Our previous work with CDHs confirms the presence of proteins, collagens,

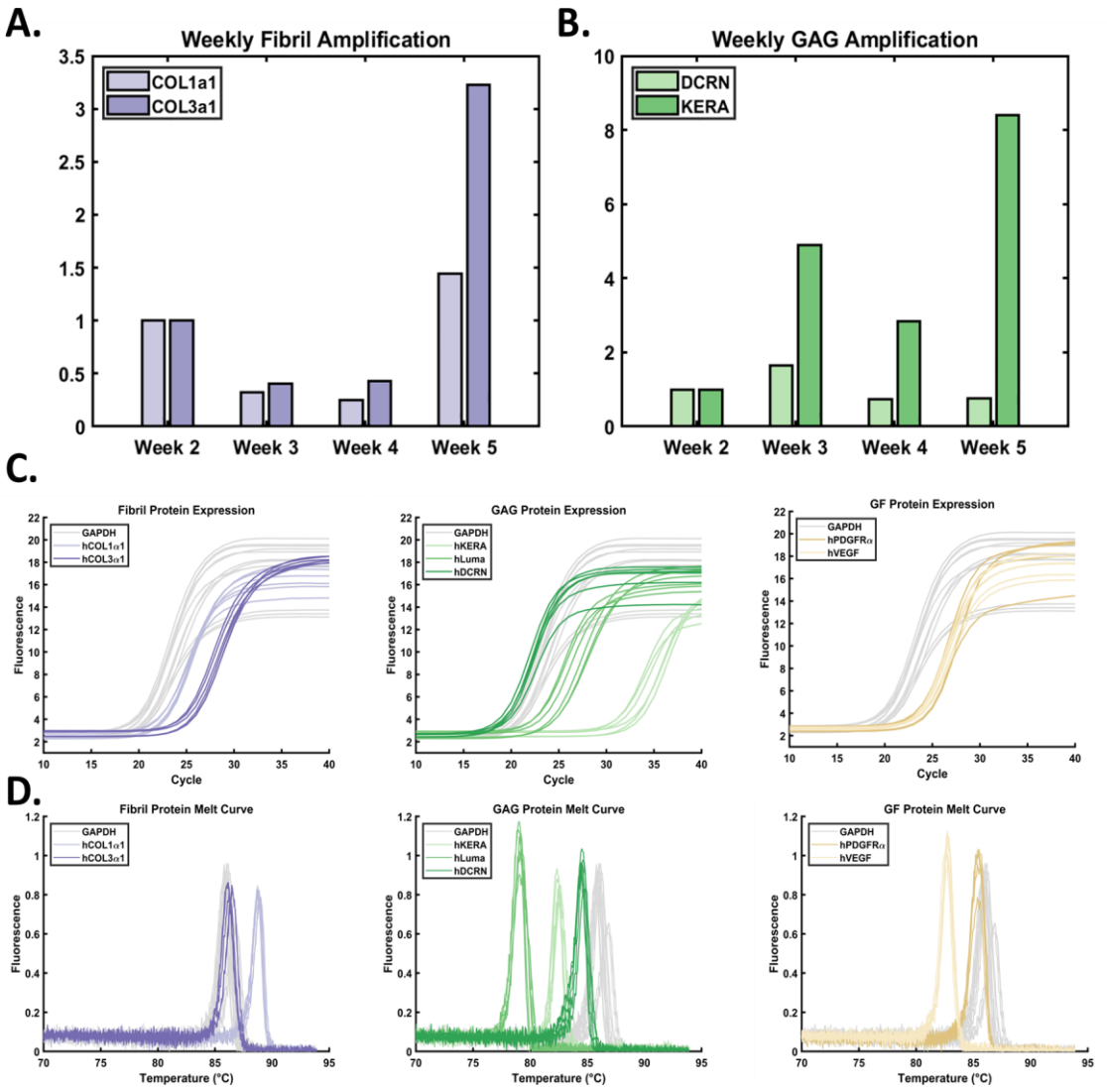
and GAGs consistent with decellularized tissue. In the current work, we further demonstrate transcript level expression of wound-associated collagen type III, decorin, VEGF and PDGF in addition to more homeostatic corneal proteins like keratocan and lumican. Several of these biomarkers have been shown to influence the outcome of corneal grafts and can in principle be used to predict graft survival.[141] While not pursued in this work, the cytokines presented during the *in vitro* matrix production process were chosen to mimic the tissue damage and repair cycle of the cornea. Further characterization of the protein expression of these important matrix cues is of relevance to both CDM based hydrogels as well as those derived from donor tissues.

In the future, as the translational use of CDH progresses special consideration will need to be taken for the activation state of the depositing cells such as: culture duration, mechanical cues and soluble proteins present in culture media. While this is still a *de novo* field, the accessibility of *in vitro* CDH allows for customization, for example with genetic modification of the cells and specialized culture conditions to tailor the properties of the engineered tissue. By dynamically regulating engineered tissue it is possible to suppress inflammatory cytokine production and promote tissue repair and regulation as a method for smart tissues with sustained drug delivery over long periods of time. For instance, recent studies demonstrate the deployment of model-based analytics for the monitoring of regulating pathways at critical divergences of immune responses as potential targeted drug deliveries.[142] Leveraged machine learning technologies have recently been developed to predict solid organ graft failure[143,144]; similar approaches could theoretically be applied develop personalized tissues to minimize donor rejection.

To achieve this level of control and specificity of CDM/CDH, work is needed to understand the matrix deposition and assembly process *in vitro*. The development and deployment of *in vitro* CDHs is very recent; to our knowledge the first demonstration of this was published in 2021.[49] Future studies on scalability and controllability of these novel materials are needed.

Presented in this study is the framework for a viable approach to 3D bioprinting tissue with customizable bioinks that can be produced in culture and cater to tissue specific needs. The scalable production of CDHs provides a cost-effective approach to hydrogels used as bioinks with the added advantage of a biologically relevant protein composition. We expect our work to advance the production of physiologically relevant tissue models for dynamic tissue repair and therapeutics.

## 3.6 Supplementary materials




Supplemental Figure 3.S.1 Corneal Specific Protein Expression. A) A time course analysis of cornea specific fibril proteins where collagen type 1 alpha 1 (COL1a1) is the prominent fibril protein of the cornea and collagen type 3 alpha 1 (Col3a1) is a wound fibril protein. Each week was normalized against week 2 measured against RPLPO (Large Ribosomal Protein) Endogenous Control. B) Corneal specific GAG keratocan (KERA) weekly amplification compared to decoran (DCRN) a wound specific GAG also normalized to week 2 under the same conditions. C) An endpoint analysis of protein expression after a 5-week CDM culture observing fibril collagens, GAGs and growth factor protein production for corneal reconstruction measured against GADPH. D) The melt curves verification of target specific amplification and fluorescent detection in the previous graphs.

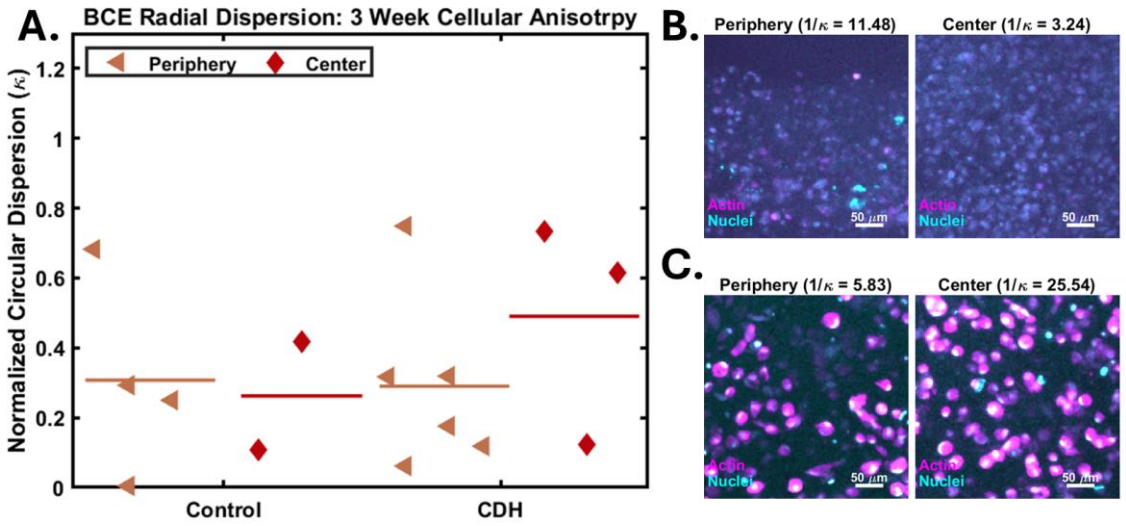



Figure 3.S.2 The Circularity of BCEs after 3 weeks in culture. A.) Preferential circular anisotropy of cells withing 3D printed BCEs. The kappa (κ) values are the circular dispersion values normalized to the mean with the red diamonds representing the average center-points of each sample and the orange triangles the leftmost and rightmost radial means. B.) Depicts collagen control confocal images of the leftmost and central point of a single sample and their respective kappa values. C.) Depicts confocal images and distributions of a single CDH sample. Scalebar is 50 μm

# Chapter 4

# Closing Statements

## 4.1 Challenges, Limitations, and Future Improvements

Due to many variations among cell types, experimental designs, and applications, identifying the best practices for CDM generation is challenging. As the field of CDM progresses more attention will need to be paid to how the matrix is deposited. More specifically the self-assembly of the ECM architecture *in vitro* as well as the variation of secreted proteins over a prolonged culture period. Better understanding and control of these processes is a critical tool for the intentional design of engineered tissue.

### 4.1.1 Scaling up Tissue Production

Determining variation in the rate at which cells deposit ECM *in vitro* stipulates the scalability and regulations optimal for streamlining production. Namely cell growth and ECM formation kinetics should be assessed so that an optimal environmental condition (i.e. stiffness, porosity, alignment, shear etc.) can be defined for adequate oxygen transfer, waste removal and nutrient selection.[145] Bioreactors and perfusion chambers are the practical choices when scaling up production to meet tissue demands.[22] However a major issue complicating the production of thick 3D constructs is the increased metabolic demands; which can become costly and hard to maintain sufficient levels in continuous cultures.[146–148]

Media demands is a major concern as studies show the more regularly media is changed (especially for crowded/confluent cultures) the more metabolic load the cells can take – increasing yields in DNA, RNA and protein synthesis.[149]

### 4.1.2 Sustainably Tackling Metabolic Demands

In line with media values is the growing demand for chemically defined medias that do not utilize non-defined animal materials (i.e. serums) and instead utilize specialized compounds, amino acids, lipids, carbohydrates, trace elements and/or vitamins to enrich protein production.[74,150,151] Indeed, providing chemically defined medias with factors like EGF,[152] TGF,[59,79] PDGF,[153] insulin[154,155] and even patented[150] specialized media blends for CDM production have shown improvements in the mechanical properties of *in vitro* tissue production. These reagents, however, can be costly. In order to combat this we have begun developing studies that genetically modify cells with an optogenetic system[114] that enables selective activation of TGF-β signaling through light patterning. We hope to circumvent the need of exogenous GFs and instead stimulate increased ECM production and remodeling with light.

### 4.1.3 Combatting Insufficient Mechanical Properties

Current CDM tissues possess an insufficient mechanical strength threshold that does not mechanically match native tissue.[35,74,156–158] We've established that certain reagents in chemically defined medias increase structural and elastic protein deposition in culture. However, in order for the tissue to mature the cells and ECM must experience the necessary forces (i.e. compression, tension and shear)[159] to develop a mechanically functional tissue. Engineering tissue with a bioreactor capable of meeting metabolic demands as well as

provide tissue-specific stretch regimes has the potential to enhance ECM and cell organization, functionality and strength.[160]

### 4.1.4 Tissue Composition Post-Decellularization

Many of these tissues are then harvested for therapeutics. Additional chemical limitations are associated with extraction methods. Denser tissues require harsh decellularization methods that strip away important biochemical components imbedded in the tissue.[41,42] What's more certain tissues, like the cornea, have a highly specific cellular network formation that is integral to tissue integrity.[161] Understanding how much of the mechanical integrity of a tissue is truly due to live cell-ECM interactions could motivate the choosing of allograft, autograft, and xenograft tissues depending on the user's needs.

### 4.1.5 The Impact of Pepsin Digestions on Gelation Properties

Reconstituting these materials into a hydrogel provides an ideal approach for many tissue engineering applications. In TDH and CDH, pepsin digestion has become a common solubilization agent for the extraction of triple helical collagen without the N- and C-terminal telopeptides.[162,163] This exposes 26-residue non-triple-helical telopeptide domains that once rehydrated form back into fibrils, which, entangle to form a hydrogel.[164] This pepsin digestion process is time-dependent in which non-collagenous proteins and glycosaminoglycans have been found to resist extraction resulting in differences in collagen cross-linkage placement.[165] This leads to gelation inconsistencies that in turn effects the resulting ECM hydrogels physical, biochemical, mechanical and biological properties.[166] As the field progresses more care will need to be placed on the concentration and rate of pepsin relative to not only collagen but ground substances in the ECM.

### 4.1.6 3D Bioprinting with CDH Bio-inks

3D bioprinting provides relative precision for tissue organization and design. The viscosity and other rheological properties of bio-inks are critical for determining printing parameters. Unfortunately, with the relative novelty of CDH these properties have not yet been characterized and are likely batch dependent. Still, we expect CDH containing bio-inks will perform similarly to others; for example, we observed increased alignment at the outer region of our printed fibers (where the most shear was applied). This is consistent with prior studies of hydrogel based bio-inks, revealing that wall shear has an impact on both collagen fiber and cellular behavior.[167,168] One such study further demonstrates the shear-induced arrangement of collagen fibrils in turn assists in the expression of keratocyte markers.[167]

### 4.1.7 Considerations for Bioinks and Crosslinkers

Many 3D printed biomaterials utilize a non-adhesive polymer such as alginate, as we did in these studies. However, these additives change the structure of the material to be more resistive to cell migration and contraction.[169] In our experiments we used sodium alginate with a $Ca^{2+}$ crosslinker and as the tissues matured alginate lyase was our removal agent. However, we found that high concentrations induced cells to quickly contract the tissue; this negatively impacted tissue integrity and size.[170] We had better success with lower concentrations over an extended period of time allowed out cells to gradually become more accustomed to these changes. An alternative approach would be to optimize the $Ca^{2+}$ of crosslinkers or the saline environment used for ion exchange, temperature and pH in order to reach the desired tensile strength, stiffness, moisture content and swelling index.[171] Finally, in the cornea the surface tissue must be smooth. However, 3D printed extrusion systems are not amenable to this unless printed directly into a gel bath.[172] Future studies will be needed to optimize and translate the work described herein.

## 4.2 Impact

Harvesting site specific ECM has immense research and therapeutic advantages in the fields of tissue engineering and regenerative medicine, which principally uses biomimetic scaffolds to repair and restore damaged tissue. Tissue extracted *in vitro*, solubilized and reconstituted as a CDH provide a fine tunable tissue specific hydrogel. Designating byproducts of these resources that facilitate the long-term storage of hydrogel constituents additionally benefits usability. We find that both the powder and the digestate are modes capable of long-term storage in the same way that TDM and TDH are.[173] This increases the bioavailability and accessibility of these products. The reconstitution of *in vitro* derived hydrogels provides a sustainable approach for tissue engineering applications such as regenerative medicine therapeutics, drug delivery systems,[174] sealants,[175] food additives,[176] transplantable tissue mediums, bio-inks, wound dressings,[177,178] and intuitive bioregulators. The primary contribution of this work is the novel demonstration of tissue-specific CDM and its application in a tissue engineered cornea. As a general tool for research or translation, tissue-specific CDM will broadly impact many biomedical fields, especially in the development of graft tissues. These advancements represent early steps to increased accessibility for tissue grafts; successfully translating these results will impact patients throughout the US and worldwide.

# Chapter 5

# Appendix

## MATLAB Analysis and Quantification

### Layered Cellular Distribution in CDM

```
ftitle = 'C:\Users\lsalmeron\Downloads\FixedAPTES_20221007_hCKp5_40x3_merge';
thrsh = 6; %published example
%ftitle = 'C:\Users\lsalmeron\Downloads\FixedAPTES_20221007_hCKp5_40x2_merge';
thrsh = 12;
%ftitle = 'C:\Users\lsalmeron\Downloads\FixedAPTES_20221007_hCKp_40x_merge';
thrsh = 12;
%ftitle = 'C:\Users\lsalmeron\Downloads\FixedAPTES_20220921_IMR90p19_40x_merge';
thrsh = 100;
%ftitle = 'C:\Users\lsalmeron\Downloads\FixedAPTES_20220923_IMR90p20_40x_merge';
thrsh = 100; %published example
%ftitle = 'C:\Users\lsalmeron\Downloads\FixedAPTES_20220923_NIH3T3_40x_merge';
thrsh = 30; %published group
%ftitle =
'C:\Users\lsalmeron\Downloads\mergedFixedAPTES_20221205_NIH3T3p00_40x_2'; thrsh
= 45;%30;
%ftitle =
'C:\Users\lsalmeron\Downloads\mergedFixedAPTES_20221205_NIH3T3p00_40x'; thrsh =
30;%30;
%ftitle = 'C:\Users\lsalmeron\Downloads\mergedFixedAPTES_20221216_IMR90p17_40x';
thrsh = 90;%20;

%load
tic
A = bfopen([ftitle '.lif']);
toc

%deinterleave
C = cat(3,A{1,1}{1:3:end-2,1});
P = cat(3,A{1,1}{2:3:end-1,1});
D = cat(3,A{1,1}{3:3:end,1});

%filter
tic;
Da = medfilt3(D,[5 5 3]); toc
Da = imtophat(Da,strel('disk',25)); toc
```

```
Db = Da>thrsh;

Dba = imopen(Db,strel('sphere',3)); toc
Dba = imclose(Dba,strel('sphere',3)); toc
Dba = imfill(Dba,'holes');
Dba = bwareaopen(Dba,2500);

ED = -bwdist(~Dba); toc
ED(~Dba) = Inf;
ED = imhmin(ED,2); %sometimes you can have 2 barely different minimas, the hmin
will suppress any small minima
Dba2 = watershed(ED); toc
Dba2(~Dba) = 0;
Dba2 = bwareaopen(Dba2,2500);

% review segmentation if needed
TEST = cat(4,Da*10,Dba2*100,Dba2*10);
sliceViewer(TEST)


%Initial Basic Stats

s = regionprops3(Dba2,'Volume',"BoundingBox","Centroid");

figure
for i = 1:length(s.BoundingBox)
    c = s.Centroid(i,:);
    b = s.BoundingBox(i,:);
    plot3([c(1) c(1)],[c(2) c(2)],[b(3) b(6)+b(3)],'r-','linewidth',2); hold on
    plot3(c(1),c(2),c(3),'b.','markersize',20)
end
title("Original Centroids and Extents")

figure
for i = 1:length(s.BoundingBox)
    c = s.Centroid(i,:);
    plot3(c(1),c(2),c(3),'b.','markersize',20); hold on
end
title("Original Centroids")

Vorig = Dba2;
Vtest = Vorig;
Vlay = {};

VlayOUT = zeros(size(Vorig),'uint8');

%set conditions for looping
Nl = 50; %increased number of layers
kl = 0;

Z = ones(size(Vorig,1),size(Vorig,2)); %initialize flexible sheet on bottom of
stack
```

```
while kl<Nl && any(Vtest,"all")

    kl = kl+1;

    %set conditions for looping
    N = 100;
    k = 0;
    temp = true(size(Z)); %need this to start loop
    [ii,jj] = find(temp);
    SE = offsetstrel('ball',11,1); %this is key parameter for controlling sheet
flex
    tic
    while k<N && any(temp(:))
        k = k+1;
        test = imerode(Z,SE);
        temp = false(size(Z));
        for i = 1:size(Vorig,1)
            for j = 1:size(Vorig,2)

                if Vtest(i,j,Z(i,j))

                elseif Z(i,j)<size(Vorig,3) && Z(i,j) <= test(i,j)+1
                    temp(i,j) = true;
                end

            end
        end
        %update Z
        Z(temp) = Z(temp)+1;

    end
    toc
    k
    Vtemp = bwselect3(Vtest,jj,ii,Z(:)); %identify nuclei touching "Z" sheet
    Vlay{kl} = Vtemp; %define volume for each layer
    Vtest(Vtemp) = false; %delete layer nuclei from test volume

    %update output volume
    for i = 1:size(Vorig,1)
        for j = 1:size(Vorig,2)
            VlayOUT(i,j,Z(i,j):end) = VlayOUT(i,j,Z(i,j):end)+1;
        end
    end

end
kl

TEST = zeros(size(Vorig),'uint8');
for il = 1:length(Vlay); TEST(Vlay{il}) = il; end
TEST(Vtest) = il+1;
figure
sliceViewer(TEST); colormap("jet"); title("Original Layers")

cl = {'b.','r.','g.','m.','c.','y.','k','b.','r.','g.','m.','c.','y.','k'};
```

```
figure
for il = 1:length(Vlay)
    s = regionprops3(Vlay{il},'Volume',"BoundingBox","Centroid");
    for i = 1:size(s.Centroid,1)
        c = s.Centroid(i,:);
        plot3(c(1),c(2),c(3),cl{il},'markersize',20); hold on
    end
end
title("Original Layers")

%merge layers if close
Vlayold = Vlay;

%collect basic info about each layer
for il = 1:length(Vlay)
    s = regionprops3(uint8(Vlay{il}),'Volume',"BoundingBox","Centroid");
    V(il) = s.Volume;
    b = s.BoundingBox;
    c = s.Centroid;
    R(il,1:2) = [b(3) b(3)+b(6)];
    Cnt(il) = c(3);
end

%identify layers less than 25% of max layer
pL = V<max(V)*0.25;
iRL = find(pL);
iKL = find(~pL);

%identify merge layers and merge layers
shiftind = 1:length(Vlay);
for il = iRL % loop over the reject layers
    RLcnt = Cnt(il);
    %identify closest keep layer to merge with
    KLdst = abs(Cnt-Cnt(il));
    KLdst(iRL) = Inf;
    [~,shiftind(il)] = min(KLdst)
    Vlay{shiftind(il)} = Vlay{shiftind(il)} | Vlay{il}; %merge the two layers

    VlayOUT(VlayOUT==il) = shiftind(il); %merge small layers into big ones
end

%clear merged layers
Vlay(iRL) = [];

%shift layer numbering as needed
for il = 1:max(VlayOUT(:))
    if ~any(VlayOUT(:)==(il+1))
        VlayOUT(VlayOUT>il) = VlayOUT(VlayOUT>il)-1;
    end
end

TEST = zeros(size(Vorig),'uint8');
for il = 1:length(Vlay); TEST(Vlay{il}) = il; end
TEST(Vtest) = il+1;
```

```
figure
sliceViewer(TEST); colormap("jet"); title("Merged Layers")


% cl = {'b.','r.','g.','m.','c.','y.','k','b.','r.','g.','m.','c.','y.','k'};
cl =
{[63,0,125]/255,[84,39,143]/255,[106,81,163]/255,[128,125,186]/255,[158,154,200]
/255,[188,189,220]/255,[218,218,235]/255,[239,237,245]/255};%purple hck
%cl =
{[8,48,107]/255,[8,81,156]/255,[33,113,181]/255,[66,146,198]/255,[107,174,214]/2
55,[158,202,225]/255,[198,219,239]/255,[222,235,247]/255};%imr90 blue
%cl =
{[103,0,13]/255,[165,15,21]/255,[203,24,29]/255,[239,59,44]/255,[251,106,74]/255
,[252,146,114]/255,[252,187,161]/255,[254,224,210]/255};%3t3 orange
map = [cl{1};cl{2};cl{3};cl{4};cl{5};cl{6};cl{7};cl{8}];
figure;
for il = 1:length(Vlay)
    s = regionprops3(Vlay{il},'Volume',"BoundingBox","Centroid");
    for i = 1:size(s.Centroid,1)
        c = s.Centroid(i,:);
        p=
plot3(c(1)*.358,c(2)*.358,c(3)*.566,'MarkerFaceColor',cl{il},'MarkerEdgeColor',c
l{il},'Marker','.','markersize',20); hold on %'MarkerFaceColor',
    end
end
title("Merged Layers")
        xlabel('Length (\mum)','FontWeight','bold')
        ylabel('Width (\mum)','FontWeight','bold')
        zlabel('Height (\mum)','FontWeight','bold')
        zlim([1,70])
        colormap(map)
        colorbar('TickLabels',{'Layer 1','Layer 2','Layer 3','Layer 4','Layer
5','Layer 6','Layer 7','Layer 8'})%'Ticks',[-5,-2,1,4,7],...
        set(gca,'LineWidth',2)

%save([ftitle '.mat'], 'Da','D','Dba2','Vorig','Vlay','VlayOUT','TEST','-v7.3');
%%
PX = 0.358/1000; PY = 0.358/1000; PZ = 0.566/1000; %correct with acount voxel
size
for i = 1:length(Vlay)
    CC = bwconncomp(Vlay{i});
    nucnum(i) = CC.NumObjects;
    vol(i) = sum(VlayOUT(:)==i) * PX * PY * PZ;
    dens(i) = nucnum(i)/vol(i);
end
dens
```

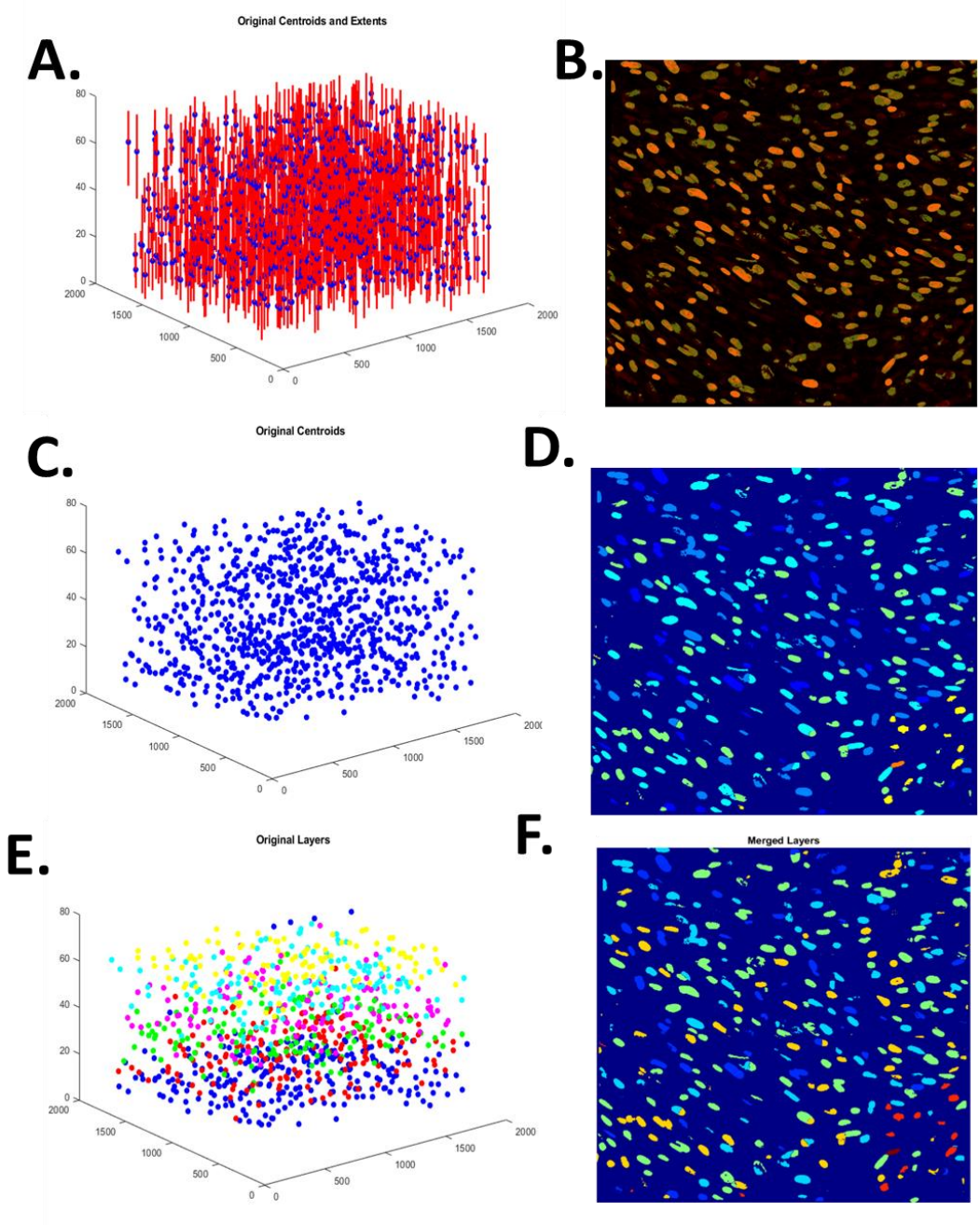



Figure 5.1 Merged Layer Distribution Breakdown. A) Binary thresholding of nuclear staining to identify centroid and extent through sample thickness in Z-axis. B) Stained nucleus confocal imaging at individual Z-slice for comparison. C) In order of code figure this is the position of the original centroid through the imaged CDM; X, Y, and Z axis units in pixels. D) Updated view of nucleus within Z-slice. Outside of plane/layer separated by color scheme. E) Color-scheme-separated nuclear centroids distributed throughout CDM. F) Finalized merged layer distribution after removing rejected layers at individual Z-slice. This information was used to create the finalized image in Figure 2.2B.

# Established Lab Protocols

## Alcian Blue Staining

### Protocol Overview

*This is a comprehensive staining protocol to visually confirm the presence of mucins (i.e. mucopolysaccharides: carbohydrates found in bone/cartilage/skin/elastic tissue). Alcian blue is a planar phthalocyanine molecule with a copper that is positively charged and will bind to acid mucins using charged interactions to stain the tissue surface. Using varying pH concentrations, one can deduce more about the tissue make up. pH 2.5 will stain most GAGs/acid mucins while pH 1 stains weakly/strongly sulphated acid mucins.*

### *1. Materials and Preliminary Preparations/Setup*

#### *Materials:*

1. ***PPE: lab coat, gloves, and laminar flow hood***
2. ***70% ethanol***
3. ***Alcian Blue***
4. ***Weigh Boat***
5. ***Scupula***
6. ***Scale***
7. ***DI water***
8. ***Glacial acetic acid***
9. ***1% glacial acetic acid***
10. ***1N HCL***
11. ***pH Strips***
12. ***Rocker***
13. ***Gloves***
14. ***vortexer***

#### *Timing and scheduling:*

*Make sure all surgical equipment and beakers are sterilized (autoclaved) before performing experiments. Perform experiments as soon as pH 1 and/or pH 2.5 staining solutions have been prepared and staining sample has been selected.*

### *Set Up instructions:*

*These experiments can be conducted in the staining bench of any Wetlab.*

## *2. Procedure*

### *Procedure Outline:*

#### *pH 2.5 Stain - 1% Alcian Blue in 3% Acetic Acid*

1. *Alcian Blue stain can be reused after multiple stains so check beforehand to be sure there is not a solution made up beforehand*
2. *to make up new solution make up 3% glacial acetic acid solution by pipetting 0.3ml of glacial acetic acid into 9.7mL of DI water*
3. *Then weigh out 100mg of alcian blue the copper in this solution makes it very static so carefully scoop out solution and transfer to weigh boat*
4. *Once weighed carefully transfer alcian blue to water it will immediately turn blue in solution*
5. *Vortex the mixture until alcian blue dissolves*
6. *Use a pH strip to confirm the pH of the solution*

#### *pH 1 Alcian Blue Solution*

7. *Add 1mL of 1 N HCL in 9mL of DI water*
8. *Carefully weigh out 100mg of Alcian blue*
9. *Transfer alcian blue into acidic solution and vortex*

#### *Staining Protocol*

10. *Rinse Isolated ECM in DI water*
11. *Add 1ml of 1% glacial acetic acid*
12. *Incubate for 3 minutes*
13. *Remove and add pH solution of Alcian blue*
14. *Stain for 30 minutes on rocker*
    - *remove staining solution after 30 minutes and return to beaker for repeated use*
15. *Rinse for 2 minutes in running tap water*
16. *Rinse for 2 minutes in DI water*
    - *Positive Stains will turn bright blue*
17. *Store tissue in PBS(+/+) with azide.*
    - *stain should last multiple months without color drop off*

# CDM Harvesting

**Protocol Overview**

*The procedure is optimized for extracellular matrix isolation by removing cellular remnants in culture. After a five-week cell culture on a functionalized surface; cellular remnants are removed via chemical treatments for the analysis of extracellular matrix components/characteristics.*

## *1.* *Materials and Preliminary Preparations/Setup*

***Materials:***

15. ***PPE: lab coat, gloves, and laminar flow hood***
16. ***70% ethanol***
17. ***Cell deposited ECM (in form of a 4 week culture on APTES functionalized surface***
18. ***PBS (+magnesium/+calcium)***
19. ***Autoclaved 50ml Beaker***
20. ***20 mM NH4OH and 0.05% triton X-100 solution in water***
21. ***Parafilm***

***Timing and scheduling:***

*Allow cells to grow on APTES functionalized surface for at least 4 weeks prior to decellularization. This will make it possible for cells to deposit ECM onto adherent surface.*

***Set Up instructions:***

*Spray laminar flow hood with 70% ethanol and wipe down surface before performing experiment. Prior to experiments make sure you have sufficient 20 mM NH4OH and 0.05% triton X-100 solution. If none is available make up molar solution of ammonium in laminar flow hood then add triton X-100 to solution.*

## *2.* *Procedure*

***Procedure Outline:***

1. *Remove cell culture dish from incubator and place in sterile biosafety cabinet.*
    a. *Make sure to wipe down surface with 70% ethanol.*
2. *Gently remove media from cell culture disk using serological pipette. Discard spent media in 50ml beaker*
    a. *Avoid using aspirator or rough pipetting in order to keep ECM intact.*
3. *Immediately after removing media gently wash dish with PBS(+/+).*
    a. *Discard PBS in the same 50ml beaker*
4. *Add ammonium/triton solution to cells*
    a. *For 90mm dish 2ml is sufficient*

    b. *35-60mm dish only requires 1ml*
    c. *Smaller dishes may only need 500ul.*
5. *Ammonium/triton solution is fast acting and does not need to be incubated. It may be removed 30 seconds after being added and can also be discarded in 50ml beaker.*
    a. *Be careful to gently remove as much liquid as possible for all washes*
6. *Perform 3-5 washes of ammonium/triton solution in order to lift and lyse cell remnants.*
7. *Finally wash out ammonium/triton solution with PBS and inspect under microscope.*
    a. *Check to make sure that cellular components are washed off and ECM remains attached to functionalized surface.*
    b. *Note that if cells were cultured on functionalized glass cellular components may remain adherent or alive underneath the glass surface. For this reason, it is recommended to remove your now decellularized glass and place in secondary containment for further analysis.*
8. *If cell remnants have not been fully removed add more ammonium/triton solution and incubate for 2-5minutes before washing.*
9. *Finally, aspirate or bleach 50ml beaker containing spent media and chemical washes. Clean biosafety cabinet*
    a. *If you decide to bleach 50ml beaker add a dash of bleach (around 3-5mls) and let sit for 10 minutes before pouring down the drain.*
10. *Solution can be stored in PBS at 4° C. To avoid bacterial growth for prolonged storage, add 0.02% sodium azide to PBS.*
    a. *Be carful not to shake azide.*

# Bibliography


(1) Kamrani, P.; Marston, G.; Arbor, T. C.; Jan, A. Anatomy, Connective Tissue. In *StatPearls*; StatPearls Publishing: Treasure Island (FL), 2024.

(2) Halper, J.; Kjaer, M. Basic Components of Connective Tissues and Extracellular Matrix: Elastin, Fibrillin, Fibulins, Fibrinogen, Fibronectin, Laminin, Tenascins and Thrombospondins. In *Progress in Heritable Soft Connective Tissue Diseases*; Halper, J., Ed.; Springer Netherlands: Dordrecht, 2014; pp 31–47. https://doi.org/10.1007/978-94-007-7893-1_3.

(3) Omelyanenko, N. P.; Slutsky, L. I.; Mironov, S. P. *Connective Tissue: Histophysiology, Biochemistry, Molecular Biology*; CRC Press, 2013.

(4) Carlson, B. M. Chapter 2 - Tissues. In *The Human Body*; Carlson, B. M., Ed.; Academic Press, 2019; pp 27–63. https://doi.org/10.1016/B978-0-12-804254-0.00002-8.

(5) Wu, M.; Cronin, K.; Crane, J. S. Biochemistry, Collagen Synthesis. In *StatPearls*; StatPearls Publishing: Treasure Island (FL), 2021.

(6) Shoulders, M. D.; Raines, R. T. COLLAGEN STRUCTURE AND STABILITY. *Annu Rev Biochem* **2009**, *78*, 929–958. https://doi.org/10.1146/annurev.biochem.77.032207.120833.

(7) Ushiki, T. Collagen Fibers, Reticular Fibers and Elastic Fibers. A Comprehensive Understanding from a Morphological Viewpoint. *Archives of Histology and Cytology* **2002**, *65* (2), 109–126. https://doi.org/10.1679/aohc.65.109.

(8) Onursal, C.; Dick, E.; Angelidis, I.; Schiller, H. B.; Staab-Weijnitz, C. A. Collagen Biosynthesis, Processing, and Maturation in Lung Ageing. *Front. Med.* **2021**, *8*. https://doi.org/10.3389/fmed.2021.593874.

(9) Yanagishita, M. Function of Proteoglycans in the Extracellular Matrix. *Acta Pathol. Jpn.* **1993**, *43* (6), 283–293.

(10) Scott, J. E. Proteoglycan:Collagen Interactions in Connective Tissues. Ultrastructural, Biochemical, Functional and Evolutionary Aspects. *International Journal of Biological Macromolecules* **1991**, *13* (3), 157–161. https://doi.org/10.1016/0141-8130(91)90041-R.

(11) Sh, K.; J, T.; S, G. Extracellular Matrix and Cell Signalling: The Dynamic Cooperation of Integrin, Proteoglycan and Growth Factor Receptor. *J Endocrinol* **2011**, *209* (2), 139–151. https://doi.org/10.1530/joe-10-0377.

(12) Miller, C.; Gasser, T. C. A Bottom-up Approach to Model Collagen Fiber Damage and Failure in Soft Biological Tissues. *Journal of the Mechanics and Physics of Solids* **2022**, *169*, 105086. https://doi.org/10.1016/j.jmps.2022.105086.

(13) Stylianou, A. Assessing Collagen D-Band Periodicity with Atomic Force Microscopy. *Materials (Basel)* **2022**, *15* (4), 1608. https://doi.org/10.3390/ma15041608.

(14) Karamanos, N. K.; Theocharis, A. D.; Piperigkou, Z.; Manou, D.; Passi, A.; Skandalis, S. S.; Vynios, D. H.; Orian-Rousseau, V.; Ricard-Blum, S.; Schmelzer, C. E. H.; Duca, L.; Durbeej, M.; Afratis, N. A.; Troeberg, L.; Franchi, M.; Masola, V.; Onisto, M. A Guide to the Composition and Functions of the Extracellular Matrix. *The FEBS Journal* **2021**, *288* (24), 6850–6912. https://doi.org/10.1111/febs.15776.

(15) *Modeling Protein–Glycosaminoglycan Complexes: Does the Size Matter? | Journal of Chemical Information and Modeling*. https://pubs.acs.org/doi/full/10.1021/acs.jcim.1c00664 (accessed 2023-07-19).

(16) Brummer, T.; Schmitz-Peiffer, C.; Daly, R. J. Docking Proteins. *The FEBS Journal* **2010**, *277* (21), 4356–4369. https://doi.org/10.1111/j.1742-4658.2010.07865.x.
(17) Frantz, C.; Stewart, K. M.; Weaver, V. M. The Extracellular Matrix at a Glance. *J Cell Sci* **2010**, *123* (24), 4195–4200. https://doi.org/10.1242/jcs.023820.
(18) Hynes, R. O. Extracellular Matrix: Not Just Pretty Fibrils. *Science* **2009**, *326* (5957), 1216–1219. https://doi.org/10.1126/science.1176009.
(19) Alberts, B.; Johnson, A.; Lewis, J.; Raff, M.; Roberts, K.; Walter, P. The Extracellular Matrix of Animals. In *Molecular Biology of the Cell. 4th edition*; Garland Science, 2002.
(20) Yue, B. Biology of the Extracellular Matrix: An Overview. *J Glaucoma* **2014**, S20–S23. https://doi.org/10.1097/IJG.0000000000000108.
(21) Mao, A. S.; Mooney, D. J. Regenerative Medicine: Current Therapies and Future Directions. *Proceedings of the National Academy of Sciences* **2015**, *112* (47), 14452–14459. https://doi.org/10.1073/pnas.1508520112.
(22) Curtis, A.; Riehle, M. Tissue Engineering: The Biophysical Background. *Phys. Med. Biol.* **2001**, *46* (4), R47. https://doi.org/10.1088/0031-9155/46/4/201.
(23) Research, C. for B. E. and. Approved Cellular and Gene Therapy Products. *FDA* **2024**.
(24) By Paul J. Kim, D. P. M. A Closer Look At Bioengineered Alternative Tissues. *Podiatry Today* **2006**, *19* (7).
(25) Stupp, S. I. Biomaterials for Regenerative Medicine. *MRS Bulletin* **2005**, *30* (7), 546–553. https://doi.org/10.1557/mrs2005.148.
(26) Kohane, D. S.; Langer, R. Polymeric Biomaterials in Tissue Engineering. *Pediatr Res* **2008**, *63* (5), 487–491. https://doi.org/10.1203/01.pdr.0000305937.26105.e7.
(27) Huang, J.; Best, S. M. Chapter 1 - Ceramic Biomaterials for Tissue Engineering. In *Tissue Engineering Using Ceramics and Polymers (Third Edition)*; Boccaccini, A. R., Ma, P. X., Liverani, L., Eds.; Woodhead Publishing Series in Biomaterials; Woodhead Publishing, 2022; pp 3–40. https://doi.org/10.1016/B978-0-12-820508-2.00007-6.
(28) Santos-Coquillat, A.; Martínez-Campos, E.; Mora Sánchez, H.; Moreno, L.; Arrabal, R.; Mohedano, M.; Gallardo, A.; Rodríguez-Hernández, J.; Matykina, E. Hybrid Functionalized Coatings on Metallic Biomaterials for Tissue Engineering. *Surface and Coatings Technology* **2021**, *422*, 127508. https://doi.org/10.1016/j.surfcoat.2021.127508.
(29) Rahaman, M. N.; Day, D. E.; Sonny Bal, B.; Fu, Q.; Jung, S. B.; Bonewald, L. F.; Tomsia, A. P. Bioactive Glass in Tissue Engineering. *Acta Biomaterialia* **2011**, *7* (6), 2355–2373. https://doi.org/10.1016/j.actbio.2011.03.016.
(30) Berrier, A. L.; Yamada, K. M. Cell–Matrix Adhesion. *Journal of Cellular Physiology* **2007**, *213* (3), 565–573. https://doi.org/10.1002/jcp.21237.
(31) Mase, V. J.; Hsu, J. R.; Wolf, S. E.; Wenke, J. C.; Baer, D. G.; Owens, J.; Badylak, S. F.; Walters, T. J. Clinical Application of an Acellular Biologic Scaffold for Surgical Repair of a Large, Traumatic Quadriceps Femoris Muscle Defect. *Orthopedics* **2010**, *33* (7), 511. https://doi.org/10.3928/01477447-20100526-24.
(32) Kaplan, A. V.; Baim, D. S.; Smith, J. J.; Feigal, D. A.; Simons, M.; Jefferys, D.; Fogarty, T. J.; Kuntz, R. E.; Leon, M. B. Medical Device Development. *Circulation* **2004**, *109* (25), 3068–3072. https://doi.org/10.1161/01.CIR.0000134695.65733.64.
(33) Fernández-Pérez, J.; Ahearne, M. The Impact of Decellularization Methods on Extracellular Matrix Derived Hydrogels. *Sci Rep* **2019**, *9* (1), 14933. https://doi.org/10.1038/s41598-019-49575-2.
(34) Badylak, S. F. The Extracellular Matrix as a Scaffold for Tissue Reconstruction. *Seminars in Cell & Developmental Biology* **2002**, *13* (5), 377–383. https://doi.org/10.1016/S1084952102000940.

(35) E. Fitzpatrick, L.; C. McDevitt, T. Cell-Derived Matrices for Tissue Engineering and Regenerative Medicine Applications. *Biomaterials Science* **2015**, *3* (1), 12–24. https://doi.org/10.1039/C4BM00246F.
(36) Rubi-Sans, G.; Castaño, O.; Cano, I.; Mateos-Timoneda, M. A.; Perez-Amodio, S.; Engel, E. Engineering Cell-Derived Matrices: From 3D Models to Advanced Personalized Therapies. *Advanced Functional Materials* **2020**, *30* (44), 2000496. https://doi.org/10.1002/adfm.202000496.
(37) Zhang, J.; Yun, S.; Du, Y.; Zannettino, A.; Zhang, H. Hydrogel-Based Preparation of Cell Aggregates for Biomedical Applications. *Applied Materials Today* **2020**, *20*, 100747. https://doi.org/10.1016/j.apmt.2020.100747.
(38) Kim, M.-H.; Takeuchi, K.; Kino-oka, M. Role of Cell-Secreted Extracellular Matrix Formation in Aggregate Formation and Stability of Human Induced Pluripotent Stem Cells in Suspension Culture. *Journal of Bioscience and Bioengineering* **2019**, *127* (3), 372–380. https://doi.org/10.1016/j.jbiosc.2018.08.010.
(39) Franco-Barraza, J.; Beacham, D. A.; Amatangelo, M. D.; Cukierman, E. Preparation of Extracellular Matrices Produced by Cultured and Primary Fibroblasts. *Current Protocols in Cell Biology* **2016**, *71* (1), 10.9.1-10.9.34. https://doi.org/10.1002/cpcb.2.
(40) Pinnell, S. R. Regulation of Collagen Biosynthesis by Ascorbic Acid: A Review. *Yale J Biol Med* **1985**, *58* (6), 553–559.
(41) Rajab, T. K.; O'Malley, T. J.; Tchantchaleishvili, V. Decellularized Scaffolds for Tissue Engineering: Current Status and Future Perspective. *Artificial Organs* **2020**, *44* (10), 1031–1043. https://doi.org/10.1111/aor.13701.
(42) Crapo, P. M.; Gilbert, T. W.; Badylak, S. F. An Overview of Tissue and Whole Organ Decellularization Processes. *Biomaterials* **2011**, *32* (12), 3233–3243. https://doi.org/10.1016/j.biomaterials.2011.01.057.
(43) Gilbert, T. W.; Sellaro, T. L.; Badylak, S. F. Decellularization of Tissues and Organs. *Biomaterials* **2006**, *27* (19), 3675–3683. https://doi.org/10.1016/j.biomaterials.2006.02.014.
(44) Xing, Q.; Yates, K.; Tahtinen, M.; Shearier, E.; Qian, Z.; Zhao, F. Decellularization of Fibroblast Cell Sheets for Natural Extracellular Matrix Scaffold Preparation. *Tissue Engineering Part C: Methods* **2015**, *21* (1), 77–87. https://doi.org/10.1089/ten.tec.2013.0666.
(45) King, S. J.; Parsons, M. Imaging Cells Within 3D Cell-Derived Matrix. In *Cell Migration: Developmental Methods and Protocols*; Wells, C. M., Parsons, M., Eds.; Humana Press: Totowa, NJ, 2011; pp 53–64. https://doi.org/10.1007/978-1-61779-207-6_5.
(46) Badylak, S. F.; Freytes, D. O.; Gilbert, T. W. Extracellular Matrix as a Biological Scaffold Material: Structure and Function. *Acta Biomaterialia* **2009**, *5* (1), 1–13. https://doi.org/10.1016/j.actbio.2008.09.013.
(47) Hussey, G. S.; Dziki, J. L.; Badylak, S. F. Extracellular Matrix-Based Materials for Regenerative Medicine. *Nat Rev Mater* **2018**, *3* (7), 159–173. https://doi.org/10.1038/s41578-018-0023-x.
(48) Doherty, E. L.; Krohn, G.; Warren, E. C.; Patton, A.; Whitworth, C. P.; Rathod, M.; Biehl, A.; Aw, W. Y.; Freytes, D. O.; Polacheck, W. J. Human Cell-Derived Matrix Composite Hydrogels with Diverse Composition for Use in Vasculature-on-Chip Models. *Advanced Healthcare Materials n/a* (n/a), 2400192. https://doi.org/10.1002/adhm.202400192.
(49) Antich, C.; Jiménez, G.; de Vicente, J.; López-Ruiz, E.; Chocarro-Wrona, C.; Griñán-Lisón, C.; Carrillo, E.; Montañez, E.; Marchal, J. A. Development of a Biomimetic Hydrogel Based on Predifferentiated Mesenchymal Stem-Cell-Derived ECM for Cartilage Tissue Engineering. *Advanced Healthcare Materials* **2021**, *10* (8), 2001847. https://doi.org/10.1002/adhm.202001847.

(50) Walimbe, T.; Panitch, A. Best of Both Hydrogel Worlds: Harnessing Bioactivity and Tunability by Incorporating Glycosaminoglycans in Collagen Hydrogels. *Bioengineering* **2020**, *7* (4), 156. https://doi.org/10.3390/bioengineering7040156.
(51) Saldin, L. T.; Cramer, M. C.; Velankar, S. S.; White, L. J.; Badylak, S. F. Extracellular Matrix Hydrogels from Decellularized Tissues: Structure and Function. *Acta Biomaterialia* **2017**, *49*, 1–15. https://doi.org/10.1016/j.actbio.2016.11.068.
(52) Bi, Y.; Patra, P.; Faezipour, M. Structure of Collagen-Glycosaminoglycan Matrix and the Influence to Its Integrity and Stability. In *2014 36th Annual International Conference of the IEEE Engineering in Medicine and Biology Society*; 2014; pp 3949–3952. https://doi.org/10.1109/EMBC.2014.6944488.
(53) Kleinman, H. K.; Martin, G. R. Matrigel: Basement Membrane Matrix with Biological Activity. *Seminars in Cancer Biology* **2005**, *15* (5), 378–386. https://doi.org/10.1016/j.semcancer.2005.05.004.
(54) Wong, M. L.; Griffiths, L. G. Immunogenicity in Xenogeneic Scaffold Generation: Antigen Removal versus Decellularization. *Acta Biomater* **2014**, *10* (5), 1806–1816. https://doi.org/10.1016/j.actbio.2014.01.028.
(55) Zhou, Q.; Li, T.; Wang, K.; Zhang, Q.; Geng, Z.; Deng, S.; Cheng, C.; Wang, Y. Current Status of Xenotransplantation Research and the Strategies for Preventing Xenograft Rejection. *Front Immunol* **2022**, *13*, 928173. https://doi.org/10.3389/fimmu.2022.928173.
(56) Zhang, W.; Zhu, Y.; Li, J.; Guo, Q.; Peng, J.; Liu, S.; Yang, J.; Wang, Y. Cell-Derived Extracellular Matrix: Basic Characteristics and Current Applications in Orthopedic Tissue Engineering. *Tissue Engineering Part B: Reviews* **2016**, *22* (3), 193–207. https://doi.org/10.1089/ten.teb.2015.0290.
(57) Cheng, H.-W.; Tsui, Y.-K.; Cheung, K. M. C.; Chan, D.; Chan, B. P. Decellularization of Chondrocyte-Encapsulated Collagen Microspheres: A Three-Dimensional Model to Study the Effects of Acellular Matrix on Stem Cell Fate. *Tissue Engineering Part C: Methods* **2009**, *15* (4), 697–706. https://doi.org/10.1089/ten.tec.2008.0635.
(58) Lu, H.; Hoshiba, T.; Kawazoe, N.; Koda, I.; Song, M.; Chen, G. Cultured Cell-Derived Extracellular Matrix Scaffolds for Tissue Engineering. *Biomaterials* **2011**, *32* (36), 9658–9666. https://doi.org/10.1016/j.biomaterials.2011.08.091.
(59) Raghunathan, V. K.; Morgan, J. T.; Chang, Y.-R.; Weber, D.; Phinney, B.; Murphy, C. J.; Russell, P. Transforming Growth Factor Beta 3 Modifies Mechanics and Composition of Extracellular Matrix Deposited by Human Trabecular Meshwork Cells. *ACS Biomater. Sci. Eng.* **2015**, *1* (2), 110–118. https://doi.org/10.1021/ab500060r.
(60) Preibisch, S.; Saalfeld, S.; Tomancak, P. Globally Optimal Stitching of Tiled 3D Microscopic Image Acquisitions. *Bioinformatics* **2009**, *25* (11), 1463–1465. https://doi.org/10.1093/bioinformatics/btp184.
(61) Liu, Y.; Keikhosravi, A.; Mehta, G. S.; Drifka, C. R.; Eliceiri, K. W. Methods for Quantifying Fibrillar Collagen Alignment. In *Fibrosis: Methods and Protocols*; Rittié, L., Ed.; Methods in Molecular Biology; Springer: New York, NY, 2017; pp 429–451. https://doi.org/10.1007/978-1-4939-7113-8_28.
(62) Bredfeldt, J. S.; Liu, Y.; Conklin, M. W.; Keely, P. J.; Mackie, T. R.; Eliceiri, K. W. Automated Quantification of Aligned Collagen for Human Breast Carcinoma Prognosis. *J Pathol Inform* **2014**, *5* (1), 28. https://doi.org/10.4103/2153-3539.139707.
(63) Berens, P. CircStat: A MATLAB Toolbox for Circular Statistics. *Journal of Statistical Software* **2009**, *31*, 1–21. https://doi.org/10.18637/jss.v031.i10.
(64) Coulson- Thomas, V.; Gesteira, T. Dimethylmethylene Blue Assay (DMMB). *BIO-PROTOCOL* **2014**, *4*. https://doi.org/10.21769/BioProtoc.1236.

(65) Brown, R. A.; Wiseman, M.; Chuo, C.-B.; Cheema, U.; Nazhat, S. N. Ultrarapid Engineering of Biomimetic Materials and Tissues: Fabrication of Nano- and Microstructures by Plastic Compression. *Advanced Functional Materials* **2005**, *15* (11), 1762–1770. https://doi.org/10.1002/adfm.200500042.
(66) Medberry, C. J.; Crapo, P. M.; Siu, B. F.; Carruthers, C. A.; Wolf, M. T.; Nagarkar, S. P.; Agrawal, V.; Jones, K. E.; Kelly, J.; Johnson, S. A.; Velankar, S. S.; Watkins, S. C.; Modo, M.; Badylak, S. F. Hydrogels Derived from Central Nervous System Extracellular Matrix. *Biomaterials* **2013**, *34* (4), 1033–1040. https://doi.org/10.1016/j.biomaterials.2012.10.062.
(67) Pouliot, R. A.; Young, B. M.; Link, P. A.; Park, H. E.; Kahn, A. R.; Shankar, K.; Schneck, M. B.; Weiss, D. J.; Heise, R. L. Porcine Lung-Derived Extracellular Matrix Hydrogel Properties Are Dependent on Pepsin Digestion Time. *Tissue Engineering Part C: Methods* **2020**, *26* (6), 332–346. https://doi.org/10.1089/ten.tec.2020.0042.
(68) Freytes, D. O.; Martin, J.; Velankar, S. S.; Lee, A. S.; Badylak, S. F. Preparation and Rheological Characterization of a Gel Form of the Porcine Urinary Bladder Matrix. *Biomaterials* **2008**, *29* (11), 1630–1637. https://doi.org/10.1016/j.biomaterials.2007.12.014.
(69) Sanchez, M. M.; Morgan, J. T. Generation of Self-Assembled Vascularized Human Skin Equivalents. *JoVE (Journal of Visualized Experiments)* **2021**, No. 168, e62125. https://doi.org/10.3791/62125.
(70) Logan, A. C.; Nightingale, S. J.; Haas, D. L.; Cho, G. J.; Pepper, K. A.; Kohn, D. B. Factors Influencing the Titer and Infectivity of Lentiviral Vectors. *Human Gene Therapy* **2004**, *15* (10), 976–988. https://doi.org/10.1089/hum.2004.15.976.
(71) Hu, B.; Thirtamara-Rajamani, K. K.; Sim, H.; Viapiano, M. S. FIBULIN-3 IS UNIQUELY UPREGULATED IN MALIGNANT GLIOMAS AND PROMOTES TUMOR CELL MOTILITY AND INVASION. *Mol Cancer Res* **2009**, *7* (11), 1756–1770. https://doi.org/10.1158/1541-7786.MCR-09-0207.
(72) Kaukonen, R.; Jacquemet, G.; Hamidi, H.; Ivaska, J. Cell-Derived Matrices for Studying Cell Proliferation and Directional Migration in a Complex 3D Microenvironment. *Nat Protoc* **2017**, *12* (11), 2376–2390. https://doi.org/10.1038/nprot.2017.107.
(73) The Ridgelet and Curvelet Transforms. In *Sparse Image and Signal Processing: Wavelets, Curvelets, Morphological Diversity*; Murtagh, F., Fadili, J. M., Starck, J.-L., Eds.; Cambridge University Press: Cambridge, 2010; pp 89–118. https://doi.org/10.1017/CBO9780511730344.006.
(74) Ahlfors, J.-E. W.; Billiar, K. L. Biomechanical and Biochemical Characteristics of a Human Fibroblast-Produced and Remodeled Matrix. *Biomaterials* **2007**, *28* (13), 2183–2191. https://doi.org/10.1016/j.biomaterials.2006.12.030.
(75) Gargotti, M.; Lopez-Gonzalez, U.; Byrne, H. J.; Casey, A. Comparative Studies of Cellular Viability Levels on 2D and 3D in Vitro Culture Matrices. *Cytotechnology* **2018**, *70* (1), 261–273. https://doi.org/10.1007/s10616-017-0139-7.
(76) D'Aniello, C.; Cermola, F.; Patriarca, E. J.; Minchiotti, G. Vitamin C in Stem Cell Biology: Impact on Extracellular Matrix Homeostasis and Epigenetics. *Stem Cells Int* **2017**, *2017*, 8936156. https://doi.org/10.1155/2017/8936156.
(77) Guo, X.; Hutcheon, A. E. K.; Melotti, S. A.; Zieske, J. D.; Trinkaus-Randall, V.; Ruberti, J. W. Morphologic Characterization of Organized Extracellular Matrix Deposition by Ascorbic Acid–Stimulated Human Corneal Fibroblasts. *Investigative Ophthalmology & Visual Science* **2007**, *48* (9), 4050–4060. https://doi.org/10.1167/iovs.06-1216.
(78) Fujisawa, K.; Hara, K.; Takami, T.; Okada, S.; Matsumoto, T.; Yamamoto, N.; Sakaida, I. Evaluation of the Effects of Ascorbic Acid on Metabolism of Human Mesenchymal Stem Cells. *Stem Cell Research & Therapy* **2018**, *9* (1), 93. https://doi.org/10.1186/s13287-018-0825-1.

(79) Mann, B. K.; Schmedlen, R. H.; West, J. L. Tethered-TGF-β Increases Extracellular Matrix Production of Vascular Smooth Muscle Cells. *Biomaterials* **2001**, *22* (5), 439–444. https://doi.org/10.1016/S0142-9612(00)00196-4.
(80) Funderburgh, J. L.; Funderburgh, M. L.; Mann, M. M.; Corpuz, L.; Roth, M. R. Proteoglycan Expression during Transforming Growth Factor β-Induced Keratocyte-Myofibroblast Transdifferentiation*. *Journal of Biological Chemistry* **2001**, *276* (47), 44173–44178. https://doi.org/10.1074/jbc.M107596200.
(81) Wolchok, J. C.; Tresco, P. A. Using Growth Factor Conditioning to Modify the Properties of Human Cell Derived Extracellular Matrix. *Biotechnology Progress* **2012**, *28* (6), 1581–1587. https://doi.org/10.1002/btpr.1625.
(82) Gong, X.; Kulwatno, J.; Mills, K. L. Rapid Fabrication of Collagen Bundles Mimicking Tumor-Associated Collagen Architectures. *Acta Biomaterialia* **2020**, *108*, 128–141. https://doi.org/10.1016/j.actbio.2020.03.019.
(83) Saidi, I. S.; Jacques, S. L.; Tittel, F. K. Mie and Rayleigh Modeling of Visible-Light Scattering in Neonatal Skin. *Appl. Opt., AO* **1995**, *34* (31), 7410–7418. https://doi.org/10.1364/AO.34.007410.
(84) Lai, V. K.; Frey, C. R.; Kerandi, A. M.; Lake, S. P.; Tranquillo, R. T.; Barocas, V. H. Microstructural and Mechanical Differences between Digested Collagen–Fibrin Co-Gels and Pure Collagen and Fibrin Gels. *Acta Biomaterialia* **2012**, *8* (11), 4031–4042. https://doi.org/10.1016/j.actbio.2012.07.010.
(85) Parry, D. A. D. The Molecular Fibrillar Structure of Collagen and Its Relationship to the Mechanical Properties of Connective Tissue. *Biophysical Chemistry* **1988**, *29* (1), 195–209. https://doi.org/10.1016/0301-4622(88)87039-X.
(86) Christiansen, D. L.; Huang, E. K.; Silver, F. H. Assembly of Type I Collagen: Fusion of Fibril Subunits and the Influence of Fibril Diameter on Mechanical Properties. *Matrix Biology* **2000**, *19* (5), 409–420. https://doi.org/10.1016/S0945-053X(00)00089-5.
(87) Gilbert, T. W.; Stolz, D. B.; Biancaniello, F.; Simmons-Byrd, A.; Badylak, S. F. Production and Characterization of ECM Powder: Implications for Tissue Engineering Applications. *Biomaterials* **2005**, *26* (12), 1431–1435. https://doi.org/10.1016/j.biomaterials.2004.04.042.
(88) Dziki, J. L.; Wang, D. S.; Pineda, C.; Sicari, B. M.; Rausch, T.; Badylak, S. F. Solubilized Extracellular Matrix Bioscaffolds Derived from Diverse Source Tissues Differentially Influence Macrophage Phenotype. *Journal of Biomedical Materials Research Part A* **2017**, *105* (1), 138–147. https://doi.org/10.1002/jbm.a.35894.
(89) Tsai, C.-H.; Chou, M.-Y.; Jonas, M.; Tien, Y.-T.; Chi, E. Y. A composite graft material containing bone particles and collagen in osteoinduction in mouse. *Journal of Biomedical Materials Research* **2002**, *63* (1), 65–70. https://doi.org/10.1002/jbm.10089.
(90) Mizuno, S.; Glowacki, J. Three-Dimensional Composite of Demineralized Bone Powder and Collagen for *in Vitro* Analysis of Chondroinduction of Human Dermal Fibroblasts. *Biomaterials* **1996**, *17* (18), 1819–1825. https://doi.org/10.1016/0142-9612(96)00041-5.
(91) Jin, G.-Z.; Kim, H.-W. Effects of Type I Collagen Concentration in Hydrogel on the Growth and Phenotypic Expression of Rat Chondrocytes. *Tissue Eng Regen Med* **2017**, *14* (4), 383–391. https://doi.org/10.1007/s13770-017-0060-3.
(92) Gelman, R. A.; Poppke, D. C.; Piez, K. A. Collagen Fibril Formation in Vitro. The Role of the Nonhelical Terminal Regions. *Journal of Biological Chemistry* **1979**, *254* (22), 11741–11745. https://doi.org/10.1016/S0021-9258(19)86545-6.
(93) Oliva, M. S.; Schottman, T.; Gulati, M. Turning the Tide of Corneal Blindness. *Indian J Ophthalmol* **2012**, *60* (5), 423–427. https://doi.org/10.4103/0301-4738.100540.

(94) Gain, P.; Jullienne, R.; He, Z.; Aldossary, M.; Acquart, S.; Cognasse, F.; Thuret, G. Global Survey of Corneal Transplantation and Eye Banking. *JAMA Ophthalmol* **2016**, *134* (2), 167–173. https://doi.org/10.1001/jamaophthalmol.2015.4776.
(95) Espana, E. M.; Birk, D. E. Composition, Structure and Function of the Corneal Stroma. *Exp Eye Res* **2020**, *198*, 108137. https://doi.org/10.1016/j.exer.2020.108137.
(96) Poole, C. A.; Brookes, N. H.; Clover, G. M. Keratocyte Networks Visualised in the Living Cornea Using Vital Dyes. *Journal of Cell Science* **1993**, *106* (2), 685–691.
(97) Müller, L. J.; Pels, L.; Vrensen, G. F. Novel Aspects of the Ultrastructural Organization of Human Corneal Keratocytes. *Invest. Ophthalmol. Vis. Sci.* **1995**, *36* (13), 2557–2567.
(98) Wilson, S. E. Corneal Myofibroblasts and Fibrosis. *Exp Eye Res* **2020**, *201*, 108272. https://doi.org/10.1016/j.exer.2020.108272.
(99) Yam, G. H. F.; Riau, A. K.; Funderburgh, M. L.; Mehta, J. S.; Jhanji, V. Keratocyte Biology. *Experimental Eye Research* **2020**, *196*, 108062. https://doi.org/10.1016/j.exer.2020.108062.
(100) Torricelli, A. A. M.; Wilson, S. E. Cellular and Extracellular Matrix Modulation of Corneal Stromal Opacity. *Experimental Eye Research* **2014**, *129*, 151–160. https://doi.org/10.1016/j.exer.2014.09.013.
(101) Sugioka, K.; Mishima, H.; Kodama, A.; Itahashi, M.; Fukuda, M.; Shimomura, Y. Regulatory Mechanism of Collagen Degradation by Keratocytes and Corneal Inflammation: The Role of Urokinase-Type Plasminogen Activator. *Cornea* **2016**, *35*, S59. https://doi.org/10.1097/ICO.0000000000000995.
(102) Guérin, L.-P.; Le-Bel, G.; Desjardins, P.; Couture, C.; Gillard, E.; Boisselier, É.; Bazin, R.; Germain, L.; Guérin, S. L. The Human Tissue-Engineered Cornea (hTEC): Recent Progress. *International Journal of Molecular Sciences* **2021**, *22* (3), 1291. https://doi.org/10.3390/ijms22031291.
(103) Ruberti, J. W.; Zieske, J. D. Prelude to Corneal Tissue Engineering – Gaining Control of Collagen Organization. *Progress in Retinal and Eye Research* **2008**, *27* (5), 549–577. https://doi.org/10.1016/j.preteyeres.2008.08.001.
(104) Zieske, J. D.; Mason, V. S.; Wasson, M. E.; Meunier, S. F.; Nolte, C. J.; Fukai, N.; Olsen, B. R.; Parenteau, N. L. Basement Membrane Assembly and Differentiation of Cultured Corneal Cells: Importance of Culture Environment and Endothelial Cell Interaction. *Exp. Cell Res.* **1994**, *214* (2), 621–633. https://doi.org/10.1006/excr.1994.1300.
(105) Tidu, A.; Schanne-Klein, M.-C.; Borderie, V. M. Development, Structure, and Bioengineering of the Human Corneal Stroma: A Review of Collagen-Based Implants. *Experimental Eye Research* **2020**, *200*, 108256. https://doi.org/10.1016/j.exer.2020.108256.
(106) Parekh, M.; Romano, V.; Hassanin, K.; Testa, V.; Wongvisavavit, R.; Ferrari, S.; Haneef, A.; Willoughby, C.; Ponzin, D.; Jhanji, V.; Sharma, N.; Daniels, J.; Kaye, S. B.; Ahmad, S.; Levis, H. J. Biomaterials for Corneal Endothelial Cell Culture and Tissue Engineering. *J Tissue Eng* **2021**, *12*, 2041731421990536. https://doi.org/10.1177/2041731421990536.
(107) Ahearne, M.; Lynch, A. P. Early Observation of Extracellular Matrix-Derived Hydrogels for Corneal Stroma Regeneration. *Tissue Engineering Part C: Methods* **2015**, *21* (10), 1059–1069. https://doi.org/10.1089/ten.tec.2015.0008.
(108) Zhang, S.; Zhang, M.; Li, X.; Huang, S.; Han, D.; Chang, L.; Ling, L.; Huo, Y.; Alzogool, M.; Yang, N.; Ye, Q.; Wang, Y. Development of a Novel Bioartificial Cornea Using 3D Bioprinting Based on Electrospun Micro-Nanofibrous Decellularized Extracellular Matrix. *Biofabrication* **2024**, *16* (2), 025039. https://doi.org/10.1088/1758-5090/ad35ea.
(109) Dickman, C. T. D.; Russo, V.; Thain, K.; Pan, S.; Beyer, S. T.; Walus, K.; Getsios, S.; Mohamed, T.; Wadsworth, S. J. Functional Characterization of 3D Contractile Smooth Muscle Tissues

Generated Using a Unique Microfluidic 3D Bioprinting Technology. *The FASEB Journal* **2020**, *34* (1), 1652–1664. https://doi.org/10.1096/fj.201901063RR.
(110) Kim, W. J.; Mohan, R. R.; Mohan, R. R.; Wilson, S. E. Effect of PDGF, IL-1alpha, and BMP2/4 on Corneal Fibroblast Chemotaxis: Expression of the Platelet-Derived Growth Factor System in the Cornea. *Investigative Ophthalmology & Visual Science* **1999**, *40* (7), 1364–1372.
(111) Saghizadeh, M.; Chwa, M.; Aoki, A.; Lin, B.; Pirouzmanesh, A.; Brown, D. J.; Ljubimov, A. V.; Kenney, M. C. Altered Expression of Growth Factors and Cytokines in Keratoconus, Bullous Keratopathy and Diabetic Human Corneas. *Exp Eye Res* **2001**, *73* (2), 179–189. https://doi.org/10.1006/exer.2001.1028.
(112) Scott, S.-G.; Jun, A. S.; Chakravarti, S. Sphere Formation from Corneal Keratocytes and Phenotype Specific Markers. *Experimental Eye Research* **2011**, *93* (6), 898–905. https://doi.org/10.1016/j.exer.2011.10.004.
(113) Li, Y.; Liu, Y.; Xia, W.; Lei, D.; Voorhees, J. J.; Fisher, G. J. Age-Dependent Alterations of Decorin Glycosaminoglycans in Human Skin. *Scientific Reports* **2013**, *3* (1), 2422. https://doi.org/10.1038/srep02422.
(114) Li, Y.; Lee, M.; Kim, N.; Wu, G.; Deng, D.; Liu, X.; Heo, W. D.; Zi, Z. Spatiotemporal Control of TGF-β Signaling with Light. *ACS Synth. Biol.* **2018**, *7* (2), 443–451. https://doi.org/10.1021/acssynbio.7b00225.
(115) Han, H.; Wecker, T.; Grehn, F.; Schlunck, G. Elasticity-Dependent Modulation of TGF-β Responses in Human Trabecular Meshwork Cells. *Investigative Ophthalmology & Visual Science* **2011**, *52* (6), 2889–2896. https://doi.org/10.1167/iovs.10-6640.
(116) Janin-Manificat, H.; Rovère, M.-R.; Galiacy, S. D.; Malecaze, F.; Hulmes, D. J. S.; Moali, C.; Damour, O. Development of Ex Vivo Organ Culture Models to Mimic Human Corneal Scarring. *Mol Vis* **2012**, *18*, 2896–2908.
(117) Prydal, J. I.; Franc, F.; Dilly, P. N.; Kerr Muir, M. G.; Corbett, M. C.; Marshall, J. Keratocyte Density and Size in Conscious Humans by Digital Image Analysis of Confocal Images. *Eye (Lond)* **1998**, *12 ( Pt 3a)*, 337–342. https://doi.org/10.1038/eye.1998.82.
(118) Neel, E. A. A.; Cheema, U.; Knowles, J. C.; Brown, R. A.; Nazhat, S. N. Use of Multiple Unconfined Compression for Control of Collagen Gel Scaffold Density and Mechanical Properties. *Soft Matter* **2006**, *2* (11), 986–992. https://doi.org/10.1039/B609784G.
(119) Hassell, J. R.; Birk, D. E. The Molecular Basis of Corneal Transparency. *Experimental Eye Research* **2010**, *91* (3), 326–335. https://doi.org/10.1016/j.exer.2010.06.021.
(120) Hassell, J. R.; Cintron, C.; Kublin, C.; Newsome, D. A. Proteoglycan Changes during Restoration of Transparency in Corneal Scars. *Archives of Biochemistry and Biophysics* **1983**, *222* (2), 362–369. https://doi.org/10.1016/0003-9861(83)90532-5.
(121) Kao, W. W.-Y.; Liu, C.-Y. Roles of Lumican and Keratocan on Corneal Transparency. *Glycoconj J* **2002**, *19* (4), 275–285. https://doi.org/10.1023/A:1025396316169.
(122) Parapuram, S. K.; Hodge, W. The Integrin Needle in the Stromal Haystack: Emerging Role in Corneal Physiology and Pathology. *J. Cell Commun. Signal.* **2014**, *8* (2), 113–124. https://doi.org/10.1007/s12079-014-0230-1.
(123) Grzetić-Lenac, R.; Merlak, M.; Balog, T.; Markusić, V.; Dekaris, I. The Expression of Interleukin-1 Alpha, TNF and VEGF in Corneal Cells of Patients with Bullous Keratopathy. *Coll Antropol* **2011**, *35 Suppl 2*, 171–173.
(124) Meek, K. M.; Boote, C. The Organization of Collagen in the Corneal Stroma. *Experimental Eye Research* **2004**, *78* (3), 503–512. https://doi.org/10.1016/j.exer.2003.07.003.
(125) Meek, K. M.; Boote, C. The Use of X-Ray Scattering Techniques to Quantify the Orientation and Distribution of Collagen in the Corneal Stroma. *Progress in Retinal and Eye Research* **2009**, *28* (5), 369–392. https://doi.org/10.1016/j.preteyeres.2009.06.005.

(126) Boularaoui, S.; Al Hussein, G.; Khan, K. A.; Christoforou, N.; Stefanini, C. An Overview of Extrusion-Based Bioprinting with a Focus on Induced Shear Stress and Its Effect on Cell Viability. *Bioprinting* **2020**, *20*, e00093. https://doi.org/10.1016/j.bprint.2020.e00093.
(127) Bron, A. J. The Architecture of the Corneal Stroma. *British Journal of Ophthalmology* **2001**, *85* (4), 379–381. https://doi.org/10.1136/bjo.85.4.379.
(128) Watsky, M. A. Keratocyte Gap Junctional Communication in Normal and Wounded Rabbit Corneas and Human Corneas. *Invest. Ophthalmol. Vis. Sci.* **1995**, *36* (13), 2568–2576.
(129) Chakravarti, S.; Wu, F.; Vij, N.; Roberts, L.; Joyce, S. Microarray Studies Reveal Macrophage-like Function of Stromal Keratocytes in the Cornea. *Invest. Ophthalmol. Vis. Sci.* **2004**, *45* (10), 3475–3484. https://doi.org/10.1167/iovs.04-0343.
(130) Elsheikh, A.; Brown, M.; Alhasso, D.; Rama, P.; Campanelli, M.; Garway-Heath, D. Experimental Assessment of Corneal Anisotropy. *Journal of refractive surgery (Thorofare, N.J. : 1995)* **2008**, *24*, 178–187. https://doi.org/10.3928/1081597X-20080201-09.
(131) Crouch, J. R.; Merriam, J. C.; Crouch, E. R. Finite Element Model of Cornea Deformation. In *Medical Image Computing and Computer-Assisted Intervention – MICCAI 2005*; Duncan, J. S., Gerig, G., Eds.; Springer: Berlin, Heidelberg, 2005; pp 591–598. https://doi.org/10.1007/11566489_73.
(132) Smith, C. M.; Christian, J. J.; Warren, W. L.; Williams, S. K. Characterizing Environmental Factors That Impact the Viability of Tissue-Engineered Constructs Fabricated by a Direct-Write Bioassembly Tool. *Tissue Engineering* **2007**, *13* (2), 373–383. https://doi.org/10.1089/ten.2006.0101.
(133) Restan Perez, M.; Sharma, R.; Masri, N. Z.; Willerth, S. M. 3D Bioprinting Mesenchymal Stem Cell-Derived Neural Tissues Using a Fibrin-Based Bioink. *Biomolecules* **2021**, *11* (8), 1250. https://doi.org/10.3390/biom11081250.
(134) Malda, J.; Visser, J.; Melchels, F. P.; Jüngst, T.; Hennink, W. E.; Dhert, W. J. A.; Groll, J.; Hutmacher, D. W. 25th Anniversary Article: Engineering Hydrogels for Biofabrication. *Advanced Materials* **2013**, *25* (36), 5011–5028. https://doi.org/10.1002/adma.201302042.
(135) Kimura, K.; Orita, T.; Morishige, N.; Nishida, T.; Sonoda, K.-H. Role of the JNK Signaling PathWay in Downregulation of Connexin43 by TNF-α in Human Corneal Fibroblasts. *Current Eye Research* **2013**, *38* (9), 926–932. https://doi.org/10.3109/02713683.2013.798419.
(136) Grupcheva, C. N.; Laux, W. T.; Rupenthal, I. D.; McGhee, J.; McGhee, C. N. J.; Green, C. R. Improved Corneal Wound Healing through Modulation of Gap Junction Communication Using Connexin43-Specific Antisense Oligodeoxynucleotides. *Investigative Ophthalmology & Visual Science* **2012**, *53* (3), 1130–1138. https://doi.org/10.1167/iovs.11-8711.
(137) Stramer, B. M.; Fini, M. E. Uncoupling Keratocyte Loss of Corneal Crystallin from Markers of Fibrotic Repair. *Invest. Ophthalmol. Vis. Sci.* **2004**, *45* (11), 4010–4015. https://doi.org/10.1167/iovs.03-1057.
(138) Petroll, W. M.; Cavanagh, H. D.; Jester, J. V. Dynamic Three-Dimensional Visualization of Collagen Matrix Remodeling and Cytoskeletal Organization in Living Corneal Fibroblasts. *Scanning* **2004**, *26* (1), 1–10. https://doi.org/10.1002/sca.4950260102.
(139) Niederer, R. L.; McGhee, C. N. J. Clinical *in Vivo* Confocal Microscopy of the Human Cornea in Health and Disease. *Progress in Retinal and Eye Research* **2010**, *29* (1), 30–58. https://doi.org/10.1016/j.preteyeres.2009.11.001.
(140) Hahnel, C.; Somodi, S.; Weiss, D. G.; Guthoff, R. F. The Keratocyte Network of Human Cornea: A Three-Dimensional Study Using Confocal Laser Scanning Fluorescence Microscopy. *Cornea* **2000**, *19* (2), 185.

(141) Di Zazzo, A.; Lee, S.-M.; Sung, J.; Niutta, M.; Coassin, M.; Mashaghi, A.; Inomata, T. Variable Responses to Corneal Grafts: Insights from Immunology and Systems Biology. *Journal of Clinical Medicine* **2020**, *9* (2), 586. https://doi.org/10.3390/jcm9020586.
(142) Green, L. N.; Naghshnejad, P.; Dankwa, D.; Tang, X. Model-Guided Design of Biological Controller for Septic Wound Healing Regulation. bioRxiv January 18, 2023, p 2023.01.16.523937. https://doi.org/10.1101/2023.01.16.523937.
(143) Mark, E.; Goldsman, D.; Gurbaxani, B.; Keskinocak, P.; Sokol, J. Using Machine Learning and an Ensemble of Methods to Predict Kidney Transplant Survival. *PLOS ONE* **2019**, *14* (1), e0209068. https://doi.org/10.1371/journal.pone.0209068.
(144) Senanayake, S.; White, N.; Graves, N.; Healy, H.; Baboolal, K.; Kularatna, S. Machine Learning in Predicting Graft Failure Following Kidney Transplantation: A Systematic Review of Published Predictive Models. *International Journal of Medical Informatics* **2019**, *130*, 103957. https://doi.org/10.1016/j.ijmedinf.2019.103957.
(145) Zhong, J.-J. Recent Advances in Bioreactor Engineering. *Korean J. Chem. Eng.* **2010**, *27* (4), 1035–1041. https://doi.org/10.1007/s11814-010-0277-5.
(146) Janssen, F. W.; Hofland, I.; Oorschot, A. van; Oostra, J.; Peters, H.; Blitterswijk, C. A. van. Online Measurement of Oxygen Consumption by Goat Bone Marrow Stromal Cells in a Combined Cell-Seeding and Proliferation Perfusion Bioreactor. *Journal of Biomedical Materials Research Part A* **2006**, *79A* (2), 338–348. https://doi.org/10.1002/jbm.a.30794.
(147) Maier, U.; Büchs, J. Characterisation of the Gas–Liquid Mass Transfer in Shaking Bioreactors. *Biochemical Engineering Journal* **2001**, *7* (2), 99–106. https://doi.org/10.1016/S1369-703X(00)00107-8.
(148) Hu, W.-S.; Weichang, Z.; Europa, L. F. Controlling Mammalian Cell Metabolism in Bioreactors. *Journal of Microbiology and Biotechnology* **1998**, *8* (1), 8–13.
(149) Griffiths, J. B. The Effect of Medium Changes on the Growth and Metabolism of the Human Diploid Cell, W1-38. *Journal of Cell Science* **1971**, *8* (1), 43–52. https://doi.org/10.1242/jcs.8.1.43.
(150) Lee, C.; Ly, C.; Moore, G.; Perkinson, R. Chemically Defined Medium for Cultured Mammalian Cells. US6900056B2, May 31, 2005. https://patents.google.com/patent/US6900056B2/en (accessed 2024-07-11).
(151) van der Valk, J.; Brunner, D.; De Smet, K.; Fex Svenningsen, Å.; Honegger, P.; Knudsen, L. E.; Lindl, T.; Noraberg, J.; Price, A.; Scarino, M. L.; Gstraunthaler, G. Optimization of Chemically Defined Cell Culture Media – Replacing Fetal Bovine Serum in Mammalian *in Vitro* Methods. *Toxicology in Vitro* **2010**, *24* (4), 1053–1063. https://doi.org/10.1016/j.tiv.2010.03.016.
(152) Throm, A. M.; Liu, W.-C.; Lock, C.-H.; Billiar, K. L. Development of a Cell-Derived Matrix: Effects of Epidermal Growth Factor in Chemically Defined Culture. *Journal of Biomedical Materials Research Part A* **2010**, *92A* (2), 533–541. https://doi.org/10.1002/jbm.a.32369.
(153) Farahani, R. M.; Xaymardan, M. Platelet-Derived Growth Factor Receptor Alpha as a Marker of Mesenchymal Stem Cells in Development and Stem Cell Biology. *Stem Cells Int* **2015**, *2015*, 362753. https://doi.org/10.1155/2015/362753.
(154) Hassell, J. R.; Kane, B. P.; Etheredge, L. T.; Valkov, N.; Birk, D. E. Increased Stromal Extracellular Matrix Synthesis and Assembly by Insulin Activated Bovine Keratocytes Cultured under Agarose. *Experimental Eye Research* **2008**, *87* (6), 604–611. https://doi.org/10.1016/j.exer.2008.09.010.
(155) Ross, J. J.; Tranquillo, R. T. ECM Gene Expression Correlates with in Vitro Tissue Growth and Development in Fibrin Gel Remodeled by Neonatal Smooth Muscle Cells. *Matrix Biology* **2003**, *22* (6), 477–490. https://doi.org/10.1016/S0945-053X(03)00078-7.

(156) Maia, F. R.; Reis, R. L.; Oliveira, J. M. Cell-Derived Matrices for Scaffolds Improvement. In *Handbook of the Extracellular Matrix*; Maia, F. R. A., Oliveira, J. M., Reis, R. L., Eds.; Springer International Publishing: Cham, 2023; pp 1–21. https://doi.org/10.1007/978-3-030-92090-6_38-1.
(157) Rowland, C. R.; Colucci, L. A.; Guilak, F. Fabrication of Anatomically-Shaped Cartilage Constructs Using Decellularized Cartilage-Derived Matrix Scaffolds. *Biomaterials* **2016**, *91*, 57–72. https://doi.org/10.1016/j.biomaterials.2016.03.012.
(158) Yong, I.; Oh, S. W.; Kim, P. Chapter 9 - Re-Engineered Cell-Derived Extracellular Matrix as a New Approach to Clarify the Role of Native ECM. In *Methods in Cell Biology*; Caballero, D., Kundu, S. C., Reis, R. L., Eds.; Cell-derived Matrices - Part A; Academic Press, 2020; Vol. 156, pp 205–231. https://doi.org/10.1016/bs.mcb.2019.12.007.
(159) Davidson, M. D.; Burdick, J. A.; Wells, R. G. Engineered Biomaterial Platforms to Study Fibrosis. *Advanced Healthcare Materials* **2020**, *9* (8), 1901682. https://doi.org/10.1002/adhm.201901682.
(160) Riehl, B. D.; Park, J.-H.; Kwon, I. K.; Lim, J. Y. Mechanical Stretching for Tissue Engineering: Two-Dimensional and Three-Dimensional Constructs. *Tissue Engineering Part B: Reviews* **2012**, *18* (4), 288–300. https://doi.org/10.1089/ten.teb.2011.0465.
(161) Müller, L. J.; Pels, E.; Vrensen, G. F. J. M. The Specific Architecture of the Anterior Stroma Accounts for Maintenance of Corneal Curvature. *British Journal of Ophthalmology* **2001**, *85* (4), 437–443. https://doi.org/10.1136/bjo.85.4.437.
(162) Qian, J.; Okada, Y.; Ogura, T.; Tanaka, K.; Hattori, S.; Ito, S.; Satoh, J.; Takita, T.; Yasukawa, K. Kinetic Analysis of the Digestion of Bovine Type I Collagen Telopeptides with Porcine Pepsin. *Journal of Food Science* **2016**, *81* (1), C27–C34. https://doi.org/10.1111/1750-3841.13179.
(163) Nalinanon, S.; Benjakul, S.; Visessanguan, W.; Kishimura, H. Use of Pepsin for Collagen Extraction from the Skin of Bigeye Snapper (*Priacanthus Tayenus*). *Food Chemistry* **2007**, *104* (2), 593–601. https://doi.org/10.1016/j.foodchem.2006.12.035.
(164) Maher, M. K.; White, J. F.; Glattauer, V.; Yue, Z.; Hughes, T. C.; Ramshaw, J. A. M.; Wallace, G. G. Variation in Hydrogel Formation and Network Structure for Telo-, Atelo- and Methacrylated Collagens. *Polymers* **2022**, *14* (9), 1775. https://doi.org/10.3390/polym14091775.
(165) Carmichael, D. J.; Dodd, C. M.; Veis, A. The Solubilization of Bone and Dentin Collagens by Pepsin Effect of Cross-Linkages and Non-Collagen Components. *Biochimica et Biophysica Acta (BBA) - Protein Structure* **1977**, *491* (1), 177–192. https://doi.org/10.1016/0005-2795(77)90054-X.
(166) Chamkouri, H.; Chamkouri, M. A Review of Hydrogels, Their Properties and Applications in Medicine. *AJBSR* **2021**, *11* (5), 485.
(167) Kim, H.; Jang, J.; Park, J.; Lee, K.-P.; Lee, S.; Lee, D.-M.; Kim, K. H.; Kim, H. K.; Cho, D.-W. Shear-Induced Alignment of Collagen Fibrils Using 3D Cell Printing for Corneal Stroma Tissue Engineering. *Biofabrication* **2019**, *11* (3), 035017. https://doi.org/10.1088/1758-5090/ab1a8b.
(168) Guo, T.; Ringel, J. P.; Lim, C. G.; Bracaglia, L. G.; Noshin, M.; Baker, H. B.; Powell, D. A.; Fisher, J. P. Three Dimensional Extrusion Printing Induces Polymer Molecule Alignment and Cell Organization within Engineered Cartilage. *Journal of Biomedical Materials Research Part A* **2018**, *106* (8), 2190–2199. https://doi.org/10.1002/jbm.a.36426.
(169) Osagie, J. O.; Syeda, S. S.; Turner-Brannen, E.; Guimond, M.; Parrenas, L.; Haroon, A.; Imasuen, P.; West, A. R. Development of a 3D Bioprinted Airway Smooth Muscle Model for Manipulating Structure and Measuring Contraction. bioRxiv January 2, 2023, p 2022.12.15.520464. https://doi.org/10.1101/2022.12.15.520464.

(170) Bagdasarian, I. A.; Tonmoy, T. I.; Park, B. H.; Morgan, J. T. In Vitro Formation and Extended Culture of Highly Metabolically Active and Contractile Tissues. *PLOS ONE* **2023**, *18* (11), e0293609. https://doi.org/10.1371/journal.pone.0293609.
(171) Wang, J.; Liu, S.; Huang, J.; Ren, K.; Zhu, Y.; Yang, S. Alginate: Microbial Production, Functionalization, and Biomedical Applications. *International Journal of Biological Macromolecules* **2023**, *242*, 125048. https://doi.org/10.1016/j.ijbiomac.2023.125048.
(172) Xie, Z.-T.; Kang, D.-H.; Matsusaki, M. Resolution of 3D Bioprinting inside Bulk Gel and Granular Gel Baths. *Soft Matter* **2021**, *17* (39), 8769–8785. https://doi.org/10.1039/D1SM00926E.
(173) Wolf, M. T.; Daly, K. A.; Brennan-Pierce, E. P.; Johnson, S. A.; Carruthers, C. A.; D'Amore, A.; Nagarkar, S. P.; Velankar, S. S.; Badylak, S. F. A Hydrogel Derived from Decellularized Dermal Extracellular Matrix. *Biomaterials* **2012**, *33* (29), 7028–7038. https://doi.org/10.1016/j.biomaterials.2012.06.051.
(174) Mikhail, A. S.; Morhard, R.; Mauda-Havakuk, M.; Kassin, M.; Arrichiello, A.; Wood, B. J. Hydrogel Drug Delivery Systems for Minimally Invasive Local Immunotherapy of Cancer. *Advanced Drug Delivery Reviews* **2023**, *202*, 115083. https://doi.org/10.1016/j.addr.2023.115083.
(175) Yang, J.; Yu, H.; Wang, L.; Liu, J.; Liu, X.; Hong, Y.; Huang, Y.; Ren, S. Advances in Adhesive Hydrogels for Tissue Engineering. *European Polymer Journal* **2022**, *172*, 111241. https://doi.org/10.1016/j.eurpolymj.2022.111241.
(176) Li, J.; Jia, X.; Yin, L. Hydrogel: Diversity of Structures and Applications in Food Science. *Food Reviews International* **2021**, *37* (3), 313–372. https://doi.org/10.1080/87559129.2020.1858313.
(177) Vriend, L.; Sinkunas, V.; Camargo, C. P.; van der Lei, B.; Harmsen, M. C.; van Dongen, J. A. Extracellular Matrix-Derived Hydrogels to Augment Dermal Wound Healing: A Systematic Review. *Tissue Engineering Part B: Reviews* **2022**, *28* (5), 1093–1108. https://doi.org/10.1089/ten.teb.2021.0120.
(178) Torregrossa, M.; Kakpenova, A.; Simon, J. C.; Franz, S. Modulation of Macrophage Functions by ECM-Inspired Wound Dressings – a Promising Therapeutic Approach for Chronic Wounds. *Biological Chemistry* **2021**, *402* (11), 1289–1307. https://doi.org/10.1515/hsz-2021-0145.